University of Alberta

Characterization of a diamond detector for intensity modulated point dose measurements

by

Erin Rae Barnett ©

A thesis submitted to the Faculty of Graduate studies and Research in partial fulfillment of the requirements for the degree of Master of Science

in

Medical Physics

Department of Physics

Edmonton, Alberta

Spring 2004

Library and Archives Canada

Published Heritage Branch

395 Wellington Street
Ottawa ON K1A 0N4
Canada

Bibliothèque et Archives Canada

Direction du Patrimoine de l'édition

395, rue Wellington
Ottawa ON K1A 0N4
Canada

Your file Votre référence
ISBN: 0-612-96448-5
Our file Notre référence
ISBN: 0-612-96448-5

The author has granted a non-exclusive license allowing the Library and Archives Canada to reproduce, loan, distribute or sell copies of this thesis in microform, paper or electronic formats.

L'auteur a accordé une licence non exclusive permettant à la Bibliothèque et Archives Canada de reproduire, prêter, distribuer ou vendre des copies de cette thèse sous la forme de microfiche/film, de reproduction sur papier ou sur format électronique.

The author retains ownership of the copyright in this thesis. Neither the thesis nor substantial extracts from it may be printed or otherwise reproduced without the author's permission.

L'auteur conserve la propriété du droit d'auteur qui protège cette thèse. Ni la thèse ni des extraits substantiels de celle-ci ne doivent être imprimés ou aturement reproduits sans son autorisation.

In compliance with the Canadian Privacy Act some supporting forms may have been removed from this thesis.

Conformément à la loi canadienne sur la protection de la vie privée, quelques formulaires secondaires ont été enlevés de cette thèse.

While these forms may be included in the document page count, their removal does not represent any loss of content from the thesis.

Bien que ces formulaires aient inclus dans la pagination, il n'y aura aucun contenu manquant.

Canada

Abstract

The introduction of 3D intensity modulated radiotherapy through the use of multi-leaf collimation into the field of radiation oncology has given rise smaller radiation fields than were previously encountered in conventional radiotherapy. In addition within these intensity modulated radiation fields high dose gradients can be present. Difficulties in obtaining accurate dose measurements in these smaller fields and fields containing high dose gradients with conventional dosimeters have led to the investigation of new dosimeters to overcome these problems. Diamond detectors are dosimeters with sufficiently high spatial resolution to make accurate dose measurements in these fields.

The characterization of a PTW-Freiburg type 60003 diamond detector (S/N 9-032) for use in megavoltage photon beam dosimetry is the basis of this thesis, particularly with respect to small fields and intensity modulated fields. Basic properties such as the pre-irradiation effect, detector stability, spatial resolution and radiation sensitivity have been observed and quantified. The dose rate dependence of this dosimeter has been measured for the following beam qualities: ^{60}Co as well as 6 MV and 15 MV linear accelerator photon beams. The effect of this dose rate dependence on the conversion of diamond current to dose rate has been investigated. The dose measured with the diamond detector in 6 and 15 MV square radiation fields as small as 1 x 1 cm^2 was compared with doses measured with other point dosimeters as well as with the dose determined using an electronic portal imaging device. Comparison between doses measured in simple intensity modulated fields with the diamond detector, large and small volume ion chambers and the electronic portal imaging device was made.

To my family

Acknowledgements

First and foremost I would like to thank the Medical Physics graduate students sharing the office space on the other side. They have made this experience bearable and I would even go so far to say that coming to school was at times bordering on enjoyable. I thank Tara, MadDog, Monajemi for all of her zany stories, Alana for all the wonderful event co-ordination and outfitting for events when I was ill prepared, Steven for being who he is and Keith and Anna for seamlessly joining our group of windowless basement dwellers. I thank them all for their friendship.

I would also like to thank numerous people in the Medical Physics Department who have been extremely helpful throughout both the course and research components of this degree. In particular thanks go to Heather Thompson for her willingness to help when HELAX proved too complicated for me and Dr. Stephen Steciw and Brad Warkentin for sharing their work and letting me make use of their EPID dose software along with many useful discussions. I also would like to thank B. G. Fallone for selling Medical Physics to me the first time I walked into the Cross Cancer Institute. Without his influence I may have returned to Italy to soak up the culture and sun while overindulging in great wine, coffee and food with my fine friend Julia.

I would like to thank Marc MacKenzie for all of the good ideas that went into this project, his great sense of humour and offering encouragement and support when things were looking dark and broken.

My thanks go to my family that has been supportive of me always. Thanks go to my mother who among countless other things has outfit me with flannel pajamas to face the cold cold winter in Edmonton, to my father for his no nonsense encouragement and to my sister, Ellen, for giving me lots to laugh about, particularly the running man and generally being a great friend. Without you all, this thesis would not exist.

Abbreviations

AAPM	American Association of Physicists in Medicine
CAX	Central Axis
CRT	Conformal Radiotherapy
d_{max}	Depth of maximum dose
EPID	Electronic Portal Imaging Devices
ICRU	International Commission of Radiation Units and Measurements
IMB	Intensity Modulated Beam
IMRT	Intensity Modulated Radiation Therapy
MLC	Multileaf Collimator
MOSFET	Metal Oxide Silicon Field Effect Transistors
MU	Monitor Units
OAR	Organ At Risk
PDD	Percent Depth Dose
PRF	Pulse Repetition Frequency
RT	Radiation Therapy/Radiotherapy
SSD	Source to Surface Distance
TLD	Thermoluminescent Device
TMR	Tissue Maximum Ratio
TPS	Treatment Planning System

TABLE OF CONTENTS

CHAPTER 1 ..... **1**

1.1 THESIS OVERVIEW 1
1.1.1 Thesis Overview – Chapter 2 - Introduction *1*
1.1.2 Thesis Overview – Chapter 3 – Materials and Methods *2*
1.1.3 Thesis Overview – Chapter 4 – Results and Discussion *3*
1.1.4 Thesis Overview – Chapter 5 - Conclusions *3*

CHAPTER 2 INTRODUCTION **4**

2.1 CANCER AND ITS TREATMENT 4
2.2 RADIATION THERAPY 5
2.3 IMPROVEMENTS IN RADIOTHERAPY 6
2.3.1 Conformal Radiotherapy *7*
2.3.2 Intensity Modulated Radiation Therapy *8*
2.3.3 Tomotherapy *11*
2.4 SMALL RADIATION FIELD DOSIMETRY 12
2.5 DOSIMETERS IN CLINICAL USE 14
2.5.1 Ionization Chambers *14*
2.5.2 Solid State Dosimeters *16*
2.5.2.1 Diodes 16
2.5.2.2 MOSFET dosimetry 18
2.5.3 Thermoluminescent Dosimetry *19*
2.5.4 Film Dosimetry *20*
2.5.5 Flat-panel detectors *22*
2.6 DIAMOND DETECTOR PROPERTIES 22
2.6.1 Basic Operation Principles *22*
2.6.2 Dose Rate Dependence *24*
2.6.3 High Spatial Resolution *30*
2.6.4 High Sensitivity *31*
2.6.5 Near Tissue Equivalence *31*
2.6.6 Radiation Priming and Radiation Stability *33*
2.6.7 Temperature Dependence *36*
2.6.8 Resistant to Radiation Damage *36*
2.6.9 Directional Independence *37*
2.6.10 Diamond use in clinical dosimetry *38*
CHAPTER 2 REFERENCES 39

CHAPTER 3 MATERIALS AND METHODS **44**

3.1 MATERIALS 44
3.1.1 Dosimeters *44*
3.1.1.1 Diamond Detector 44
3.1.1.2 Exradin A12 ionization chamber 46
3.1.1.3 PinPoint ionization chamber 46
3.1.1.4 IC10 Ionization Chamber 47
3.1.1.5 Scanditronix Photon Diode 47
3.1.1.6 PR-06C Farmer type chamber 47
3.1.1.7 aS500 EPID 47
3.1.2 Electrometers *48*
3.1.2.1 Capintec Model 192 Electrometer 48
3.1.2.2 Keithley 6514 System Electrometer 48
3.1.2.3 Wellhöfer Beam Data Acquisition System 48
3.1.3 Phantoms *49*
3.1.3.1 Solid Water Phantom 49

3.1.3.2 Wellhöfer water phantom 49
3.1.4 Computer Software *50*
3.1.4.1 HELAX Treatment Planning System 50
3.1.4.2 WP700 Software 50
3.1.4.3 Matlab 50
3.2 MEASUREMENTS 50
3.2.1 Basic Diamond Detector Operation *51*
3.2.2 Pre-Irradiation Measurements *52*
3.2.3 Detector Stability Measurements *52*
3.2.4 Beam Profile Measurements *53*
3.2.5 Dose Rate Dependence Measurements *54*
3.2.5.1 Source Surface Distance (SSD) Variation 57
3.2.5.3 Tissue Maximum Ratio (TMR) Measurements 58
3.2.5.4 Pulse Repetition Frequency Variation 59
3.2.6 R Value Determination *60*
3.2.7 Arc Treatment *61*
3.2.8 Effect of dose rate dependence *62*
3.2.9 Wellhöfer dose measurements *62*
3.2.10 Small Field Dosimetry Measurements *63*
3.2.11 Simple Intensity Modulated Beams *65*
3.2.12 Dosimetry of clinical prostate intensity modulated beam *66*
3.2.13 Dosimetry of clinical prostate intensity modulated beam at improved detector positions *66*
3.2.14 Intensity Modulated Beam Calculations *67*
CHAPTER 3 REFERENCES 68

CHAPTER 4 RESULTS AND DISCUSSION 69

4.1 PRE-IRRADIATION 69
4.2 STABILITY 71
4.3 BEAM PROFILE MEASUREMENTS 73
4.4 DOSE RATE DEPENDENCE MEASUREMENTS 77
4.5 R VALUE DETERMINATION 81
4.6 ARC TREATMENT 82
4.7 THEORETICAL EFFECT OF DOSE RATE DEPENDENCE 84
4.8 SMALL FIELD DOSIMETRY 86
4.9 DOSIMETRY OF SIMPLE INTENSITY MODULATED BEAMS 89
4.10 DOSIMETRY OF CLINICAL PROSTATE INTENSITY MODULATED BEAM 93
4.11 DOSIMETRY OF CLINICAL PROSTATE INTENSITY MODULATED BEAM AT IMPROVED DETECTOR POSITIONS 98
CHAPTER 4 REFERENCES 103

CHAPTER 5 CONCLUSIONS 104

APPENDIX 107

APPENDIX A - CALCULATION OF ERROR IN DOSE RATE FOR DIAMOND DETECTOR 107
APPENDIX B – WEIGHTED REGRESSION 108
APPENDIX C – ERROR PROPAGATION 109

REFERENCES 110

LIST OF FIGURES

FIGURE 2.1 SHAPE OF SEVEN STEP AND SHOOT SEGMENTS THAT COMPRISE SINGLE INTENSITY MODULATED BEAM AND "FLUENCE MAP" RESULTING FROM DELIVERY OF SEVEN STEP AND SHOOT SEGMENTS - THICK LINES ILLUSTRATE SEGMENT GEOMETRY, THIN LINES ILLUSTRATE MAIN COLLIMATOR SETTINGS 11

FIGURE 2.2 BASIC DIAMOND DETECTOR OPERATION 23

FIGURE 3.1 SCHEMATIC DIAGRAM OF DIAMOND DETECTOR SHOWING LOCATION OF SENSITIVE VOLUME AS SHOWN IN PTW-FREIBURG TYPE 60003 DIAMOND DETECTOR INSTRUCTION MANUAL 45

FIGURE 3.2 PTW-FREIBURG TYPE 60003 DIAMOND DETECTOR EXPERIMENTAL SET-UP SHOWING CONNECTIONS TO POWER SUPPLY AND ELECTROMETER 51

FIGURE 3.3 DIAMOND DETECTOR PROBE ORIENTATIONS USED IN MAKING BEAM PROFILE MEASUREMENTS (A) PROBE STEM ORIENTED PARALLEL TO BEAM CAX AND (B) PROBE STEM ORIENTED PERPENDICULAR TO BEAM CAX 54

FIGURE 3.4 EXPERIMENTAL SET-UP EMPLOYED FOR DELIVERY OF PHOTON BEAM ARC TREATMENT 61

FIGURE 4.1 DIAMOND DETECTOR PRE-IRRADIATION RESPONSE TO BEAMS OF COBALT, 6 MV AND 15 MV PHOTONS 70

FIGURE 4.2 DIAMOND DETECTOR RESPONSE TO PULSE OF COBALT-60 RADIATION FOLLOWING 1 MINUTE AND 60 MINUTES OF NO IRRADIATION 72

FIGURE 4.3 VARIATIONS IN DETECTOR RESPONSE TO COBALT-60 IRRADIATION WITH INCREASING TIME BETWEEN SUBSEQUENT IRRADIATIONS 73

FIGURE 4.4 CROSSPLANE BEAM PROFILES AT 10 CM DEPTH WITH SSD = 90 CM OF 5 X 5 CM^2 VARIAN 600C GENERATED 6 MV PHOTON BEAM AS MEASURED WITH DIAMOND DETECTOR WITH PERPENDICULAR AND PARALLEL ORIENTATIONS AS WELL AS IC10 ION CHAMBER 74

FIGURE 4.5 CROSSPLANE BEAM PROFILES AT 10 CM DEPTH WITH SSD = 90 CM OF 3 X 3 CM^2 VARIAN 600C GENERATED 6 MV PHOTON BEAM AS MEASURED WITH DIAMOND DETECTOR WITH PERPENDICULAR AND PARALLEL ORIENTATIONS AS WELL AS IC10 ION CHAMBER 75

FIGURE 4.6 LINEAR RELATIONSHIP BETWEEN LOGARITHMS OF NORMALIZED DIAMOND RESPONSE AND NORMALIZED DOSE RATE FOR 15 MV PHOTONS GENERATED BY A VARIAN 2300 EX LINAC. VARIATIONS IN SSD WERE USED TO OBTAIN DOSE RATE VARIATIONS. THE INSET SHOWS THE VARIATION IN THE ION CHAMBER CORRECTION FACTORS WITH DOSE RATE 79

FIGURE 4.7 DIAMOND DETECTOR CURRENT AS A FUNCTION OF TIME DURING 6 MV ARC TREATMENT 83

FIGURE 4.8 DOSES MEASURED AT FIELD SIZES RANGING FROM 1 X 1 CM^2 TO 10 X 10 CM^2 USING DIAMOND DETECTOR, A12 AND PINPOINT FOR 6 MV IRRADIATIONS 88

FIGURE 4.9 DOSES MEASURED AT FIELD SIZES RANGING FROM 1 X 1 CM^2 TO 10 X 10 CM^2 USING DIAMOND DETECTOR, A12, PINPOINT AND EPID FOR 15 MV IRRADIATIONS 89

FIGURE 4.10 SHAPE OF INDIVIDUAL SEGMENTS COMPRISING 5 SEGMENT SIMPLE STEP AND SHOOT INTENSITY MODULATED BEAM – THICK LINES ILLUSTRATE SEGMENT GEOMETRY, THIN LINES ILLUSTRATE MAIN COLLIMATOR SETTINGS 91

FIGURE 4.11 DOSE RATE DURING DELIVERY OF 5 SEGMENT STEP AND SHOOT IMRT FIELD AT ISOCENTRE AT 10 CM DEPTH IN PHANTOM AS MEASURED WITH DIAMOND DETECTOR AND EXRADIN A12 ION CHAMBER 91

FIGURE 4.12 COMPARISON OF RESPONSE OF THREE POINT DOSIMETERS' RESPONSE TO 8 SEGMENT INTENSITY MODULATED FIELD AT ISOCENTRE 94

FIGURE 4.13 SHAPE OF EIGHT SEGMENTS THAT COMPRISE SINGLE IMB AND "FLUENCE MAP" RESULTING FROM DELIVERY OF EIGHT STEP AND SHOOT SEGMENTS - THICK LINES ILLUSTRATE SEGMENT GEOMETRY, THIN LINES ILLUSTRATE MAIN COLLIMATOR SETTINGS 95

FIGURE 4.14 MAP USED TO DETERMINE APPROPRIATE PROBE POSITIONS FOR A CLINICAL PROSTATE IMB 99

FIGURE 4.15 COMPARISON OF RESPONSE OF THREE POINT DOSIMETERS' RESPONSE TO 8 SEGMENT IMRT FIELD AT IMPROVED DETECTOR POSITION 1 (-1.3 CM, 1.7 CM) AS DETERMINED BY EDGE EXCLUDE SOFTWARE 100

FIGURE 4.16 COMPARISON OF RESPONSE OF THREE POINT DOSIMETERS' RESPONSE TO 8 SEGMENT IMRT FIELD AT IMPROVED DETECTOR POSITION 2 (0.7 CM, 3.0 CM) AS DETERMINED BY EDGE EXCLUDE SOFTWARE 101

LIST OF TABLES

TABLE 3.1 COMPARISON OF SENSITIVE VOLUMES OF POINT DOSIMETERS EMPLOYED IN THIS THESIS AND RATIO OF SENSITIVE VOLUMES TO THAT OF DIAMOND DETECTOR 44

TABLE 3.2 PHYSICAL AND OPERATING CHARACTERISTICS OF PTW-FREIBERG TYPE 60003 DIAMOND DETECTOR AS GIVEN BY THE MANUFACTURER 46

TABLE 4.1 DOSE REQUIRED TO STABILIZE PTW-FREIBURG TYPE 60003 DIAMOND DETECTOR (S/N 9-032) RESPONSE FOLLOWING PERIOD OF UNBIASED CONDITIONS 70

TABLE 4.2 20-80 % DOSE LEVEL PENUMBRAL WIDTHS MEASURED WITH DIAMOND DETECTOR AND IC10 ION CHAMBER FOR 6 MV PHOTON BEAM GENERATED WITH A VARIAN 600C LINAC 76

TABLE 4.3 10-90 % DOSE LEVEL PENUMBRAL WIDTHS MEASURED WITH DIAMOND DETECTOR AND IC10 ION CHAMBER FOR 6 MV PHOTON BEAM GENERATED WITH A VARIAN 600C LINAC 77

TABLE 4.4 Δ VALUES DETERMINED FROM SSD VARIATION 78

TABLE 4.5 Δ VALUES DETERMINED FROM PDD MEASUREMENTS 79

TABLE 4.6 Δ VALUES DETERMINED FROM TMR VARIATION 79

TABLE 4.7 Δ VALUES DETERMINED FROM PRF VARIATION 80

TABLE 4.8 R VALUES OF PTW-FREIBURG TYPE 60003 DIAMOND DETECTOR (S/N 9-032) FOR DIFFERENT BEAM QUALITIES USED IN THIS INVESTIGATION 81

TABLE 4.9 DOSES MEASURED WITH PR-06C ION CHAMBER AND DIAMOND DETECTOR DURING 6 AND 15 MV ARC TREATMENT 83

TABLE 4.10 THEORETICAL DOSES CALCULATED FOR 6 MV ARC TREATMENT ILLUSTRATING EFFECT OF DIAMOND DETECTOR'S Δ VALUE ON CONVERSION FROM DIAMOND CURRENT TO DOSE RATE 84

TABLE 4.11 THEORETICAL DOSES CALCULATED FOR 15 MV ARC TREATMENT ILLUSTRATING EFFECT OF DIAMOND DETECTOR'S Δ VALUE ON CONVERSION FROM DIAMOND CURRENT TO DOSE RATE 85

TABLE 4.12 DOSES AT ISOCENTER FOR SIMPLE IMRT PLANS MEASURED USING A12, PINPOINT, DIAMOND DETECTOR AND AS500 EPID 92

TABLE 4.13 DOSES MEASURED AT ISOCENTRE DURING DELIVERY OF 8 SEGMENT CLINICAL PROSTATE INTENSITY MODULATED BEAM 97

TABLE 4.14 DOSES MEASURED AT IMPROVED DETECTOR POSITION 1 (-1.3 CM 1.7 CM) DURING DELIVERY OF 8 SEGMENT IMRT FIELD 101

TABLE 4.15 DOSES MEASURED AT IMPROVED DETECTOR POSITION 2 (0.7 CM, 3.0 CM) DURING DELIVERY OF 8 SEGMENT IMRT FIELD 102

Chapter 1

1.1 Thesis Overview

The advent of any new technology is accompanied by the evaluation of that technology and a thorough investigation into the viability of implementation of that technology into everyday practices. This thesis constitutes an evaluation of a PTW-Freiburg type 60003 diamond detector (S/N 9-032) for the purpose of megavoltage photon beam dosimetry of linear accelerator and cobalt-60 generated radiotherapy beams. The aim of this thesis was to demonstrate that following the characterization of this dosimeter, it can be employed to make accurate point dose measurements in situations where other dosimeters are known to perform poorly, particularly in intensity modulated beams (IMB).

This thesis chapter provides an introduction to this thesis and gives a breakdown of chapter content.

1.1.1 Thesis Overview – Chapter 2 - Introduction

Chapter 2 serves as a brief introduction to this thesis. To put this work in perspective, this chapter opens with some current cancer statistics as well as a description of progress in the field of radiotherapy. In order to illustrate the need for the implementation of a diamond detector clinically, small field dosimetry is discussed in some detail. To contrast the diamond detector, a brief description of the following competing dosimeters is included in this chapter: ion chambers, diodes, MOSFETs, thermoluminescent devices (TLD), film and flat panel imaging devices. Basic diamond detector operation is described also in this section. The dose rate dependence of diamond detectors is then described. A literature review of some of the properties of diamond as a dosimeter such as spatial resolution, sensitivity, near tissue equivalence, radiation priming dose and stability follows. A look at the temperature and directional dependence as well as the resistance of diamond detectors is also included in this chapter.

1.1.2 Thesis Overview – Chapter 3 – Materials and Methods

Chapter 3 entitled Materials and Methods is a description of the experimental techniques used throughout the duration of this thesis. A description of each dosimeter and each electrometer used in this study is included for completeness. Also included in this chapter are brief descriptions of each of the phantoms employed in this study. The descriptions of the measurements provide sufficient information to enable one to repeat these measurements. This chapter includes a short description of basic diamond detector operation as well as a description of the measurement techniques used to quantify some of the basic properties of the diamond detector such as the required pre-irradiation dose to ensure detector stability. This chapter also includes a description of the method used to establish the stability of the detector response with increasing time between subsequent measurements. Beam profile measurements were made to observe the improved spatial resolution exhibited by the diamond detector as compared with other point dosimeters. A description of the four techniques employed to quantify the dose rate dependence of this diamond detector are included in this chapter. The different techniques include varying the source surface distance (SSD) and varying the depth of the probe in phantom both at fixed and changing SSDs. The final method which is only applicable to linear accelerator generated beams, involved the variation of the pulse repetition frequency of the accelerator. Prior to making use of the diamond detector in complicated radiation beams such as intensity modulated beams, it was of interest to observe the effect of the dose rate dependence and verify our ability to correct for this dependence. An arc treatment during which the dose rate varied significantly, yet no high dose gradients were present in the field served as a test of our ability to correct for the dose rate dependence. Comparison was subsequently made between the dose rate dependent corrected dose measured with the diamond and an ion chamber measured dose for the arc treatment. The complexity of the radiation treatments delivered to the phantom and quantified using the diamond detector increased with time, leading to the primary aim of this study – point dose verification in intensity modulated fields. The methods used to

measure dose with varying field size and in simple intensity modulated beams are described. The dose measurements made in the clinical intensity modulated beams are also described in this chapter. This chapter also includes a description of the technique proposed in this thesis to select better positions for point dose measurements.

1.1.3 Thesis Overview – Chapter 4 – Results and Discussion

Chapter 4 contains the results obtained during the period of experimentation leading to this thesis. Results are presented both in a graphical and tabular form. The first sections of this chapter include basic diamond detector characterization measurements. The latter sections of this chapter tend to focus on the use of this dosimeter in clinically relevant dose measurements and the comparison of the diamond detector response with that of other dosimeters.

1.1.4 Thesis Overview – Chapter 5 - Conclusions

Chapter 5 consists of concluding remarks of this work. Possibilities for future work stemming from this thesis are included in this chapter.

Chapter 2 Introduction

2.1 Cancer and its treatment

The National Cancer Institute of Canada in its report *Canadian Cancer Statistics 2002* estimated that 136 900 new cases of cancer would be diagnosed in 2002 and an estimated 66 200 people would die from the disease (NCIC 2003). Although diseases of the circulatory system cause a larger number of deaths than cancer (StatsCanada 1999), cancer deaths are the cause of the greatest number of years of lost life in Canada. Untimely cancer deaths result in 30 % of all years of potential life that are lost in this country (NCIC 2003). This disease will infect 38 % of women and 41 % of men during their lives according to present incident rates (NCIC 2003).

Upon diagnosis of a cancer, patients are staged according to the severity of the cancer and the extent to which it has spread throughout the body. Staging of cancer at the time of diagnosis evaluates the size of the primary tumor, the invasion of the cancer into the nodes of the lymphatic system and the presence or absence of distant metastases. The stage of the cancer at the time of diagnosis is used by oncologists to determine the intent of the treatment: palliative or curative. Radiation therapy plays a role in both palliative and curative treatment regimes. Half of patients diagnosed with cancer will receive radiation either as their primary treatment modality or in conjunction with other treatment modalities, namely surgery and chemotherapy. Of those treated for cancer with radiation therapy, one third of them will receive only radiation (NCIC 2003). The prevalence of this treatment modality in cancer therapy indicates that improvements in radiotherapy could improve the survival of thousands of people in this country alone each year.

2.2 Radiation Therapy

The goal of radiation therapy (RT) is to deliver a dose of radiation to the cancerous volume that is sufficiently high to kill all the clonogenic cells within the tumor while minimizing the amount of damage to healthy tissues. Irradiation of healthy tissues can result in acute and chronic effects with the possibility of carcinogenesis in the future (Van Dyk 1999). For these reasons it is also of primary importance to protect organs at risk (OAR) that surround the tumor site.

When ionizing radiation is incident upon tissue, energy is imparted to that tissue. The deposition of energy within the cells making up a tissue can cause a number of effects: cell killing, mutation and carcinogensis (Hall 2000). RT is complicated by the fact that ionizing radiation kills both healthy and diseased tissue. Radiation doses that can be delivered to tumors are limited by the tolerances of the healthy tissues surrounding the target. Early experimenters investigating the properties of radiation in the late 1800s soon realized that extended exposure to radiation resulted in damage to healthy tissue. Shortly thereafter ionizing radiation's potential to kill diseased cells was recognized. In the early part of 1896, the first therapeutic radiation treatment was delivered by E. H. Grubbe (Brady, Kramer et al. 2001). The treatment consisted of exposure of diseased breast tissue to radiation emitted from an x-ray tube for an hour. Grubbe, familiar with the threat that x-rays posed to healthy tissue from his experience testing vacuum tubes with his hand, attempted to protect the patient's healthy tissues by separating the healthy tissue from the x-ray source with a lead sheet. There is no record of the outcome of this treatment (Radiology Centennial 1993). Of course, drastic improvements in the field of RT have been made since this first treatment.

The RT modality can be sub-divided into two major categories: brachytherapy and external beam (Khan 1994). Brachytherapy involves the insertion of sealed radioactive sources into the body. The appropriateness of brachytherapy radionuclides is assessed based on the particle type and energy of the emission from the nuclide. Availability and decay of radioactive sources are also factors in the selection of radionuclides for the purpose of brachytherapy.

The depth dose deposition characteristics of the particles emitted from the sources make brachytherapy suitable for certain cancer sites. Brachytherapy has been used to treat cancers occurring throughout the body, but this modality has been most successful in the following sites: prostate, cervix, ovaries. Because brachytherapy sources are positioned within the diseased volume, the damage to healthy tissue surrounding the disease site is minimal. This treatment modality is only applicable to well confined tumors with no distant metastases (Glasgow 1999b). External beam therapy also referred to as teletherapy involves the deposition of energy by photons, electrons or heavy particles that originate externally to the body, for example in a linear accelerator. This type of RT makes up the majority of radiation treatments; 85 to 95 % of cancer patients being treated with radiation will receive external beam radiotherapy (Glasgow 1999a).

Although classified as part of nuclear medicine, it would be remiss not to mention radioimmunotherapy in a discussion of RT. This modality is similar to brachytherapy in that radiation sources are inserted inside the body, however these sources are unsealed. By labeling compounds that bind to cancer cells with radioactive atoms or radionuclides, a radiation dose can be deposited locally to the diseased cells. This modality is presently being used in the treatment of B cell lymphomas with some success and will therefore likely become increasingly important in the treatment of cancer with the increasing occurrence of lymphomas (Williams, Liu et al. 1999).

2.3 Improvements in Radiotherapy

Advancements in technology allowing for the creation of higher energy x-rays and other particles were instrumental in improving the outcome of RT. Higher energy photons give rise to more desirable depth dose deposition properties for deep-seated tumors. The invention of a cobalt treatment unit in the early 1950s improved upon the dose deposition properties over those that were previously available based on the ortho-voltage and radium teletherapy technology (Glasgow 1999a). Further improvements were achieved with the

introduction of linear accelerator technology to the field of RT. Additional improvements in radiotherapy are described in the following sections.

2.3.1 Conformal Radiotherapy

It was the damage of healthy tissues observed by early experimenters investigating the properties of x-rays and gamma rays that led to the use of radiation to destroy unhealthy or cancerous tissue. Radiation damages tissues indiscriminately; both healthy and diseased cells can be damaged or killed by ionizing radiation. Because of this indiscriminate killing, measures must be made to protect healthy tissues while simultaneously delivering a sufficient dose to the target volume to ensure local control of the tumor. Conformal radiotherapy (CRT) is a technique capable of reducing the risk of radiation induced damage to neighboring healthy structures while ensuring a high absorbed radiation dose to the target volume.

Historically, the doses of absorbed radiation that were prescribed to treat certain cancers were limited by the dose tolerances of the healthy tissues that surrounded the target. Increasing the dose to the target volume while ensuring the protection of the organs at risk is the goal of CRT. CRT is a term used to describe a treatment delivery technique whereby the dose to healthy tissues surrounding the target volume is reduced as much as possible. Avoidance of delivering high doses to the healthy tissues allows for a higher dose deposition within the target volume which has been shown to increase the probability of local tumor control (Webb 1997; Webb 2001). The dose that is delivered in a CRT treatment is confined closely to the perceived tumor volume, with the dose dropping off drastically outside the target volume. For this reason, CRT is only applicable to treat tumors that have clearly defined boundaries. If a patient's tumor volume is not clearly defined then CRT is not an appropriate treatment option. If the tumor volume extends into the margins of the treated volume, the presence of the steep dose gradients in this region reduce the probability of local control (Olivera, Shepard et al. 1999). Due to the fine treatment margins, positioning of patients becomes increasingly important when using CRT to ensure that the treated

volume corresponds to the target volume. Misalignment of patients when using CRT with close margins reduces the probability of local control (Webb 2001).

CRT can make use of Multileaf Collimators (MLC) to shape the radiation beam. This technique delivers a dose of radiation that conforms to the geometry of the target volume, however the energy fluence of the beam is not intensity modulated. CRT also includes the increasingly common technique of intensity modulated radiation therapy (IMRT) discussed in the following section.

2.3.2 Intensity Modulated Radiation Therapy

The present day movement in radiation therapy is towards IMRT. The aim of these conformal radiation treatments is to achieve a higher, more uniform dose within the target volume(s) while minimizing the damage to the OARs. IMRT is a particularly valuable technique when target volumes are concave in shape and closely neighbored by sensitive volumes that can tolerate very little radiation damage. IMRT makes possible the creation of concave dose distributions; approximately 30 % of cases require concave dose distributions (Webb 2001). For example, a tumor that surrounds the spinal cord is a prime candidate for IMRT. These treatments include both conventional forward planned treatments as well as the more complex technique of inverse planned treatments.

In the past intensity modulation has been achieved clinically by employment of wedges, metal compensators (Webb 2001) and wax compensators. These devices alter the intensity distribution of a photon beam by placing an attenuating material between the source and the patient. The use of a wedge in a radiation field produces a dose gradient in one direction that can be used clinically in certain treatments (Boyer, Xing et al. 1999). Desired dose distributions can be attained by custom building compensators that meet the need of a treatment. Compensators continue to be used in radiotherapy to achieve desired isodose curves in cases where the beam travels different distances before reaching the target, and in the presence of internal tissue inhomogeneities (Khan 1994). In

addition, some groups are investigating improvement of dose homogeneity within breast tumors by means of IMBs created by tissue compensators (Webb 2001).

Technological advances have allowed further conformation of beams to targets with the key advancement being the MLC. In addition to the aspect of beam conformation, MLCs can be used to achieve intensity modulation within the treatment field. MLCs are being used in two modes of operation namely i) step and shoot and ii) sliding window or dynamic. Intensity modulation in step and shoot IMRT is achieved by superimposing the radiation fields of a number of beam segments which have varying shape and weight as shown in Figure 2.1. The intensity modulation created by the superposition of the beam segments is illustrated in the net energy fluence map in the lower right hand corner of Figure 2.1. The individual segments that constitute an IMB can be relatively small being limited in one direction by the width of the individual leaves of the MLC. The Varian Millenium 120 leaf MLC [Varian Medical Systems, Palo Alto, CA] employed in this centre has 40 central leaf pairs that project a width of 0.5 cm at isocentre that are positioned between 2 sets of 10 leaf pairs that project a width of 1 cm in the plane of isocentre. The creation of segments with widths as small as 0.5 cm in the plane of isocentre is therefore possible. There is no restriction on the lengths of these segments. Dosimetry of radiation fields of these small dimensions is complicated by a number of factors that will be discussed in the following section. During a step and shoot radiation delivery the MLC leaf pairs move to form a segment of the IMB as determined during the treatment planning, typically by the process of inverse treatment planning. While the leaves are in motion the radiation beam is off. When all of the leaf pairs are positioned correctly, producing a segment of the IMB, the radiation is turned on for a given number of monitor units (MU) as determined during the planning. Following the delivery of the required radiation for an individual segment, the MLC is reshaped to form the next segment. As the various segments of the IMB are delivered, the intensity modulation is achieved (Martens, Claeys et al. 2002). Once all of the segments of an individual IMB have been delivered the gantry is rotated to the next gantry angle in the plan and the delivery of the next IMB is begun. Dynamic

IMRT delivery using an MLC involves radiation delivery to the target while the leaves are in motion. During a dynamic IMRT delivery, all leaf pairs of the MLC are closed at the beginning of the treatment. While the radiation beam is on, each of the individual leaves moves according to the trajectory calculated during the planning stage. The velocity of leaf motion varies from leaf to leaf and in this way intensity modulation is obtained (Webb 2001). The use of MLC whether in the step and shoot or the dynamic mode has given rise to smaller radiation fields that were not encountered frequently previously in radiotherapy, except for in the field of stereotactic radiosurgery. Both methods of IMB creation allow for the delivery of greater and more homogeneous doses to complex shaped targets which can include convex shapes (Martens, Claeys et al. 2002). Presently in this centre, cutouts are used to protect healthy structures when electron beams are used. Lead blocks and MLCs are also used to shape photon beams and subsequently block radiation from impinging on healthy tissues. Step and shoot IMRT is also being used to treat head and neck cancer.

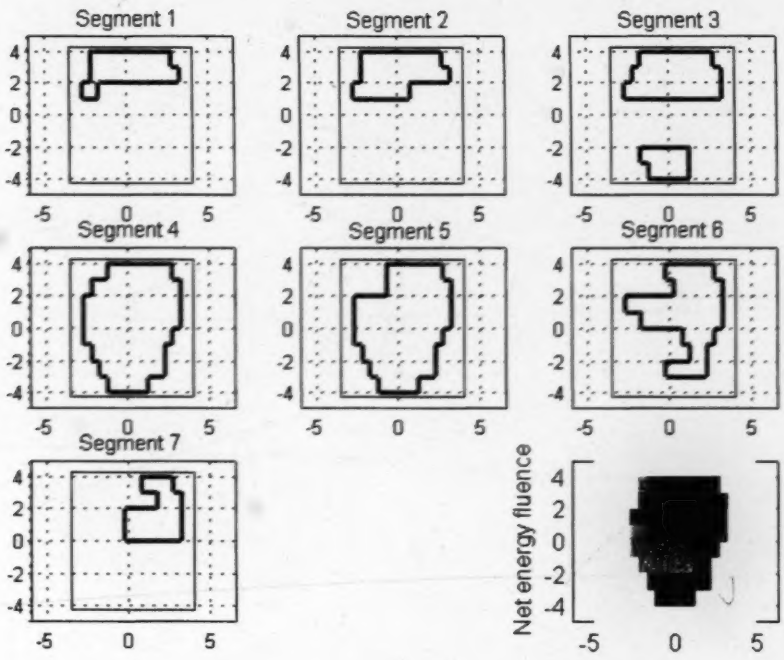

Figure 2.1 Shapes of seven step and shoot segments that comprise single intensity modulated beam and "fluence map" resulting from delivery of seven step and shoot segments - thick lines illustrate segment geometry, thin lines illustrate main collimator settings

2.3.3 Tomotherapy

Tomotherapy is a new radiotherapy technique that marries the fields of imaging and IMRT. A great deal of tomotherapy research and development has been conducted at the University of Wisconsin-Madison. The system developed in Wisconsin combines a megavoltage computed tomography (MVCT) scanner with a linear accelerator with an MLC giving IMRT capabilities (Olivera, Shepard et al. 1999).

As with IMRT treatments, tomotherapy treatments will give rise to smaller radiation fields than previously encountered in more conventional radiotherapy deliveries. The introduction of these three treatment modalities into radiotherapy departments has given rise to smaller radiation fields and the subsequent need for adequate means to make accurate dosimetric measurements in these fields.

2.4 Small Radiation Field Dosimetry

Small radiation fields are being encountered more frequently as radiotherapy embraces technologies such as IMRT and tomotherapy. There are two problems that cause difficulties in small field dosimetry: volume averaging effects (blurring of a reading over the finite size of the detector's sensitive volume) and the absence of electronic equilibrium within the fields (Martens, De Wagter et al. 2000). Volume averaging of a signal is not a significant problem if the signal is constant or changes in a linear manner, but dose "spikes" or "troughs" get averaged out within the sensitive volume of the detector (Mack, Scheib et al. 2002). Volume averaging effects are particularly pronounced in regions of high dose gradients. In these regions the response of a detector may differ substantially from the absorbed dose (Martens, De Wagter et al. 2000). A reduction in the size of the sensitive volume yields a reduction in the magnitude of volume averaging effects and therefore more accurate measurements in high gradient regions. The other primary complicating factor of small field dosimetry is electronic disequilibrium. There are two situations that can give rise to this loss of lateral electron equilibrium. When the energy of the beam becomes sufficiently high or the field size becomes sufficiently small such that the maximum range of electrons is of the same order as the field, loss of electron equilibrium can exist (Bjarngard, Tsai et al. 1990). For square field sizes with side length less than twice the maximum lateral range of electrons set in motion by primary photons, lateral electronic equilibrium may not exist at the beam central axis (CAX) (Heydarian, Hoban et al. 1996). This effect suggests that there may be a ceiling to the x-ray energies that should be used in small field radiotherapy (Bjarngard, Tsai et al. 1990), unless better dosimetry methods are established that do not require the existence of electronic equilibrium such as TLDs which do not depend on cavity theory. Ionization chambers such as the Farmer chamber are used worldwide in clinical dosimetry. In the absence of electronic equilibrium, ion chamber dose measurements do not necessarily correspond to the actual absorbed dose. In cases where electronic equilibrium

does not exist, such as in small fields being used in some of the 3D-IMRT treatments, the theories used in ion chamber dosimetry break down (Attix 1986).

Numerous small field dosimetry investigations have been conducted by various groups, particularly in the field of stereotactic radiotherapy and radiosurgery (Houdek, VanBuren et al. 1983; Arcovito, Piermattei et al. 1985; Rustgi, Rustgi et al. 1998; Zhu, Allen et al. 2000; Mack, Scheib et al. 2002). The consensus among these groups is that special attention must be paid to ensure that the detector dimensions and materials are appropriate for small field dosimetry. As IMRT is implemented clinically in more and more centers worldwide, the call for accurate small field dosimetry is becoming increasingly important. TLDs, parallel-plate chambers, micro-ionization chambers, plastic scintillators, MOSFET detectors, silicon diodes, radiographic and radiochromic film as well as diamond detectors have been investigated as possible candidates for small field dosimetry (Martens, De Wagter et al. 2000). Monte Carlo simulations have also been conducted in an effort to establish small field dosimetric effects. Although film offers the advantage of high spatial resolution, it is extremely sensitive to low-energy photons that are present in large numbers in penumbral regions of the beam (Martens, De Wagter et al. 2000). Martens *et al.* point out that the sensitive volumes of most standard dosimeters are too large when making small field measurements where high dose gradients exist. Measurements made with relatively large sensitive volumes may therefore stray from the actual dose for these small fields (Martens, De Wagter et al. 2000).

Treatment planning systems (TPS) make use of experimentally obtained data to make dose calculations. For this reason it is necessary to have extremely accurate dosimetric measurements to input into the TPS. If inaccurate data is input into the treatment planning system at the time of commissioning even the planning stage of a RT treatment will be prone to errors. There is a paucity of small field radiation data and for the reasons mentioned above there are problems associated with the collection of such data using conventional dosimeters. For this reason new dosimeters capable of making better small radiation field

measurements are required. It is for this reason that the diamond detector is being employed in this thesis.

2.5 Dosimeters in Clinical Use

There are a variety of dosimeters that are used commonly in photon beam dosimetry at the present time including ion chambers, solid state diodes, TLDs and film (Beddar, Mason et al. 1994). Depending upon the application for which the dosimetric measurements are to be made, different devices may be desirable. This section includes a description of ion chambers; ion chamber dosimetry accounts for the majority of clinical dosimetric point measurements. In addition this section provides a brief description of the properties exhibited by diodes, MOSFETs and TLDs each of which exhibits particular advantages and disadvantages.

2.5.1 Ionization Chambers

Ion chambers are presently the "gold standard" in clinical radiation dosimetry. The relationship between the delivery of dose to tissue and charge collected within the sensitive volume of a air is well understood. These devices measure ionization produced by ionizing radiation within a sensitive volume of air. The ionization must subsequently be related to absorbed dose. Presently ionization chambers play a central role in quality assurance programs in RT departments. The reference dosimetry of high energy electron and photon beams protocol described by the American Association of Physicists in Medicine's (AAPM) Task Group 51 (Almond, Biggs et al. 1999), relies on ion chamber measurements. Presently this protocol is employed across the continent stressing the importance of ion chambers as dosimeters.

For many clinical applications ion chambers perform adequately. However, the performance of ion chambers in certain applications is limited by the size of their sensitive volumes. There is a compromise between the size of the sensitive volume and the magnitude of the detector's response. As the size of the

sensitive volume is reduced, the number of ion pairs created in the chamber volume for a given radiation field is reduced, giving rise to a corresponding reduction in the signal. Although reduced volume ion chambers are made and used clinically, these devices suffer from low signal. A decrease in the size would result in a corresponding decrease in the sensitivity of the device, thereby ruling out miniaturization of ionization chambers to the level necessary to obtain similar spatial resolution of the solid state devices (Heydarian, Hoban et al. 1993).

The relatively large sensitive volume of ion chambers becomes a large problem when making dosimetric measurements in high gradient regions. In these regions volume averaging of the signal occurs and dose information is lost. In spite of the poor performance of ionization chambers in regions where the dose distribution changes greatly over a small distance, these devices are capable of making very accurate dose measurements in regions where the dose is relatively uniform (Heydarian, Hoban et al. 1993). It is desirable to make dosimeters that have sensitive volumes that are essentially tissue equivalent in a radiological sense. Energy dependence of a dosimeter is determined by the atomic number of its sensitive volume for low energy photons where the photoelectric effect is the dominant photon interaction (Attix 1986). The photoelectric cross-section is highly Z dependent and for this reason the similarity of atomic numbers of the sensitive volume and tissue is a parameter that indicates the energy dependence. For composite materials an effective atomic number can be calculated according to the following expression.

$$\overline{Z} = \sqrt[m]{a_1 \cdot Z_1^{\,m} + a_2 \cdot Z_2^{\,m} + \ldots + a_n \cdot Z_n^{\,m}}$$

where a_i is the fraction of electrons in the composite material from element Z_i and the exponent $m = 2.94$ (Khan 1994). The effective atomic number of a composite material is the atomic number of an element that would interact in the same way to photons as the composite material. The ion chamber has a relatively flat energy response relative to water since the effective atomic numbers of air and water are quite similar $\left(\left(\overline{Z}_{air}\right)_{eff} = 7.78, \left(\overline{Z}_{water}\right)_{eff} = 7.51\right)$ (Johns and Cunningham 1983). Because of this relationship, ion chambers respond equally to particles of

different energies. In addition to being energy independent for low energy photons, ion chambers are dose rate independent.

2.5.2 Solid State Dosimeters

In addition to the study of the diamond detector as a dosimeter in this thesis, there are various point dosimeters that can be categorized as solid state devices. This category encompasses diodes and Metal Oxide Silicon Field Effect Transistors (MOSFET) detectors. The physical dimensions of the sensitive volumes of solid state detectors are smaller than those of air-filled ionization chambers. This reduction in size can be attributed to two effects: the density of solids is substantially larger than that of air ($\rho_{solid} / \rho_{air} \approx 3 \times 10^3$) and the mean energy needed to create an electron-hole pair in a solid is an order of magnitude less than in air (Planskoy 1980). Although the increase in density of solids as compared with air contributes to a reduction in the size of the sensitive volume of solid state dosimeters, this property worsens the effect of charged particle recombination within the sensitive volume for solid state dosimeters (Hoban, Heydarian et al. 1994). In addition to high spatial resolution capabilities, diodes and diamond detectors also exhibit a good sensitivity, reproducibility, linearity and stability (Podgorsak and Podgorsak 1999). In the following section, diodes will be discussed. Diamond detectors will be discussed in significantly more detail in section 2.6.

2.5.2.1 Diodes

Diodes, which are semi-conducting devices capable of making dosimetric measurements, are essentially a solid-state version of ionization chambers. The sensitive volume of diodes consists of silicon or germanium doped semi-conductor material. By appropriate doping of the different semi-conductor regions making up the diode, dose rate information about the incident radiation beam can be made. When ionizing radiation is incident upon a diode's sensitive volume, a current is produced. This current is proportional to the dose rate of the

radiation impinging on the detector. This current can also be integrated with respect to time to obtain the dose. As mentioned previously, the main advantages that diodes have over ion chambers are superior spatial resolution and improved sensitivity. These advantages can be attributed to the differences in densities of the sensitive volumes and the differences in energy required to produce electron-hole pairs in the detectors' respective sensitive volumes. The mean energy required to create an ion pair in air is 33.97 eV compared to 3.68 eV required in silicon (Attix 1986). Because the energy required in silicon is about one-tenth of that in air, the sensitive volume of the diode can be substantially smaller than that of an ion chamber, reducing the volume averaging effects that plague ion chambers.

There are a number of problems associated with using diodes to make dosimetric measurements including energy, directional and temperature dependence. If a detector is not water equivalent in a radiological sense, the presence of the detector in the radiation field will disturb the electron transport through that volume. The non-water equivalence of diodes is best seen by comparing the atomic number of silicon and the effective atomic number of water, 14 and 7.51 respectively (Johns and Cunningham 1983). As a result of this difference, diodes exhibit an energy dependence; diodes respond more strongly to photons at energies below 400 keV (Beddar, Mason et al. 1994). Due to the large low-energy component of the spectrum in the penumbral regions of photon beams, differences exist between the penumbra measured with a diode and the actual penumbra (Beddar, Mason et al. 1994). This difference is of increasing importance in radiosurgical beams and small fields potentially encountered in IMRT. In spite of this weakness, diodes have been used to measure beam profiles in many centres. They have also been employed in determining dose distributions of the very small fields that are encountered in radiosurgery (Beddar, Mason et al. 1994).

Diodes also show evidence of a strong directional dependence. An absorbed dose measurement made with a diode's axis parallel to the central beam axis will vary from a measurement with the diode's axis perpendicular to the

CAX. This effect is sufficiently pronounced that Beddar *et al.* suggested that using diodes to make photon beam measurements in an orientation other than parallel to the CAX is best avoided (Beddar, Mason et al. 1994). Another study found that a Scanditronics silicon p-type diode exhibited a strong directional dependence. Measurements were made in air with acrylic build-up caps of thicknesses of d_{max} for cobalt, 6 MV and 18 MV energies. The detector response was measured as a function of the angle between the detector stem and the central axis of the beam. The results of this investigation indicated that the diode's sensitivity dropped to 82 % of its value with the gantry at 0° when rotated to an angle of 90° and drops even further to 73 % at a gantry angle of 135° for a cobalt beam (Theratron 780 Unit). Results for the higher energy beams were similar, dropping sensitivity with increasing gantry angle – 78 % and 85 % at 90 ° for 6 MV and 18 MV, respectively (Rustgi 1995).

Other disadvantages of diodes include temperature dependence (Attix 1986) and dose rate dependence (Wilkins, Li et al. 1997). Diodes are susceptible to radiation damage and therefore have a time varying response. This effect can be attributed to the formation of recombination centres due to the removal of the silicon atoms from their lattice positions by ionizing radiation. The formation of these recombination centres causes a decrease in the distance that minority carriers diffuse through the sensitive volume (Wilkins, Li et al. 1997). The loss of diode sensitivity with accumulated dose makes these devices inappropriate for absolute dosimetry measurements, but does not make then unattractive for relative measurements.

2.5.2.2 MOSFET dosimetry

Another solid state device that is being employed for dosimetric measurements is the MOSFET. Like other solid state devices, MOSFETs boast an extremely small sensitive volume. The active area of these detectors is a 0.2 x 0.2 mm^2 region of a small silicon chip measuring 1 x 1 mm^2. These small dimensions make these dosimeters useful for *in vivo* dosimetry and for IMRT verification (Chuang, Verhey et al. 2002). MOSFETs are integrating dosimeters; radiation

impinging on the active area causes a permanent change in the operating characteristics of the device. Specifically, the voltage required to allow charge to flow through the device can be related to the dose deposited in the oxide layer of the MOSFET (Chuang, Verhey et al. 2002). The operating characteristics of the MOSFET are obtained before and after radiation measurements, and the difference in characteristics is related to the integrated dose absorbed during the irradiation (Chuang, Verhey et al. 2002).

Chuang *et al.* have reported that MOSFETs are not as accurate as ion chambers, and exhibit a high directional dependence (Chuang, Verhey et al. 2002).

2.5.3 Thermoluminescent Dosimetry

The property of thermoluminescence is exhibited by a number of different materials. Impurities within these thermoluminescent crystals serve as electron traps at intermediate energy levels between the conduction and valence energy bands. Upon irradiation, these traps can become occupied by electrons. In order to free these trapped electrons, additional energy must be applied to the system. Upon addition of energy to the previously irradiated crystal, the trapped electrons return to the valence band and a photon of the energy difference between the trap level and the valence band is emitted. It is this emission of light upon heating that is the process of thermoluminescence. The measurement of these emitted photons following irradiation allows for the determination of the absorbed dose. This extra energy is delivered by a well-controlled heating cycle and the light that is emitted is measured using a photomultiplier tube. A plot of the thermoluminescence as a function of time is called a glow curve. Within a given thermoluminescent crystal there can be traps at various energy levels. As a result of this property, there are a number of peaks on a typical glow curve. Integration of the area under this curve provides a measure of the integrated absorbed dose following the proper calibration of the TLD. A disadvantage of these dosimeters is that they are sensitive to their radiation history. In order to eliminate the effects of previous irradiations, TLDs must be annealed in an appropriate manner. For

LiF, a typical TLD material, this annealing process consists of heating at 400° C and 80° C for periods of 1 hour and 24 hours, respectively. The response of TLDs to irradiation is linear up to a certain dose level, 10^3 cGy for TLD-100 which is a mixture of 7.5 % ^{6}Li and 92.5 % ^{7}Li (Khan 1994). Beyond this dose level TLD response deviates from linearity becoming supralinear. In order to generate accurate dose measurements using TLDs many conditions must be met including consistent use of the same TLD reader. For a measurement of a specific absorbed dose and beam quality, calibrations must be conducted to similar absorbed dose levels and essentially the same beam quality. When these conditions are met, measurements can be obtained to a precision level of 3 % (Khan 1994). Unfortunately, the response of TLDs is not energy independent. The degree of this energy dependence depends upon the thermoluminescent crystal that is employed with LiF exhibiting a substantially smaller energy dependence than CaF_2:Mn. These small crystals can be used *in vivo*. This is a desirable feature for verification of dose delivered to patient tissues (Khan 1994).

2.5.4 Film Dosimetry

Film is an integrating dosimeter that offers superior spatial resolution when compared with that of other dosimeters. In addition, film is an imaging detector because it offers two-dimensional spatial information of dose distributions (Barrett and Swindell 1981). Radiographic film is composed of a silver halide crystal emulsion layer whose chemical composition is altered when ionizing radiation is incident upon it. Following development of an exposed film, the darkness of the film is a measure of the amount of radiation incident upon the film (Barrett and Swindell 1981). A densitometer can be used to measure the degree of opacity, referred to as the optical density, of the developed film. This device directs light of a known intensity through a narrow aperture through the film and then measures the intensity of light that is transmitted through the film. The device then displays the optical density at that position of the film. The optical density, OD is defined as the logarithm of the ratio of the incident light intensity, I_o, to the transmitted intensity I_t.

$$OD = \log\left(\frac{I_o}{I_t}\right) \qquad (2.5.4.1)$$

The optical density on the developed film can subsequently be related to the dose by means of an H-D (Hurter and Driffield) curve.

Film dosimetry is plagued by differences in optical density caused by variations in processing, emulsion composition, as well as, artifacts that can arise from air gaps neighboring the film. In spite of these negative characteristics, film has been recognized as a useful dosimeter for electron beams. Various properties of electron beams, such as practical range, isodose curves and beam flatness, can be evaluated using film. However, film dosimetry of electron beams is not dependable because the optical density of developed film can vary for a number of reasons including development conditions and film batch (Khan 1994).

In spite of film's usefulness in relative electron beam dosimetry, its use in the dosimetry of photon beams is more restricted. The primary reason for this limitation is due to the composition of the film emulsion. Due to the high atomic number of the silver halide crystals within the film emulsion, film is highly susceptible to the absorption of low energy photons that are generated by scatter. The absorption of low energy scattered photons can lead to elevated estimates of absorbed dose particularly in regions where the spectrum consists primarily of scattered photons (in penumbral regions of beams). Film can however be useful for a number of clinical quality assurance tests including: field flatness, symmetry, light-field coincidence (Khan 1994). Other clinical uses of film include determination of isodose lines within a radiation field, penumbral sizes, radiation leakage external to the collimated field and measurement of the buildup region of a beam (Johns and Cunningham 1983).

Various groups have employed film clinically for verification of IMRT fields. The major difficulty of film is its over-response to low energy (scattered) photons which are amplified in penumbral regions. IMRT verification would, therefore subject film to conditions where its performance is poorest (Ju, Ahn et al. 2002). In spite of this, various groups have employed Kodak EDR2 film in IMRT verification with success. Zhu *et al.* state that EDR2 film is appropriate for

step and shoot IMRT verification using clinical daily fractions in most cases (Zhu, Jursinic et al. 2002).

2.5.5 Flat-panel detectors

Although film offers extremely high spatial resolution, development time and storage requirements have encouraged researchers to seek alternatives. Flat panel detectors are a very attractive alternative to film and are presently the subject of much research. The properties of two materials have been investigated for flat panel imaging: amorphous silicon and amorphous selenium. Amorphous silicon technology is more developed than amorphous selenium, although amorphous selenium exhibits properties that are more desirable than amorphous silicon. Electronic Portal Imaging Devices (EPID) based on amorphous silicon flat panel technology are becoming commonplace in cancer treatment centres. These devices are being used to confirm proper patient positioning and IMRT dose verification (Steciw, Warkentin et al. 2003; Warkentin, Steciw et al. 2003). In our centre, the use of EPIDs in compensator quality assurance is also being investigated (Menon and Sloboda 2003).

2.6 Diamond Detector Properties

Natural diamonds can be used to make dosimetric measurements. The characteristics of these dosimeters make them attractive options for specific applications especially in high dose gradient regions where volume averaging effects become more prominent for larger volume dosimeters. These devices are also being employed in small field dosimetry. Various diamond detector properties will be described in the sections that follow.

2.6.1 Basic Operation Principles

The diamond employed in this study is a natural diamond crystal that contains impurities and imperfections within the crystal structure. Nitrogen is the most prevalent impurity found in diamond crystals with concentrations ranging from 1 to 3000 atomic parts per million. The nitrogen concentration within a

diamond crystal affects their properties, specifically their response to radiation (Kanda, Akaishi et al. 1999). Electrical defects within the sensitive volume also influence the x-ray sensitivity of diamond detectors. In fact, a non-uniform distribution of these defects within the diamond sensitive volume can lead to appreciable changes in the detector response with location within the diamond. Differences in the imperfection and impurity concentration among diamond detectors gives rise to large differences in the collection efficiency (Tromson, Amosov et al. 2001).

As charged particles with sufficient energy (above the band gap) traverse the sensitive volume of a diamond detector, electron-hole pairs are created along the charged particles' trajectories (Mainwood 2000). Some of the electrons and holes created become trapped at imperfection sites and impurites within the crystal. An accumulation of these trapped charges can contribute to space charge which subsequently results in polarization of the crystal (Mainwood 2000). The charged particles that do not become trapped within the crystal drift across the sensitive volume under the influence of an applied external bias and are collected at the electrodes as shown in Figure 2.2. The collected charged particles contribute to the electrical current that is subsequently related to the dose rate of the radiation impinging on the detector.

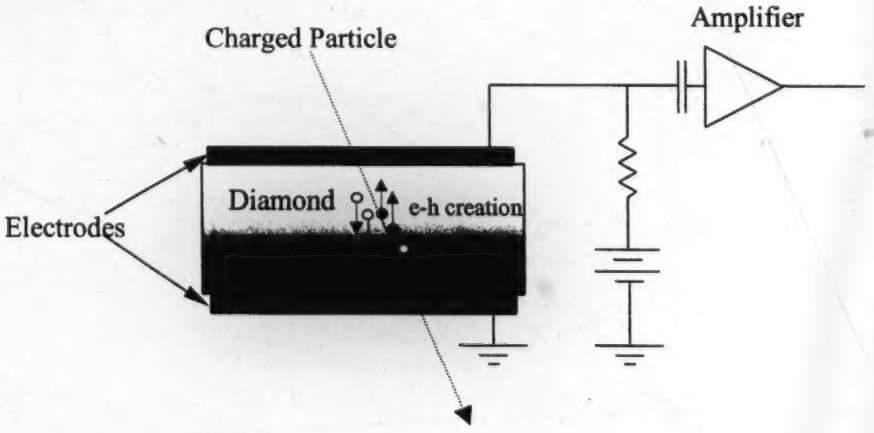

Figure 2.2 Basic diamond detector operation

2.6.2 Dose Rate Dependence

When ionizing radiation interacts with solid state materials, electron-hole pairs are created. The creation of the charge pairs acts to alter the conductivity of the solid. The conductivity is short-lived; when the source of irradiation is removed or switched off, the material returns to its normal state at a rate specific to the material (Fowler and Attix 1966).

The diamond detector literature that discusses the dose rate dependence of these dosimeters, makes reference to a chapter entitled, "Solid State Electrical Conductivity Dosimeters", written by J. F. Fowler appearing in Attix's Volume II of Radiation Dosimetry in 1966 (Fowler and Attix 1966). The relevant theory outlined in this chapter follows. In pure crystals, the theory indicates that the sensitivity of a detector varies with the square root of the rate of ion pair production (Fowler and Attix 1966). Since the rate of ion pair production and dose rate are proportional, one expects to observe a decrease in the detector sensitivity with increasing dose rate for pure crystals (Hoban, Heydarian et al. 1994). To avoid this loss of detector sensitivity with increasing dose rate, crystals with a certain amount of impurity are required to make dosimetric measurements. A sufficient quantity of crystal impurities and defects can trap a large proportion of the electrons freed by the incident radiation. In the case of a large number of electron trapping centres, the number of vacant holes will increase in a manner that is nearly independent of the dose rate which is a desirable characteristic of a dosimeter. However as the number of vacant holes increases, the probability that a free electron will encounter a vacant hole increases correspondingly, thereby decreasing the average time to recombine. This effect can give rise to a signal loss. Vacant holes will continue to be produced as long as the number of trapping sites is larger than the number of electrons freed. This effect will reduce the dose rate dependence of the recombination rate and the charge collection efficiency (Hoban, Heydarian et al. 1994). Thus, there is a fine balance between the amount of impurity; if the impurity level is too high, the reduced recombination time yields a signal reduction, and if the impurity level is too low, detector sensitivity is dose-rate dependent (Hoban, Heydarian et al. 1994). A greater concentration of

traps decreases the dose-rate dependence of a solid state detector, but simultaneously increases the amount of radiation required for the response of the detector to stabilize. Furthermore, greater concentration of traps results in decreased detector sensitivity (De Angelis, Onori et al. 2002).

Natural diamonds have been used as medical dosimeters by researchers over the last several decades. High cost and low availability of natural diamond coupled with improvements in the chemical vapour deposition (CVD) process of diamond synthesis have recently attracted much attention to the use of synthetic diamonds as dosimeters (Tapper 2000). However it appears that the properties of natural diamond are superior to those of these synthetic CVD diamonds. The variation in the operational characteristics of different diamond dosimeters is a result of differing levels of impurity within the sensitive volume. If m is used to denote the number of electrons that are trapped in the electron traps, and n represents the number of free electrons at equilibrium during an irradiation, the number of vacant holes when the system is in equilibrium is given by the sum, $m+n$. In order for the creation of an ion pair to be detected, the ions must traverse the dimensions of the crystal before recombining with other ions of the opposite sign. Therefore, an important property of insulating materials used in dosimetry is the average lifetime of the charge carriers, τ. This quantity can be related to the velocity of the charge carriers, v, and the free electron capture cross section of a hole, s, by the following expression:

$$\tau = \frac{1}{vs(m+n)}. \qquad (2.6.1)$$

Since the number of traps is very large compared with the number of free electrons $(m+n) \approx m$, the above expression is reduced to the following expression:

$$\tau \approx \frac{1}{vsm}. \qquad (2.6.2)$$

The charge carrier lifetime is subsequently related to the induced conductivity of the insulator, σ, by the following expression.

$$\sigma \approx \frac{fe\mu}{vsm}, \qquad (2.6.3)$$

where f is the rate at which ion pairs are formed per unit volume, e is the electronic charge and μ is the mobility of an electron (Fowler and Attix 1966). The conductivity can be related to the current through the insulating material, i, when a bias voltage, V, is applied across the material. If the insulator is considered to have plane parallel geometry, having a cross sectional area of A and a length of L, the current is given by the following expression:

$$i = \frac{AV\sigma}{L} = \frac{AVne\mu}{L} = \frac{AVe\mu f\tau}{L}. \qquad (2.6.4)$$

Since f is the rate at which ion pairs are formed per unit volume and AL is the volume of the insulating material, then $F = fAL$ corresponds to the total rate of ion-pair formation within the entire crystal. Therefore the above expression can be simplified to the following expression:

$$i = \frac{Ve\mu\tau F}{L^2}. \qquad (2.6.5)$$

The relationship between absorbed dose rate, $\dot{D}$, and the induced conductivity, σ, is described by the following power law:

$$\sigma \propto (\dot{D})^{\Delta}, \qquad (2.6.6)$$

where Δ is a parameter that quantifies the sublinear response of the diamond detector with dose rate and can be determined experimentally. The Δ value is specific to the individual diamond detector, and is related to the concentration and distribution of the impurity traps and defects within the sensitive volume. The conductivity, σ, is proportional to the current, i, when a bias voltage is applied as indicated in equation 2.6.4:

$$i \propto (\dot{D})^{\Delta}. \qquad (2.6.7)$$

Therefore, the slope of a log-log plot of the detector current as a function of the dose rate corresponds to Δ. A variety of groups have reported that the Δ values for their diamond detectors exhibit a sub-linear detector response with increasing dose rate (Planskoy 1980; Hoban, Heydarian et al. 1994; Laub, Kaulich et al.

1997; Bjork, Knoos et al. 2000; Fidanzio, Azario et al. 2000; De Angelis, Onori et al. 2002). In order to convert the proportional relationship of equation 2.6.7, a constant of proportionality, R, and the dark current of the detector, i_{dark}, must be introduced:

$$i = R \cdot \left(\dot{D} \right)^{\Delta} + i_{dark} . \qquad (2.6.8)$$

The magnitude of the current that is generated in the sensitive volume of diamond detectors in the absence of radiation is sufficiently small that it can be neglected when compared with the current generated when these detectors are irradiated. The negligible magnitude of the dark current is a result of the relatively large band gap (5.45 to 5.47 eV) of diamond (Mainwood 2000; Tapper 2000). The negligible dark current of these devices allows for the simplification of equation 2.6.8 to the following expression

$$i \approx R \cdot \left(\dot{D} \right)^{\Delta} \qquad (2.6.9)$$

According to Hoban *et al.*, (Hoban, Heydarian et al. 1994) diamond dosimeters exhibit a dose rate dependence for dose rate variations arising from changes in the dose per pulse, as well as, pulse frequency changes. This suggests that this dependence is sensitive to variations in average dose rate and not instantaneous dose rate. However, the authors state that this dose-rate dependence is more sensitive to changes in the average dose rate as opposed to the dose per pulse from a linear accelerator.

The dose-rate dependence of diamond detectors was studied by Planskoy (Planskoy 1980). The response of several diamond detectors to cobalt-60 and cesium-137 sources was observed at various distances from the sources thereby varying the dose rate in an inverse square fashion. These measurements were performed in air and in paraffin wax, polystyrene and water phantoms. The measured photocurrent was slightly sublinear with the dose rate. This group also investigated the dose-rate dependence for higher energy accelerator produced x-rays. The pulse repetition frequency was varied within the range 25 to 400 pulses per second. The total charge collected by the detector for a given number of

monitor units at each pulse repetition frequency was recorded. The author of this study found the Δ value of one of the diamond detectors to be dependent on the dose rate; a Δ value of 0.92 at dose rates ranging from 0.002 to about 0.5 cGy/min was found. The Δ value gradually decreased to 0.89 at the higher dose rates ranging from 1.0 to 6.0 cGy/min.

The dose rate dependence of the Burgemeister *et al.* (Burgemeister 1981) diamond was investigated using irradiations from three different sources: ^{60}Co, ^{137}Cs and 2.7 MV x-rays from an 8 MV linear accelerator. This examination revealed that this detector exhibited the same response to radiations of the energies used in the study, and that the conductivity of the diamond detector was linearly dependent on the dose rate for dose rates between 0.1 to 30 cGy/s.

The dose rate dependence of diamond detectors was investigated by Keddy *et al.* by varying the source detector distance from a ^{60}Co source. At each distance from the source the diamond detector response was measured as was the dose rate using a Farmer chamber fitted with an appropriate build up cap. The diamond detector's responses were measured using three different bias voltages: 9V, 30V and 60V. A deviation from linearity of the detector response-dose rate relationship was noted at increasing dose rates for all three bias voltages. By using a higher voltage across the detector it was observed that the linear portion of the detector response – dose rate relationship is stretched to higher dose rates (Keddy, Nam et al. 1987).

Hoban *et al.* also investigated the dose rate effects on a PTW Riga diamond detector using a 6 MV photon beam. This group measured the diamond detector output at a depth of 5 cm in solid water for a variety of SSDs. At each SSD, a Farmer 2577 ion chamber was used to measure the dose rate. Comparison was made between the performance of the diamond detector, a p-Si photon diode and an RK 83-05 thimble ionization chamber both manufactured by Scanditronix. Their findings indicate that the diamond detector under-responded at high dose rates. The authors attribute the increasing under-response with a reduction in the recombination time as the population of vacant holes increases with increasing dose rate (Hoban, Heydarian et al. 1994). The authors state that a Δ value of 0.98

gives a good fit to the data, however they also determined a dose rate dependent value of $\Delta = 0.99 - \log\left(\dot{D}_{norm}\right)$ indicating a decrease in Δ with increasing dose rate.

Fidanzio *et al.* varied the pulse repetition frequency (PRF) and the SSD for a 10 MV x-ray beam and a 21 MeV electron beam to evaluate the dose-rate dependence of a PTW type 60003 diamond detector. A PRF of 100 Hz corresponding to a monitor unit rate of 200 MU/min was used for the photon beam measurements, while monitor units rates of 200 and 400 MU/min (PRFs of 100 and 200 Hz, respectively) were used in the electron beam measurements. Measurements were made in a Nucleation automatic water phantom at a depth of d_{max} at a variety of SSDs. Simultaneous measurements were made using a PTW parallel plate ionization chamber and a Scanditronix high-doped silicon diode. The diamond detector response was compared to the dose measured with the parallel plate ion chamber in order to extract the Δ values. Analysis of the dose rate data indicated a Δ value of 0.994 ± 0.002 for both the 100 Hz photon and electron beams and 0.991 ± 0.002 for the 200 Hz electron beam. This study indicated that the Δ values were within experimental uncertainty of each other for both types of particles investigated and both PRFs for the electron beams. This group states that the diamond detector exhibits an under-response which is independent of particle type and the PRF for high dose rates (Fidanzio, Azario et al. 2000). The silicon diode to which the diamond detector was compared in this study over-responds with increasing dose and it was found that this over-response was dependent upon the energy and particle type.

In De Angelis *et al.*'s comparison of two PTW type 60003 diamond detectors, a difference in the dose rate dependence of the two detectors was observed. When the dose rate was increase from 0.9 to 4.65 Gy/min the drops in detector sensitivities were 1.9 % for one detector and 3.2 % for the other. In the range of dose rates investigated in the study by De Angelis *et al.* the Δ values for their two detectors were determined to be 0.979 and 0.987 (De Angelis, Onori et al. 2002). The authors offer the difference in impurity trap and defect

concentration as a possible explanation for this difference with the more dose-rate dependent detector having a lower concentration of impurities. As a result of these differences, the authors stress the importance of evaluating each diamond detector's performance individually to avoid unnecessary uncertainties in dose measurement.

2.6.3 High Spatial Resolution

The high spatial resolution exhibited by diamond detectors has attracted researchers to these devices (Heydarian, Hoban et al. 1993). Diamond detectors, falling into the category of solid state devices, benefit from the properties of high density of the sensitive volume relative to air and lower energy required to produce an electron-hole pair than to produce an electron-ion pair in air. The energy necessary to produce an electron-hole pair in diamond is 13 eV (Mainwood 2000) while the energy to produce an electron-ion pair in air is 33.97 eV (Johns and Cunningham 1983). This reduction in energy to produce an electron hole pair in diamond gives rise to a larger signal per charged particle interacting within the sensitive volume as compared with air. The ratio of density of diamond to air at room temperature is 2.7×10^3. These characteristics allow the use of small sensitive volumes that are much smaller than those of ionization chambers consequently yielding a greater spatial resolution. This property indicates that the diamond detector should play a role in the dose measurement especially in regions of high dose gradients (Vatnitsky and Jarvinen 1993).

Beam profile measurements of small beams (1×1 cm^2 and 2×2 cm^2) carried out by Vatnitsky *et al.* indicated that the spatial resolution of the diamond detector and the silicon diode were quite comparable, while the diamond detector performed better than the 0.1 cm^3 RK thimble ionization chamber (Vatnitsky and Jarvinen 1993). The penumbral widths measured as the distance between and 80 % and 20 % dose level were 4.5 mm for both the diamond detector and the diode detector for the 2×2 cm^2 field at a depth of 30 mm using 18 MV photons. When the penumbral measurements were made for a 14 MV photon beam with a field size of 1×1 cm^2 at a depth of 50 mm, the penumbral widths for the diamond

detector were 4.8 mm and 3.4 mm while those of the ionization chamber were 6.2 mm and 5.5 mm for in-plane and cross plane scans, respectively.

2.6.4 High Sensitivity

Vatnitsky *et al.* reported that diamond detectors produced a signal ranging between four and forty times that of the silicon diode when exposed to radiation of the same dose rate. The difference in the signal magnitude was due to the difference in the sensitive volumes of the diamond plates. The authors suggested that if the sensitive volume of the diamond was as large as the silicon diode's volume the diamond signal would be 160 times as large as the diode signal (Vatnitsky and Jarvinen 1993). Following an appropriate priming dose of radiation (described in section 2.6.6) diamond detectors are sufficiently stable and sensitive to determine dose distributions even for low-dose rate sources such as those encountered in afterloading equipment (Vatnitsky and Jarvinen 1993). Hoban *et al.* state that the PTW diamond detector measured a current approximately 50 times that measured by an RK 83-05 ionization chamber at a dose rate of 2.0 Gy/min (Hoban, Heydarian et al. 1994). Burgemeister also claims that the diamond detector had a high sensitivity and a very high ratio of signal to noise (Burgemeister 1981).

2.6.5 Near Tissue Equivalence

The energy dependence of a dosimeter is dictated by the effective atomic number, Z_{eff}, of the detector. This dependence arises because of differences between the mass energy absorption coefficient of the detector material and that of water (Attix 1986). Because of the similarity in atomic numbers of diamond and soft tissue, Z = 6 and Z = 7.42 respectively, diamond is a desirable dosimetric material due to its near soft tissue equivalence (Planskoy 1980; Burgemeister 1981; Heydarian, Hoban et al. 1993; Hoban, Heydarian et al. 1994). The sensitive volume of ion chambers consists of air which has an effective atomic number of 7.78 (Khan 1994) while the sensitive volume of silicon diodes has an atomic number of Z = 14. Therefore the sensitive volume of the diamond detector is

much more similar to tissue in a radiological sense than other solid state detectors. Fat has an effective atomic number of 6.46 and muscle has an effective atomic number of 7.64 (Khan 1994). The similarity of effective atomic number of the sensitive volume is most significant within the photon energy range where the photoelectric effect dominates (Mobit, Nahum et al. 1997).

There are other properties of diamond that emphasize the near tissue equivalence of this material. In the conversion of electron beam measurements to dose the ratio of the stopping power of the sensitive volume of the detector being employed to water must be introduced. Over a range of electron energies of 0.1 to 20 MeV the stopping power ratio of water to carbon varies from 1.12 to 1.14 (ICRU 1984) and is almost constant over an electron energy range of 1 to 20 MeV (Heydarian, Hoban et al. 1993). Over the same range of electron energies the stopping power ratio of water to air varies significantly with a maximum value of 1.135 for electron energies of 0.1 MeV to a minimum of 0.96 at 20 MeV (ICRU 1984). The small variation in stopping power ratio of carbon to water eliminates the need to convert depth ionization curves made with a diamond detector to depth dose curves by introduction of stopping power ratio (Vatnitsky and Jarvinen 1993). Ion chamber depth ionization curves must be corrected for the variation of stopping power ratio with increasing depth in phantom. In a work by Heydarian *et al.* 6 and 15 MeV electron beam depth-dose curves were measured using a PTW Riga diamond detector, Scanditronix p type silicon diode and a Scanditronix RK 8305 ion chamber. The measured ion chamber depth ionization curve was converted to a depth dose curve by correcting for the variation of the stopping power ratio. In a comparison between the uncorrected diamond and diode depth ionization curves with the corrected ion chamber depth dose curve, good agreement is obtained between the diamond and the ion chamber curves for both the 6 and 15 MeV electron beams (Heydarian, Hoban et al. 1993). This result illustrates a distinct advantage that diamond detectors offer over ionization chambers in electron beam dosimetry; depth–ionization curves measured with a diamond detector can be used directly as depth-dose curves with the correction for variation in stopping power ratio.

2.6.6 Radiation Priming and Radiation Stability

Prior to making dosimetric measurements with a diamond detector, a pre-irradiation dose is required to ensure that the detector response has reached a stable level. The manufacturer of the PTW type 60003 diamond detector used in our center recommends that a pre-irradiation dose less than 10 Gy is required for satisfactory diamond detector operation. The specifications accompanying this detector indicate that it can be used for photons ranging in energy from 80 keV to 20 MV. The manufacturers do not indicate that the required pre-irradiation dose for detector stability is energy dependent. The need for a delivery of this pre-irradiation dose is related to the filling of traps within the sensitive volume of the detector. Electrons trapped in the impurity trapping sights within the sensitive volume form a space charge that generates an electric field that opposes the applied bias voltage. This polarization effect necessitates a pre-irradiation dose to ensure an equilibrium level of trap filling (Hoban, Heydarian et al. 1994). After leaving the detector in unbiased conditions for a period of time, many of the traps empty. Thus when the detector returns to biased conditions, the polarization effect generated by the space charge created by trapped electrons is at a minimum and the net electric field within the sensitive volume is at a maximum. With this higher electric field within the sensitive volume, the sensitivity of the detector is at a maximum. The sensitivity of the detector continues to decrease with radiation until an equilibrium level of filled traps is reached. The response of the diamond detector stabilizes when the filled traps have reached an equilibrium (Hoban, Heydarian et al. 1994), and then the detector can be used for measurements.

The effect of priming the diamond detectors with radiation prior to dosimetric measurements has been observed by various groups. Planskoy investigated the effect of ^{60}Co irradiation on an in-house diamond detector with an applied bias voltage of 150 V. Initially, use of the detector revealed an immediate rise in the detector current when the beam was switched on followed by a current drop of 10 – 15 % of the initial current over a five minute irradiation period. This drop in signal was not observed after the detector had been irradiated to a

cumulative dose of 15 – 20 Gy. The delivery of this initial current stabilizing dose is referred to as priming, and was found not to be necessary unless the detector was left unused for a period of several months (Planskoy 1980). Conflicting results were observed by Laub *et al.* (Laub, Kaulich et al. 1999), who report the necessity of pre-irradiation of the PTW detector following a period of only a few minutes of non-use.

A priming dose of 2–3 Gy was required to stabilize the response of the three diamond detectors used in a study conducted by Vatnitsky *et al.* The detectors were considered to be adequately pre-irradiated when the detectors' responses varied less than 0.5 % hr^{-1} when exposed to a constant dose rate (Vatnitsky and Jarvinen 1993).

De Angelis *et al.* reported the disagreement between various experimental groups exists regarding the proper use of the diamond detector following the priming irradiation dose. De Angelis *et al.* investigated the effect of radiation priming on two PTW type 60003 diamond detectors with a 6 MV photon irradiation. The diamond detectors' relative sensitivities (detector response to ionization chamber dose ratio) were seen to be initially greater than unity at low accumulated doses. One of the detectors had a relative sensitivity greater than 1.3 after only 1 Gy had been delivered, but stabilized after an administration of 15 Gy. Another detector had a relative sensitivity near 1.1 after delivery of 1 Gy, but stabilized to 1.0 after delivery of 5.0 Gy (De Angelis, Onori et al. 2002). De Angelis *et al.* suggested that if detectors are used on a daily basis, a dose of 3 Gy is adequate to ensure a stable response. However, if the detectors are left unused for larger periods of time, larger priming doses are required to ensure stability. This group also verified that the pre-irradiation dose required is independent of the type of particles used in the irradiation (De Angelis, Onori et al. 2002).

Hoban *et al.* found that the PTW Riga diamond detector's response dropped initially. They offered two explanations for this sensitivity drop: a decrease in the electric field because of increasing polarization of the detector as the electron traps are filled, and a decrease in the time between recombination as the population of vacant holes increases. These effects necessitate a priming dose

of irradiation to arrive at an equilibrium population of filled traps prior to making any measurements (Hoban, Heydarian et al. 1994).

Diamond detector use in the field of radiotherapy is primarily limited to megavoltage energies. However, some work has been conducted at diagnostic energies. Hugtenburg et al. pre-irradiated a PTW-Freiburg type 60003 diamond detector to a dose of approximately 8 Gy at 100 kVp and 45 kVp to ensure detector stability. With this pre-irradiation dose, the diamond response varied by less than 1 % between measurements (Hugtenburg, Johnston et al. 2001).

To verify that short-term losses in counting ability did not occur, Planskoy irradiated four detectors to 500 Gy with 8 MV photons. After each 100 Gy portion of the dose was delivered, the calibration was checked using ^{60}Co. No damage to the detectors was observed during this irradiation indicating that the responses of the detectors were stable (Planskoy 1980).

Following delivery of an adequate priming dose of irradiation (15 Gy was found to be sufficient to stabilize the detector's response after three weeks of non-use) the detector's response was measured over a three-week period to verify the constancy of the output. The measurements made during this period were found to have a standard deviation of 0.67 % (Hoban, Heydarian et al. 1994). De Angelis *et al.* noted that PTW type 60003 detectors have a short-range stability of 0.1 % over periods of minutes. For various measurement series on a detector that remained biased throughout a day, however, the maximum variation of the detector response was 1%. In an effort to evaluate the long term stability of the detector De Angelis *et al.* used a 6 MV photon beam to measure the detector sensitivity on a weekly basis with the detector left unbiased between measurements. The long-term stability was determined to be quite good - a maximum variation of 1 % of the detector sensitivity (De Angelis, Onori et al. 2002).

2.6.7 Temperature Dependence

Some groups have investigated the temperature dependence of diamond detectors. Planskoy (Planskoy 1980) irradiated several diamond detectors with a ^{60}Co beam delivering 1.5 Gy/min at various temperatures, ranging from 4°C to 40°C. One of the detectors in this study exhibited a 1 % per °C increase in current with increasing temperature while two of the detectors showed a larger temperature dependence. The photocurrent of these two detectors stepped up by about 3 % between 11 – 16°C and 23 – 27°C.

Burgemeister *et al.* (Burgemeister 1981) exposed their in-house probe to cobalt-60 γ-rays and x-rays produced by a 8 MV linear accelerator at temperatures ranging from 0°C to 70°C at a fixed dose rate of 2.0 cGy/s. The results indicate that a temperature correction of -0.5% per °C is required to correct for the temperature dependence of their probe in the vicinity of room temperature.

De Angelis *et al.* varied the temperature in 5°C increments from 15°C to 40°C of two PTW type 60003 diamond detectors. The detector response to a delivery of 1 Gy was observed at each of the temperatures. One of the detector responses was observed to vary by 0.03% / °C, while the other varied by 0.1 % / °C (De Angelis, Onori et al. 2002). The reduced temperature dependence observed by De Angelis *et al.* over that observed by Planskoy and Burgemeister *et al.* is an indication of the improvements made in diamond detector technology over the past two decades.

2.6.8 Resistance to Radiation Damage

Diamond detectors are appealing for dosimetric measurements in part due to their resistance to radiation induced damage (Planskoy 1980). Diamond detectors are more resistant to radiation damage than silicon diodes (Vatnitsky and Jarvinen 1993; Fidanzio, Azario et al. 2000). In addition to being virtually immune to radiation damage, diamonds can be subjected to electric fields with magnitudes as high as 10^6 V cm^{-1} without being damaged (Planskoy 1980; Mainwood 2000) and are not fragile (Burgemeister 1981).

2.6.9 Directional Independence

Some detectors demonstrate a directional response to radiation. This property becomes increasingly important when making beam profile measurements. As the beam profile is measured, the angle of incidence of the particles changes considerably from 90° on the central axis to larger angles as the measurement moves further off axis (Heydarian, Hoban et al. 1993). Heydarian *et al.* investigated the directional dependence of a PTW Riga diamond detector and a Scanditronix p-Si electron diode. These detectors were positioned at the centre of polyethylene cylinders with their sensitive volumes at a depth of d_{max} for electron beams of energies 6 MeV and 15 MeV. Electrometer readings were recorded for gantry angles between 0° and 130° for both detectors. Their results indicate that both dosimeters exhibit directionally dependent behaviour. However, the directional dependence of the diode is larger (Heydarian, Hoban et al. 1993). For the 6 MeV electron beam the responses of both dosimeters are essentially the same for gantry angles between 0° and 60°. At gantry angles larger than 60°, the responses of both dosimeters drop to a minimum at a gantry angle of 105°. At this gantry angle the diamond and diode responses are 92 % and 88 % respectively of the signal at a gantry angle of 0°. Similar results were obtained for the 15 MeV electron beam (Heydarian, Hoban et al. 1993).

De Angelis *et al.* considered the response of two PTW type 60003 diamond detectors to photons and electrons oriented both parallel and perpendicular to the gantry axis. Their findings indicate a response variation of 1.5% for all energies investigated. With the detectors inserted into a spherical PMMA phantom both parallel and perpendicular to the gantry axis, the gantry angle was varied from 0° to 320° and irradiated with 6 MV photons. The detectors' responses over this angular range showed a maximum variation of just under 2 % when the detectors were oriented perpendicular to the gantry axis and the gantry at an angle of approximately 220°. The diamond detectors oriented parallel to the gantry axis exhibit less of a directional dependence with the relative response changing by a maximum of 0.5 % at a gantry angle of 270° (De Angelis, Onori et al. 2002).

2.6.10 Diamond use in clinical dosimetry

The diamond detector properties discussed in Sections 2.6.3 to 2.6.9 make these dosimeters particularly appealing for dosimetric measurements. It is the properties of high spatial resolution, high sensitivity and energy independence that make these devices particularly applicable in dose measurements. The primary shortcoming of these dosimeters is the dose rate dependence discussed in section 2.6.2. However, upon characterization the dose-rate dependence of an individual diamond detector, the diamond response can be corrected for this effect to obtain accurate dosimetric information.

Chapter 2 References

Almond, P. R., P. J. Biggs, B. M. Coursey, W. F. Hanson, M. S. Huq, R. Nath and D. W. Rogers (1999). "AAPM's TG-51 protocol for clinical reference dosimetry of high-energy photon and electron beams." Med Phys **26**(9): 1847-70.

Arcovito, G., A. Piermattei, G. D'Abramo and F. A. Bassi (1985). "Dose measurements and calculations of small radiation fields for 9-MV x rays." Med Phys **12**(6): 779-84.

Attix, F. H. (1986). Introduction to Radiological Physics and Radiation Dosimetry. New York, John Wiley & Sons.

Barrett, H. H. and W. Swindell (1981). Radiological Imaging - The Theory of Image Formation, Detection and Processing. New York, Academic Press, Inc.

Beddar, A. S., D. J. Mason and P. F. O'Brien (1994). "Absorbed dose perturbation caused by diodes for small field photon dosimetry." Med Phys **21**(7): 1075-9.

Bjarngard, B. E., J. S. Tsai and R. K. Rice (1990). "Doses on the central axes of narrow 6-MV x-ray beams." Med Phys **17**(5): 794-9.

Bjork, P., T. Knoos and P. Nilsson (2000). "Comparative dosimetry of diode and diamond detectors in electron beams for intraoperative radiation therapy." Med Phys **27**(11): 2580-8.

Boyer, A. L., L. Xing and P. Xia (1999). Chapter 12 Beam Shaping and Intensity Modulation. The Modern Technology of Radiation Oncology. J. Van Dyk. Madison, Wisconsin, Medical Physics Publishing: 437-479.

Brady, L. W., S. Kramer, S. H. Levitt, R. G. Parker and W. E. Powers (2001). "Radiation Oncology: Contributions of the United States in the Last Years of the 20th Century." Radiology **219**: 1-5.

Burgemeister, E. A. (1981). "Dosimetry with a diamond operating as a resistor." Phys Med Biol **26**(2): 269-75.

Chuang, C. F., L. J. Verhey and P. Xia (2002). "Investigation of the use of MOSFET for clinical IMRT dosimetric verification." Med Phys **29**(6): 1109-15.

De Angelis, C., S. Onori, M. Pacilio, G. A. Cirrone, G. Cuttone, L. Raffaele, M. Bucciolini and S. Mazzocchi (2002). "An investigation of the operating characteristics of two PTW diamond detectors in photon and electron beams." Med Phys **29**(2): 248-54.

Fidanzio, A., L. Azario, R. Miceli, A. Russo and A. Piermattei (2000). "PTW-diamond detector: dose rate and particle type dependence." Med Phys **27**(11): 2589-93.

Fowler, J. F. and F. H. Attix (1966). Solid state electrical conductivity doseimeters. Radiation Dosimetry. F. H. Attix and W. C. Roesch. New York, Academic. **1**.

Glasgow, G. P. (1999a). Chapter 10 Cobalt-60 Teletherapy. The Modern Technology of Radiation Oncology. J. Van Dyk. Madison, Wisconsin, Medical Physics Publishing: 313-348.

Glasgow, G. P. (1999b). Chapter 18 Brachytherapy. The Modern Technology of Radiation Oncology. J. Van Dyk. Madison, Wisconsin, Medical Physics Publishing: 695-752.

Hall, E. J. (2000). Radiobiology for the radiologist. Philidelphia, Lippincott Williams & Wilkins.

Heydarian, M., P. W. Hoban, W. A. Beckham, I. M. Borchardt and A. H. Beddoe (1993). "Evaluation of a PTW diamond detector for electron beam measurements." Phys Med Biol **38**: 1035-1042.

Heydarian, M., P. W. Hoban and A. H. Beddoe (1996). "A comparison of dosimetry techniques in stereotactic radiosurgery." Phys Med Biol **41**(1): 93-110.

Hoban, P. W., M. Heydarian, W. A. Beckham and A. H. Beddoe (1994). "Dose rate dependence of a PTW diamond detector in the dosimetry of a 6 MV photon beam." Phys Med Biol **39**: 1219-1229.

Houdek, P. V., J. M. VanBuren and J. V. Fayos (1983). "Dosimetry of small radiation fields for 10-MV x rays." Med Phys **10**(3): 333-6.

Hugtenburg, R. P., K. Johnston, G. J. Chalmers and A. H. Beddoe (2001). "Application of dimaond detectors fo the dosimetry of 45 and 100 kVp therapy beams: comparison with a parallel-plate ionization chamber and Monte Carlo." Phys Med Biol **46**: 2489-2501.

ICRU (1984). "Radiation dosimetry: electron beams with energies between 1 and 50 MeV." ICRU Report 35.

Johns, H. E. and J. R. Cunningham (1983). The Physics of Radiology. Springfield, Charles C. Thomas.

Ju, S. G., Y. C. Ahn, S. J. Huh and I. J. Yeo (2002). "Film dosimetry for intensity modulated radiation therapy: dosimetric evaluation." Med Phys **29**(3): 351-5.

Kanda, H., M. Akaishi and S. Yamaoka (1999). "Synthesis of diamond with the highest nitrogen concentration." Diamond and Related Materials **8**: 1441-1443.

Keddy, R. J., T. L. Nam and R. C. Burns (1987). "Synthetic diamonds as ionisation chamber radiation detectors in biological environments." Phys Med Biol **32**(6): 751-9.

Khan, F. M. (1994). The Physics of Radiation Therapy. Baltimore, Williams and Wilkins.

Laub, W. U., T. W. Kaulich and F. Nusslin (1997). "Energy and dose rate dependence of a diamond detector in the dosimetry of 4-25 MV photon beams." Med Phys **24**(4): 535-6.

Laub, W. U., T. W. Kaulich and F. Nusslin (1999). "A diamond detector in the dosimetry of high-energy electron and photon beams." Phys Med Biol **44**(9): 2183-92.

Mack, A., S. G. Scheib, J. Major, S. Gianolini, G. Pazmandi, H. Feist, H. Czempiel and H. J. Kreiner (2002). "Precision dosimetry for narrow photon beams used in radiosurgery-determination of Gamma Knife output factors." Med Phys **29**(9): 2080-9.

Mainwood, A. (2000). "Recent developments of diamond detectors for particles and UV radiation." Semicond Sci Technol **15**: R55-R63.

Martens, C., I. Claeys, C. De Wagter and W. De Neve (2002). "The value of radiographic film for the characterization of intensity-modulated beams." Phys Med Biol **47**(13): 2221-34.

Martens, C., C. De Wagter and W. De Neve (2000). "The value of the PinPoint ion chamber for characterization of small field segments used in intensity-modulated radiotherapy." Phys Med Biol **45**(9): 2519-30.

Menon, G. V. and R. S. Sloboda (2003). "Compensator quality control with an amorphous silicon EPID." Med Phys **30**(7): 1816-24.

Mobit, P. N., A. E. Nahum and P. Mayles (1997). "A Monte Carlo study of the quality dependence of diamond thermoluminescent dosimeters in radiotherapy beams." Phys Med Biol **42**: 1913-1927.

NCIC (2003). National Cancer Institute of Canada. http://www.ncic.cancer.ca, accessed September 2003.

Olivera, G. H., D. M. Shepard, K. Ruchala, J. S. Aldridge, J. Kapatoes, E. E. Fitchard, P. J. Reckwerdt, G. Fang, J. Balog, J. Zachman and T. R. Mackie (1999). Chapter 15 Tomotherapy. The Modern Technology of Radiation Oncology. J. Van Dyk. Madison, Wisconsin, Medical Physics Publishing: 521-587.

Planskoy, B. (1980). "Evaluation of diamond radiation dosemeters." Phys Med Biol **25**(3): 519-32.

Podgorsak, E. B. and M. B. Podgorsak (1999). Chapter 16 Stereotactic Irradiation. The Modern Technology of Radiation Oncology. J. Van Dyk. Madison, Wisconsin, Medical Physics Publishing: 589-639.

Radiology Centennial, I. (1993). Magical Roentgen Rays in Early Therapy http://www.xray.hmc.psu.edu/rci/ss9/ss9_2.html, accessed October 2003.

Rustgi, S. N. (1995). "Evaluation of the dosimetric characteristics of a diamond detector for photon beam measurements." Med Phys **22**(5): 567-70.

Rustgi, S. N., A. K. Rustgi, S. B. Jiang and K. M. Ayyangar (1998). "Dose perturbation caused by high-density inhomogeneities in small beams in stereotactic radiosurgery." Phys Med Biol **43**: 3509-3518.

StatsCanada (1999). Mortality - Summary List of Causes, 1997. http://www.statcan.ca/english/IPS/Data/84F0209XPB.htm#abstract, accessed September 2003.

Steciw, S., B. Warkentin, S. Rathee and B. G. Fallone (2003). "A Monte Carlo based method for accurate IMRT verification using the aS500 EPID." Med Phys **30**: 1331.

Tapper, R. J. (2000). "Diamond detectors in particle physics." Rep Prog Phys **63**: 1273-1316.

Tromson, D., V. N. Amosov, A. Brambilla, C. Mer, F. Foulon, R. Barrett and P. Bergonzo (2001). "Influence of defect inhomogeneities in high quality natural diamond detectors." Diamond and Related Materials **10**: 469-473.

Van Dyk, J. (1999). Chapter 1 Radiation Oncology Overview. The Modern Technology of Radiation Oncology. J. Van Dyk. Madison, Wisconsin, Medical Physics Publishing: 1-17.

Vatnitsky, S. and H. Jarvinen (1993). "Application of a natural diamond detector for the measurement of relative dose distributions in radiotherapy." Phys Med Biol **38**(1): 173-84.

Webb, S. (1997). The Physics of Conformal Radiotherapy. Bristol, Institute of Physics Publishing Ltd.

Webb, S. (2001). Intensity-Modulated Radiation Therapy. Bristol, Institute of Physics Publishing Ltd.

Wilkins, D., X. A. Li, J. Cygler and L. Gerig (1997). "The effect of dose rate dependence of p-type silicon detectors on linac relative dosimetry." Med Phys **24**(6): 879-81.

Williams, L. E., A. Liu and G. Wong (1999). Chapter 25 Monoclonal Antibody and Other Internal Emitter Therapies. The Modern Technology of Radiation Oncology. J. Van Dyk. Madison, Wisconsin, Medical Physics Publishing: 1021-1042.

Zhu, X. R., J. J. Allen, J. Shi and W. E. Simon (2000). "Total scatter factors and tissue maximum ratios for small radiosurgery fields: comparison of diode detectors, a parallel-plate ion chamber, and radiographic film." Med Phys **27**(3): 472-7.

Zhu, X. R., P. A. Jursinic, D. F. Grimm, F. Lopez, J. J. Rownd and M. T. Gillin (2002). "Evaluation of Kodak EDR2 film for dose verification of intensity modulated radiation therapy delivered by a static multileaf collimator." Med Phys **29**(8): 1687-92.

Chapter 3 Materials and Methods

3.1 Materials

The materials employed throughout this thesis are described in the following sections. The materials are subdivided into categories of dosimeters, electrometers and phantoms. Descriptions of the software, as well as the TPS used in this study are also included in this chapter.

3.1.1 Dosimeters

In addition to the diamond detector, various other dosimeters were employed throughout this investigation. Table 3.1 summarizes the size of the sensitive volumes of the point dosimeters employed in this study.

Table 3.1 Comparison of sensitive volumes of point dosimeters employed in this thesis and ratio of sensitive volumes to that of diamond detector

Probe	Sensitive Volume (cm^3)	Ratio of Sensitive Volume to Diamond Detector
Exradin A12	0.651	383
Wellhöfer Dosimetrie IC-10	0.14	82
PTW PinPoint (31006)	0.015	9
PTW Diamond Detector (60003)	0.0017	1
Scanditronix p-type Si diode (FP 1207)	0.0012	0.7

3.1.1.1 Diamond Detector

The diamond detector used in this investigation is a PTW-Freiburg type 60003 (S/N 9-032) [PTW, Freiburg, Germany]. The sensitive volume of this probe is a naturally grown diamond. The certificate accompanying this probe indicates that the diamond has a sensitive area of 6.8 mm^2, a thickness of 0.25 mm giving a sensitive volume of 1.7 mm^3. The density of diamond is 3.51 g/cm^3 (Mobit and Sandison 1999). The sensitive volume of the probe is situated 1 mm

below the detector surface as shown in Figure 3.1. The position of the sensitive volume was verified by imaging the detector using a 40 kVp and 10 mAs radiographic technique on a Phillips Super 80 CP simulator [Philips Medical Systems, Markham, ON]. The 100.0 ± 0.1 V bias voltage required for optimal diamond detector operation was provided by a model EB100 CNMC power supply [CNMC Company, Inc., Nashville, Tennessee]. The contact electrodes of this dosimeter consist of a thin (ca. 50 nm) gold layer (Pychlau 2003).

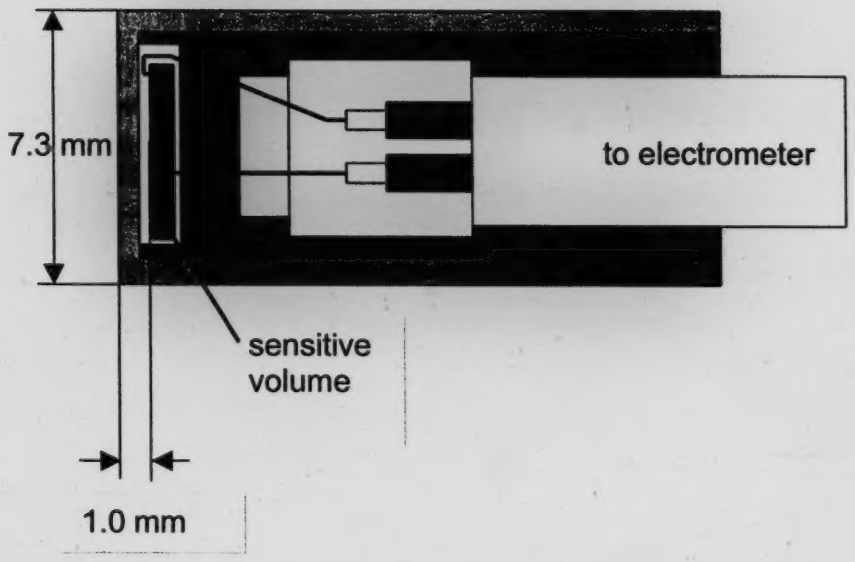

Figure 3.1 Schematic diagram of diamond detector showing location of sensitive volume as shown in PTW-Freiburg type 60003 diamond detector instruction manual

Several of the operating characteristics of the diamond detector used in this study as supplied by the manufacturer are summarized in Table 3.2.

Table 3.2 Physical and operating characteristics of PTW-Freiberg type 60003 diamond detector as given by the manufacturer

Characteristic	Nominal Value
Operating bias	100.0 ± 0.1 V
Dark current	$< 1 \times 10^{-12}$ A
Pre-irradiation dose	< 10 Gy
Sensitive volume	1.7 mm^3
Sensitive area	6.8 mm^2
Thickness of sensitive volume	0.25 mm

3.1.1.2 Exradin A12 ionization chamber

The primary substandard ion chamber used by this centre is an Exradin A12 ion chamber (S/N 396) [Standard Imaging, Middleton, WI]. This dosimeter is a Farmer type chamber and has a collecting volume of 0.651 cm^3. The diameters of the sensitive region and the collector are 6.1 mm and 1.0 mm, respectively. The wall, collector and guard material of this device are made with Shonka air-equivalent plastic C552 with a wall thickness of 0.5 mm.

3.1.1.3 PinPoint ionization chamber

The pinpoint ion chamber used in this study is a PTW-Freiburg type 31006 (S/N 0290) [PTW, Freiburg, Germany]. This detector has a 0.015 cm^3 air filled sensitive volume. The wall material is 0.56 mm of PMMA and 0.15 mm of graphite and the detector is waterproof. The sensitive volume is cylindrical in shape with a length of 5 mm and a radius of 1 mm. The central electrode of this detector is made of steel. The over-response to low-energy Compton photons due to the presence of the steel electrode has been documented for 6 and 18 MV photon beams by Marten *et al.* (Martens, De Wagter et al. 2000). The instruction manual for this device suggests a pre-irradiation dose of 2 Gy prior to dosimetric use.

3.1.1.4 IC10 Ionization Chamber

Wellhöfer Dosimetrie IC10 ionization chambers [Scanditronix Wellhofer, Bartell, TN] with 0.14 cm^3 sensitive volumes (S/N 1382, 1715) were used in this thesis. These dosimeters are commonly used in our center to obtain beam profiles and percent depth dose curves. These chambers have a diameter of 0.6 cm and an active length of 0.33 cm.

3.1.1.5 Scanditronix Photon Diode

A Scanditronix p-type silicon diode (S/N 1207) was used during this investigation. This solid state dosimeter has a very small sensitive volume of 1.2 mm^3 giving it potential to make measurements with excellent spatial resolution and does not require the application of a bias voltage and is therefore appropriate as a reference probe for use with the diamond detector.

3.1.1.6 PR-06C Farmer type chamber

Various PR-06C Farmer type chambers [CNMC Company, Nashville, TN] were employed in this thesis. These chambers are used for routine output measurements of the linear accelerators and cobalt-60 unit in this center. The practice in our center is to cross-calibrate a unit specific PR-06C chamber to absolute TG-51 dosimetry measurements to provide a quick verification of machine output.

3.1.1.7 aS500 EPID

The Varian Portalvision aS500 EPID [Varian Medical Systems, Palo Alto, CA] consists of an amorphous silicon solid state flat-panel imaging device. These devices are typically used clinically to ensure proper patient positioning prior to radiotherapy treatments, although the spectrum of uses of EPIDs is starting to be recognized. Potential uses include dose verification for dynamic IMRT treatments (Greer and Popescu 2003) and reconstruction of dose delivered to patients during treatment (Partridge, Ebert et al. 2002). Dosimetry measurements using a PortalVision aS500 EPID [Varian Medical Systems, Palo Alto, CA] were

made with a technique involving convolution-type calculations described by B. Warkentin *et al.* and S. Steciw *et al.*(Steciw, Warkentin et al. 2003; Warkentin, Steciw et al.) from our laboratory.

3.1.2 Electrometers

Several different electrometers were used in the dosimetric measurements comprising this thesis. A description of each electrometer employed in this study follows.

3.1.2.1 Capintec Model 192 Electrometer

A Capintec Model 192 electrometer [CNMC Company, Nashville, TN] was used in conjunction with both the diamond detector as well as the various ion chambers used in this study. This electrometer was used when the quantity of interest was the total or integrated response of the detector and not the instantaneous response. With this electrometer, collection potentials of –300, -150, 0, 150 and 300 V are available.

3.1.2.2 Keithley 6514 System Electrometer

A Keithley 6514 System Electrometer [Keithley Instruments, Inc., Cleveland, OH] interfaced with a personal computer was used to measure the diamond detector current as a function of time for a variety of measurements in this study. The rate of acquisition of this electrometer can be varied between 1 and 10 power line cycles thus integration times of 16.67 ms to 166.67 ms are available. A variety of acquisition sequences with various integration times were used depending upon the measurement. A bias cannot be applied by this electrometer. Thus the dosimeter with which this electrometer is used must be externally biased as is the case with the PTW-Freiburg type 60003 diamond detector.

3.1.2.3 Wellhöfer Beam Data Acquisition System

A Wellhöfer dosimetry beam data acquisition system [Scanditronix-Wellhofer, Schwarzenbruck, Germany] was used for a variety of applications

throughout this study. This system consists of a positioning apparatus within a water tank and electrometer allowing for beam profile and percent depth dose scanning. With this system the collection potential can be varied from –400 to 400 V in increments of 4 V. This feature makes this system attractive, as a zero electrometer bias must be used with the diamond detector while for ion chambers a collection voltage of 300 V is typical. This system allows the use of a reference probe to eliminate the effects of fluctuations in the output of the linear accelerator in the resulting signal.

3.1.3 Phantoms

3.1.3.1 Solid Water Phantom

For many of the measurements made in this investigation slabs of a radiologically water equivalent composite plastic called solid water [Gammex, Middleton, WI] were used. These slabs measure 25 x 25 cm^2 and have thicknesses varying from 1 mm to 2 cm. Solid water probe holders were available for the diamond detector, the A12 ion chamber and the PinPoint chamber allowing for the introduction of these probes into the phantom without the creation of air gaps.

3.1.3.2 Wellhöfer water phantom

The water phantom that makes up an integral part of this system allows scanning measurements within a volume of 48 x 48 x 41 cm^3. The design of this tank allows for in-plane, cross plane and percent depth dose measurements to be made easily and quickly. This phantom accommodates a variety of different probes making it a versatile tool for comparison of the performance of different detectors (IBA, Uppsala, Sweden).

3.1.4 Computer Software

3.1.4.1 HELAX Treatment Planning System

The treatment planning system that is presently employed at our center for all external beam treatment plans is the HELAX-TMS 6 [Nucletron, Veenendaal, The Netherlands]. The dose calculation algorithm employed by HELAX is based on the energy fluence impinging on the material within the calculation space and can be employed to calculate doses for many types of clinically encountered fields. The system used at the Cross Cancer Institute has step and shoot IMRT capabilities which were used throughout this thesis.

3.1.4.2 WP700 Software

The WP700 software that accompanies the Wellhöfer scanning water phantom provides an easy to use interface between the user and electronics. The user can select a number of parameters to obtain the desired measurement. This software allows for the specification of the type of measurement to be made easily. This workspace also allows for the easy manipulation of measured data and the extraction of important measurement parameters such as beam flatness and symmetry.

3.1.4.3 Matlab

Matlab version 6.5 [Mathworks, Natick, MA] was employed for data analysis throughout this thesis. The features of this software tool include graphics to view and aid in the analysis of data and many built in algorithms to ease data analysis.

3.2 Measurements

With the exception of all pre-irradiation measurements, the diamond detector was pre-irradiated to a total dose greater than 500 cGy ensuring the stability of the diamond's response.

3.2.1 Basic Diamond Detector Operation

For all diamond detector measurements conducted in this study the set up shown in Figure 3.2 was used. The manufacturers of this dosimeter recommend a collection voltage of 100.0 ± 0.1 V. This bias voltage was generated using the CNMC model EB100 power supply. Prior to all measurements this voltage was verified using a Marcraft SE-1038 digital multi-meter [Marcraft International Corp., Kennewick, WA]. The performance of this multi-meter was checked with another multi-meter at the outset of this investigation. When the bias voltage was determined to be outside the acceptable range as quoted by the manufacturer, the voltage was tuned to 100.0 ± 0.1 V using a potentiometer in the power supply. The bias voltage was applied for the duration of all measurement series and was verified at intervals during the measurements to ensure constant measurement conditions. The Capintec model 192 and Wellhöfer dosimetry electrometer systems employed in this centre allow for the selection of the collection voltage to be used. Since the diamond detector is externally biased, it is important to ensure that the bias voltage of the electrometer being used in conjunction with the diamond probe is switched off.

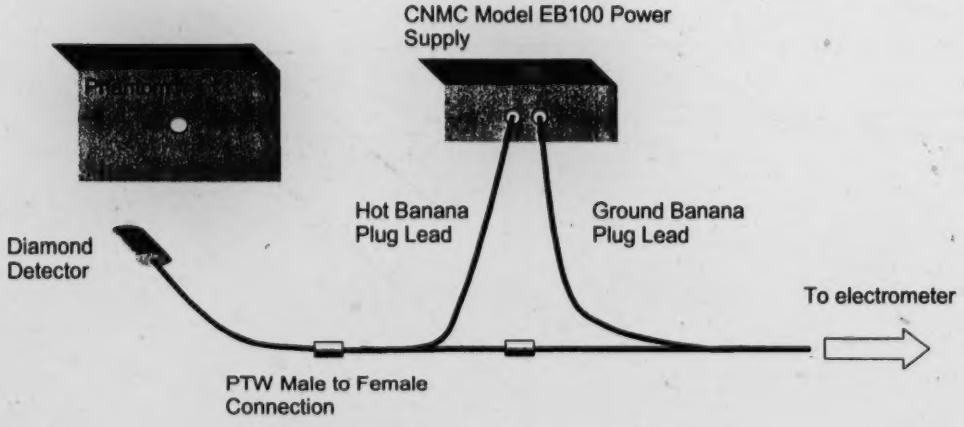

Figure 3.2 PTW-Freiburg type 60003 diamond detector experimental set-up showing connections to power supply and electrometer

3.2.2 Pre-Irradiation Measurements

The manufacturers of the PTW-Freiburg type 60003 diamond detector recommend that a pre-irradiation dose of under 10 Gy is required to ensure the stability of the detector's response. In order to firmly establish the required pre-irradiation dose to ensure detector stability, the diamond detector's signal was measured as a function of time using a Keithley 6514 System Electrometer interfaced with a computer. The probe was positioned at a depth of 5 cm in a 10 x 10 cm^2 field in the TG-51 water tank with an SSD of 75 cm from the cobalt-60 source in a Theratron 780E unit [MDS Nordion, Ottawa, Canada]. Prior to making these measurements the detector had not been used for the previous five days. The detector's signal was integrated every 1.67 s. In order to establish when the signal stopped decreasing, a short MatLab code was written. This code determines the time after beam on at which the slope of the diamond current as a function of time within error, is zero. The slope and error of the slope of this curve were determined using linear regression. At the time that this experiment was conducted, the cobalt unit delivered a dose of 182 cGy/min to a small mass of tissue at isocentre in a 10 x 10 cm^2 field. The appropriate tissue air ratio (TAR) was used to convert the time after beam on to a stable response to a dose.

This procedure was repeated for 6 and 15 MV photons generated by a Varian 2300 EX linac [Varian Medical Systems, Inc., Palo Alto, CA]. For these higher energy photons, the diamond probe was positioned at isocentre at a depth of 5 cm in a 10 x 10 cm^2 field in solid water. A pulse repetition frequency of 400 MU/min was used during the delivery of the radiation. Again the diamond current was monitored using the Keithley electrometer. In the case of these higher energy photons, the appropriate tissue maximum ratio (TMR) was used to convert the time after beam on to a stable response to a dose.

3.2.3 Detector Stability Measurements

The effect of increasing the time between successive diamond detector measurements on the detector's response was investigated. The diamond was positioned at a depth of 5 cm at isocentre of the Theratron 780E cobalt 60 unit in

a 10 x 10 cm^2 field in water. The diamond current was observed during one-minute irradiations to the cobalt beam. The Keithley 6514 electrometer was employed in this study to measure the diamond current as a function of time. The time interval between successive irradiations of the diamond was increased from 1 minute up to an hour. The detector remained biased throughout the entire measurement series.

Following the variation of the time interval between successive irradiations, the effect of switching off the diamond detector's 100.0 ± 0.1 V bias was also observed. The detector remained unbiased for 5 minutes, before turning the bias back on. Following this period in unbiased conditions the diamond detector's response to the cobalt beam was observed for 0.2 min. The accumulated dose required to obtain a stable detector response was determined following the removal of the bias.

3.2.4 Beam Profile Measurements

To compare the spatial resolution of the diamond detector with the ion chamber used in this center for beam profile measurements, beam profiles were measured with both detectors using the Wellhöfer beam data acquisition system. The diamond detector was positioned with its axis oriented both parallel and perpendicular to the beam CAX. Figure 3.3 illustrates the probe orientations employed in the beam profile measurements for the diamond detector. Beam profiles were measured with the IC10 chamber oriented perpendicular to the beam CAX only. With the diamond oriented with its axis parallel to the beam central axis (see Figure 3.3 A) the beam "sees" an area of 6.8 mm^2. When the diamond is oriented as in Figure 3.3 B the beam "sees" an area of only approximately 0.65 mm^2 suggesting that higher spatial resolution is expected when the diamond is oriented in this manner.

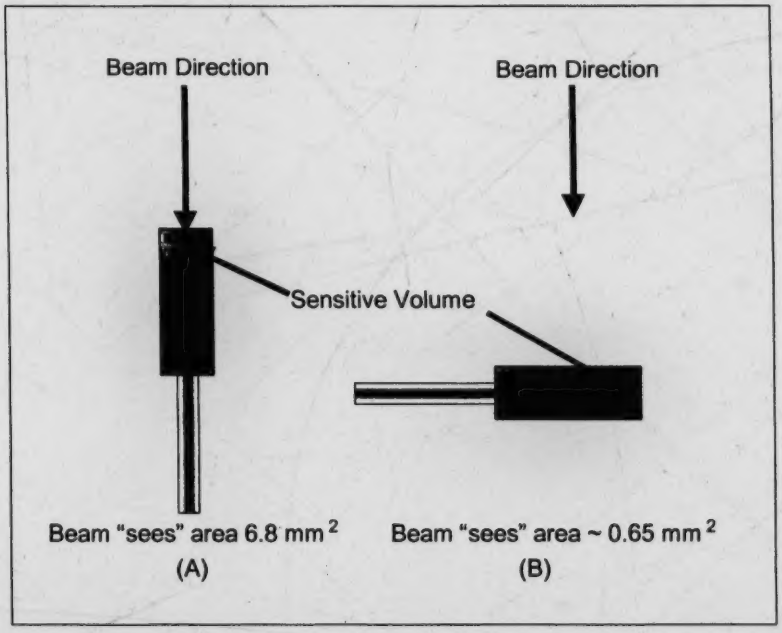

Figure 3.3 Diamond detector probe orientations used in making beam profile measurements (A) probe stem oriented parallel to beam CAX and (B) probe stem oriented perpendicular to beam CAX

In-plane and cross-plane beam profiles were measured at depths of d_{max}, 5 cm and 10 cm for a 6 MV photon beam generated by a Varian 600C linac. Efforts were made at each probe depth to centre the sensitive volume on the depth of interest. The SSD for all beam profile measurements was 90 cm and profiles were measured for 3 x 3 cm^2, 5 x 5 cm^2 and 10 x 10 cm^2 fields. In order to eliminate the effects of the fluctuations of output of the linear accelerator reference probes were used. The Scanditronix p-type silicon diode (S/N 1207) was used as the reference probe during the acquisition of the diamond beam profiles. In this center the practice during beam profile scanning is to use one IC10 ion chamber the reference probe and another IC10 probe to measure the profile.

3.2.5 Dose Rate Dependence Measurements

In order to quantify the dose rate dependence of the PTW-Freiburg type 60003 (S/N 9-032) diamond detector used in this center, the effect of varying the

dose rate on the response of the diamond detector and the ion chamber was observed. Four different methods of dose rate variation were employed in this study. In all of these approaches a measurement series was completed using the diamond detector and then repeated using an ion chamber. The ion chamber measurements have been assumed to be a true measure of dose.

The introduction of an air filled chamber in phantom perturbs the electron fluence. To compensate for this perturbation AAPM's TG-51 document states that the effective point of measurement of a cylindrical or spherical ion chamber is $0.6 \cdot r_{cav}$ shifted upstream toward the photon source where r_{cav} is the radius of the cavity of the ion chamber (Almond, Biggs et al. 1999). The diameter of the collecting volume of the A12 chamber used in this study is 6.1 mm. This corresponds to an upstream shift of 1.83 mm. Corrections for the effective point of measurement for measurements made in solid water are limited by the thickness of solid water slabs that are available. A slab of solid water with a thickness of 2 mm was placed between the surface and source while maintaining the same SSD as used for diamond detector measurements for all ion chamber measurements. The error in the shift depth is 0.17 mm and is considered to be negligible.

The effects of recombination of charged particles within the sensitive volume of the ion chamber used in this study were also considered. Incomplete charge particle collection within the sensitive volume of an ion chamber is an effect that must be corrected for in order to avoid underestimates in dose measurements. AAPM's TG-51 document includes correction factors for this effect for both pulsed and continuous radiation beams, denoted by P_{ion}. For a continuous beam, such as cobalt, the correction factor to account for incomplete ion collection is given by the following equation:

$$P_{ion}(V_H) = \frac{1 - \left(\frac{V_H}{V_L}\right)^2}{\frac{M^H_{raw}}{M^L_{raw}} - \left(\frac{V_H}{V_L}\right)^2}, \qquad [3.1a]$$

where M_{raw}^{H} and M_{raw}^{L} are the raw electrometer readings made at the high, V_H, and low, V_L, collection potentials respectively. The protocol requires that V_H be at least twice the magnitude of V_L. If the beam is pulsed in nature the correction factor is given by equation 3.1b.

$$P_{ion}(V_H) = \frac{1 - \frac{V_H}{V_L}}{\frac{M_{raw}^{H}}{M_{raw}^{L}} - \frac{V_H}{V_L}}. \qquad [3.1b]$$

The polarity of the charges that are collected within the sensitive volume affects the electrometer reading. Polarity effects change with the quality of the beam in which measurements are made. Positioning of the coaxial cable can also have an effect on the electrometer reading. For this reason, it is necessary to correct for polarity effects each time that one conducts reference dosimetry. In order to correct for this effect, measurements must be made at collection voltages of opposite polarity to a given number of monitor units. Expression 3.2 is the correction factor for this effect.

$$P_{pol} = \left| \frac{M_{raw}^{+} - M_{raw}^{-}}{2M_{raw}} \right|, \qquad [3.2]$$

where M_{raw}^{+} is the reading when positive charges generated in the sensitive volume are being collected, M_{raw}^{-} is the electrometer reading when negative charges are measured and M_{raw} is the reading for the reference dosimetry measurements (Almond, Biggs et al. 1999). The clinical practice in this centre is to use $M_{raw}^{+} = M_{raw}$.

For all ion chamber measurements conducted in the Δ value determination portion of this study, a Capintec model 192 electrometer [CNMC Company,

Nashville, TN] was employed. Ion chamber measurements were made at collection potentials of 300 V, 150 V and –300 V allowing for correction of recombination and polarity effects as outlined in AAPM's TG-51 document (Almond, Biggs et al. 1999). Also this electrometer when operated with a 0 V collection potential can be used with the diamond detector.

A Varian 2300 EX linear accelerator [Varian Medical Systems, Palo Alto, CA] was used to generate 6 and 15 MV photon beams throughout this study. The cobalt beam used in this study was created by a Theratron 780E ^{60}Co unit [MDS Nordion, Ottawa, Canada]

3.2.5.1 Source Surface Distance (SSD) Variation

To quantify the dose rate dependence of the diamond detector, this device was placed at a depth of 5 cm in solid water. For all SSD variation measurements, a field size of 5 x 5 cm^2 at isocentre was used. This field size was sufficiently large that at large SSDs the field did not extend beyond the dimensions of the phantom. 6 MV and 15 MV photon beams were generated by a Varian 2300 EX linear accelerator. A Theratron 780E ^{60}Co unit was also used in this investigation. To allow for the largest range of SSDs within the treatment vault, the gantry of the linac was rotated to an angle of 90° and the treatment couch was rotated to 270°. This set up allowed for an SSD range of 64 cm to 301 cm for the linear accelerator measurements and 60 cm to 300 cm within the cobalt unit vault. This set up gave rise to dose rate variations of 11 cGy/min to 226 cGy/min on the cobalt unit, 58 cGy/min to 1047 cGy/min for the 6 MV photon beam, and 61 cGy/min to 1165 cGy/min for the 15 MV photon beam. The diamond detector response at various SSDs within the aforementioned range to a given number of monitor units was observed. These measurements were repeated using an Exradin A12 ion chamber. A Capintec Model 192 electrometer was used in both measurement series. For the ion chamber measurements, the effective point of measurement of the ion chamber was accounted for by placement of an additional 2 mm of solid water between the surface and the source. Ion chamber response to a given number of monitor units was observed for the following

collection potentials: -300 V, -150 V and 300V. Ion chamber measurements were subsequently corrected for recombination and polarity effects as described by TG-51 (Almond, Biggs et al. 1999).

3.2.5.2 Percent Depth Dose (PDD) Measurements

The dose rate dependence of the diamond detector was observed, by varying the depth of the probe in phantom at a fixed SSD. The diamond was centered in a 10 x 10 cm^2 field. SSDs of 80 cm and 100 cm for cobalt and accelerator generated photons, respectively, were used. The diamond detector response to a given number of monitor units was observed at depths ranging from d_{max} to 25 cm for linac beams and from 1 cm to 22 cm for the cobalt beam. The d_{max} values for these 6 and 15 MV beams were 1.4 cm and 2.8 cm, respectively. The diamond detector was replaced with the Exradin A12 ion chamber and the measurement series were repeated. A Capintec Model 192 electrometer was used for both measurement series. Dose rate ranges of 175 to 600 cGy/min and 241 to 600 cGy/min were attained for the 6 MV and 15 MV photon beams. A dose rate range of 42 to 174 cGy/min was obtained by varying the depth within phantom from 1 cm to 22 cm for the ^{60}Co beam.

3.2.5.3 Tissue Maximum Ratio (TMR) Measurements

TMR measurements were made using the diamond detector and the Exradin A12 ion chamber. The diamond detector was positioned in solid water at isocentre of a Varian 2300 EX linear accelerator at a depth of 2 cm. At least 20 cm of backscatter material was used in this TMR measurement series. After a 500 cGy priming radiation dose, 50 MU were delivered to the probe and the response was monitored using a Capintec Model 192 electrometer. Additional slabs of solid water were positioned between the probe and the source thereby decreasing the dose rate. For 6 MV photons, the depth of the probe in phantom varied from 2 cm to 38 cm, while the range of depths for 15 MV photons was 3 cm to 38 cm. The difference in the ranges of the depths in phantom is to take into account the difference in the buildup regions for these photon energies.

The diamond probe was then replaced with the A12 ion chamber. For all TMR measurements, an additional 2 mm slab of solid water was placed between the probe and the source in order to account for the effective point of measurement of the ion chamber. For all depths within phantom, 50 MU were delivered and the response was monitored using the Capintec model 192 electrometer. Measurements were made at the following collection potentials of -300 V, 150 V and 300 V at each depth in order to correct for recombination and polarity effects within the sensitive volume.

This measurement series was repeated on the Theratron 780E cobalt-60 unit. Again the diamond was positioned at isocentre (80 cm for this unit) in a 10 x 10 cm^2 field at a depth of 1 cm in solid water. The response of the diamond detector to a 0.25 minute exposure to the cobalt source was observed using the Capintec model 192 electrometer. Additional layers of solid water were placed on top of the probe, thereby further attenuating the beam. The depth of solid water ranged from 1 cm to 28 cm for the cobalt beam. Following this measurement series, the diamond was replaced with the Exradin A12 probe.

3.2.5.4 Pulse Repetition Frequency Variation

The diamond detector was centered in a 10 x 10 cm^2 field at isocentre of a Varian 2300 EX linac at a depth of 10 cm in solid water. The frequency of pulse repetition of the linear accelerator was adjusted from 100 MU/min to 600 MU/min in increments of 100 MU/min giving rise to a six fold increase in the time averaged dose rate for both 6MV and 15 MV photon irradiations. The diamond detector response was monitored as a function of time at each dose rate using a Keithley 6514 system electrometer. The acquisition sequence used in the collection of this data had an integration time of 1.67 s, the maximum allowable integration time allowed by the electrometer. The length of the integration time was sufficiently long as to average out the effects of the pulsed nature of the linac output. The diamond detector was replaced with the Exradin A12 ion chamber and the measurement series was repeated using a Capintec model 192

electrometer again taking into account the effective point of measurement of the ion chamber.

3.2.6 R Value Determination

Equation 2.6.8 relates the current generated within the sensitive volume of the diamond detector to the dose rate of the incident radiation:

$$i = R \cdot \left(\dot{D}\right)^{\Delta} + i_{dark} \,. \qquad (2.6.8)$$

To relate these two quantities, both Δ and R must be determined. Following the evaluation of the Δ value, R was determined. The diamond detector was positioned at isocentre at a depth of 10 cm in solid water in a 10 x 10 cm^2 field. The diamond current was observed as a function of time with the Keithley 6514 system electrometer during irradiations of 400 MU at a pulse repetition frequency of 400 MU/min. The diamond current was observed for both 6 and 15 MV irradiations generated by a Varian 2300 EX linear accelerator. In order to relate the measured diamond currents to the dose rate, the output of the linac was measured with a PR-06C Farmer type chamber in a 10 x 10 cm^2 field in a dose constancy jig that ensures the uniform probe positioning. The output of this chamber in this "jig" has been cross calibrated to a probe and electrometer system that were calibrated at a national standards lab. This cross calibration is checked at least annually and has been shown to be stable within ± 0.3 %. The dose rate was determined from the dose measurements by dividing the absorbed dose by the time required to deliver that dose. These measurements were repeated for a ^{60}Co beam quality. The *R* value was subsequently determined from this information for all beam qualities investigated.

3.2.7 Arc Treatment

To demonstrate the response of the diamond detector in a situation where the dose rate is varying, without any high dose gradients, an arc treatment was performed. Dose gradients at the point of measurement were unwanted in this case to ensure that any differences observed in detector responses between the diamond and ion chamber arose from the dose rate dependence and not due to volume averaging effects within the sensitive volume. The diamond was positioned at isocentre at a depth of 7 cm in solid water as shown in Figure 3.4.

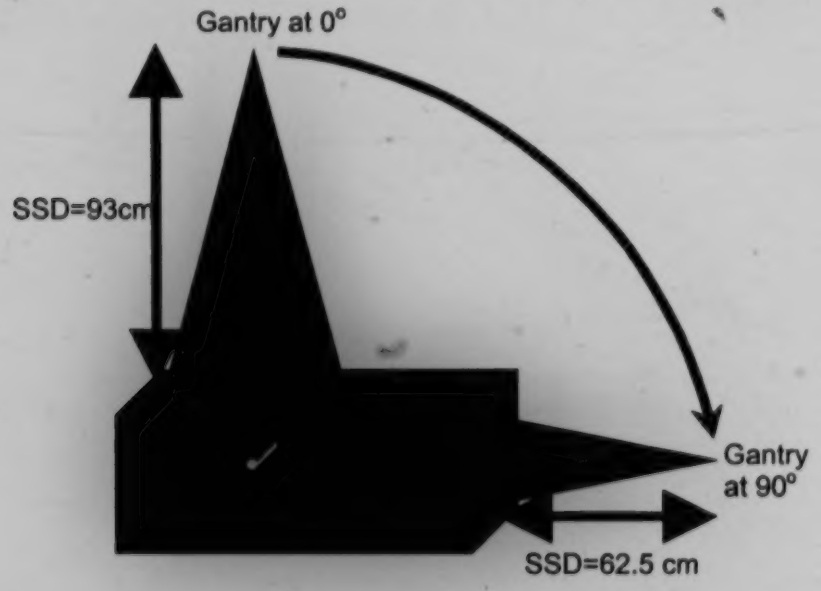

Figure 3.4 Experimental set-up employed for delivery of photon beam arc treatment

The diamond current was monitored as a function of time using the Keithley 6514 electrometer interfaced with a personal computer. 300 MU were delivered at a PRF of 300MU/min in an arc treatment fashion starting at a gantry angle of 0° and ending at 90° for a 6 MV photon beam. These measurements were repeated for a 15 MV photon beam. The diamond currents for the 6 and 15 MV arc treatments were converted to dose rates according to equation 2.6.9. The absorbed dose measured with the diamond was obtained by integrating the corrected dose rate with respect to time. The diamond detector was replaced with a PR-06C ion

chamber in the solid water and used in conjunction with a Capintec model 192 electrometer. The integrated dose during the delivery of the arc treatment was measured with this ion chamber. In order to verify that changes in recombination and polarity effects were negligible for the ion chamber throughout the arc treatment, electrometer readings at +300V, +150V and –300V collection voltages were made at fixed gantry angles between 0° and 90°.

3.2.8 Effect of dose rate dependence

Following the establishment of the Δ value, its effect on the conversion from current to dose rate was investigated for 6 and 15 MV photons. A further investigation was conducted using the arc delivery data described in the preceding section to observe the effect of the dose rate dependence on the conversion from diamond current to dose rate for this diamond detector. According to the theory of conductivity induced in insulating materials outlined by Fowler, Δ values ranging from 0.5 to 1 are typical although Δ values greater than unity have been observed (Fowler and Attix 1966). For Δ values ranging from 0.5 to 1, the diamond current was converted to a theoretical dose rate according to equation 2.6.9. An R value corresponding to each Δ value was calculated according to the following expression.

$$R = \frac{i}{\left(\dot{D}\right)^{\Delta}} \qquad (3.2.8)$$

The theoretical dose rates for each of the Δ values investigated were then integrated as a function of time to obtain the theoretical total absorbed dose delivered during the delivery. The dose measured with the ion chamber was compared with the integrated doses for each of the Δ values investigated in this study.

3.2.9 Wellhöfer dose measurements

Beam data acquisition systems such as the systems made by Wellhöfer-Scanditronix are intended to make dose measurements as a function of position.

For a fixed scanning speed, the position is proportional to time. The method described in this section can be employed to make point dose measurements as a function of time with the Wellhöfer beam data acquisition system for a variety of point dosimeters. First the probe is positioned in phantom at the point of measurement and connected to the field input of the Wellhöfer electrometer system. The motion control cable that is connected to the water phantom during normal Wellhöfer use is connected instead to a one-dimensional in air scanner which can be situated outside of the radiation vault. The in air scanning arm used in this investigation was created in house for the purpose of conducting in air one dimensional scans. This device makes use of the same probe mounts that are used by the water phantom. The measurement must be prepared to correspond with the motion capability of the in air scanning arm and the scanning speed must be selected such that the signal is collected for a sufficiently long time to ensure that no information is lost. The probe then remains fixed in phantom while the probe mount on the in air scanning arm moves. In this manner, dose rate data are collected as a function of position of the probe mount of the in air scanner. The position of the probe mount can subsequently be related to time according to the selected scanning speed. The Wellhöfer scanner used in this center has nominal scanning speeds ranging from 0.87 mm/s to 15.0 mm/s. When measured, these actual scanning speeds differ from the nominal speeds by 2 %. Thus in order to make accurate dosimetric measurements, the actual scanning speed must be measured. This measured speed is then used to convert the signal as a function of position to the signal as a function of time at a fixed point in phantom.

The signal of the Wellhöfer beam data acquisition system is a percent dose. In order to relate the percent dose to a more meaningful quantity, cross calibration must be conducted. To conduct the dosimetry measurements, a PR-06C Farmer type chamber was used as described in section 3.2.6.

3.2.10 Small Field Dosimetry Measurements

Dosimetric measurements were made at a depth of 10 cm in solid water for field sizes ranging from 1x1 cm^2 to 10x10 cm^2 using the diamond detector, the

A12 Exradin and PinPoint ion chambers using the technique described in the preceding section. Following the measurement of the relative dose as a function of time for each IMRT field, the diamond was replaced with the Exradin A12 ion chamber. In order to convert the relative dose measurements measured by the Wellhöfer to dose measurements, cross calibrations were performed. The diamond relative dose measured with the Wellhöfer in a 10 x 10 cm^2 field at a depth of 10 cm was compared with the diamond current under the same conditions measured with the Keithley 6514 electrometer, to relate diamond current with relative dose for the given sensitivity and gain settings of the Wellhöfer. This cross calibration was subsequently used to relate the relative doses of the fields of varying size measured with the Wellhöfer to the diamond current. The diamond currents were then converted to dose rate independent dose rates using expression 2.6.9. Time integration of the dose rates as a function of time allowed for the determination of the absorbed dose delivered to isocentre at each field size. The percent dose rates measured using the ion chamber were converted to dose rates by means of dose measurements conducted with the on unit jig and PR-06C ion chamber. The ion chamber dose rates were subsequently integrated to obtain the dose at each field size. Comparison of the diamond and ion chamber doses was then made.

A Varian aS500 EPID was used to image the beam at each field size. Using a novel technique developed in this department (Steciw, Warkentin et al. 2003; Warkentin, Steciw et al. 2003) the EPID images were converted to dose distributions and the central dose pixel values were extracted from the EPID dose distribution and subsequently compared with the measurements made with the point dosimeters. The manufacturers of the aS500 EPID give a specification of ± 3 mm for motion in the latitudinal and longitudinal directions. As a result, the central pixels do not necessarily correspond to the central pixels of the EPID. In order to ensure the location of the beam CAX a lead sphere (bb) measuring 1.65 mm in diameter was placed on the surface of the 2 cm solid water block that sits on the EPID surface as described in Steciw *et al.* at the centre of the crosshairs. An EPID image was acquired with the bb at the beam CAX and the pixels

corresponding to the CAX were noted. The small size of the lead bb decreases the margin of error in the location of the pixels of interest in the EPID images.

3.2.11 Simple Intensity Modulated Beams

Four simple IMBs were created that did not contain any high dose gradients at isocentre. The IMBs were created for a Varian Millenium 120 leaf MLC. Although this MLC allows for field sizes as small as 0.5 x 0.5 cm^2 in the plane of isocentre, the smallest segment size used in the creation of these IMBs was 1 x 1 cm^2. These IMBs included 5 equally weighted segments. In order to ensure that high dose gradients were not present at isocentre, edges of all segments were situated at least 0.5 cm from isocentre. The detector response of the diamond, the A12 and the PinPoint ion chamber during the delivery of these IMBs was observed using the Wellhöfer dosimetry system as described in section 3.3.10. As with the small field dosimetry measurements described in the preceding section, the detectors' responses were in the form of a percent dose rate thereby necessitating conversion from percent dose rates to meaningful quantities. The diamond percent dose rate was converted to a current by measuring the diamond current at a depth of 10 cm in a 10 x 10 cm^2 field with the Keithley 6514 electrometer. The diamond current was then converted to a dose rate according to equation 2.6.9 and integrated to obtain the total dose during the delivery of the IMB. Dosimetry measurements were made using the on unit jig and this dose was used to convert the ion chamber percent dose rate to a dose rate. The ion chamber measurements were then integrated to obtain the integrated dose during the modulated beam delivery.

EPID measurements were made using a Varian aS500 system. As for the small field dosimetry, the algorithm developed in this department was employed to convert the EPID pixel values to a dose distribution (Steciw, Warkentin et al. 2003; Warkentin, Steciw et al. 2003). The dose at isocentre was then extracted from the EPID dose distribution and compared with the diamond and ion chamber doses.

3.2.12 Dosimetry of clinical prostate intensity modulated beam

A clinical prostate step and shoot IMB was chosen. The modulation factor of an IMB is the ratio of the number of monitor units in an IMB to the monitor units for a 10 x 10 cm^2 flat field required to deliver an equivalent dose at isocentre. This factor reflects the magnitude of the dose gradient at isocentre of that beam. The closer the modulation factor is to unity the lower the dose gradient at isocentre. A beam with a modulation factor of 0.565 was selected indicating a relatively large dose gradient at isocentre. Dose measurements of this intensity modulated treatment delivery were conducted at a depth of 10 cm in solid water in the same manner as described previously for the small field dosimetry measurements. Dose calculations of this IMRT treatment delivered to a water phantom were made using HELAX-TMS. In addition to the IMBs, a 5 x 5 cm^2 field centered about a different isocentre was included in the calculation space to allow for the conversion of calculated percent doses to doses. This 5 x 5 cm^2 field was positioned sufficiently far from the IMBs so that the scatter contribution from this field to the IMB was negligible (MacKenzie, Lachaine et al. 2002). Comparison of the calculated point dose at isocentre was made to the dose measured with the various dosimeters.

3.2.13 Dosimetry of clinical prostate intensity modulated beam at improved detector positions

Due to the difficulties associated with conducting point dose measurements in high dose gradients, it is desirable to make point dose measurements at positions free of these gradients. In order to establish improved detector positions, MatLab code was written that excluded probe positions based on their vicinity to segment edges. For a given segment, possible probe positions were deemed acceptable if the beam edges were distanced 1 cm from the probe position thereby avoiding measurement positions within the penumbral regions of that segment. A probe position map for the IMB was then generated based on the acceptable probe positions for each of the segments comprising the beam according to the respective segment weightings in the IMB. Although probe

positions outside the treatment field are considered to be improved detector positions according to segment edge exclusion criteria, these positions were not considered to be improved positions. The dose within the treatment field is the quantity of interest, not the dose delivered via scatter to the surrounding volume. Comparison between measured and calculated doses was made.

Following the evaluation of the improved detector positions, the diamond detector, PinPoint chamber and the A12 ion chamber responses were measured at a depth of 10 cm in solid water at these improved detector positions. The centre of the sensitive volumes of these detectors was positioned according to the positions determined by the software. The detector signal as a function of time was monitored as a function of time using the Wellhöfer dosimetry system. For each IMB, multiple measurements were done using each detector to allow for averaging of the results for both.

3.2.14 Intensity Modulated Beam Calculations

A rectangular water phantom was created on HELAX measuring 51.2 x 51.2 x 30 cm^3. The dose calculations of the prostate treatment IMBs that were delivered to both the solid water and Wellhöfer water phantom were made using the planning software package HELAX. The doses calculated using HELAX were compared with the doses measured using the various detectors. HELAX calculates the dose distribution in terms of a percentage of the dose to the normalization point (which is isocentre in an isocentric technique). In this study the dose to a point is of interest. In order to evaluate doses within the dose plan a well characterized field must be inserted into the treatment plan. The technique used at our centre is to include a 5 x 5 cm^2 field with the normalization point at its centre in the treatment plan with the IMBs (MacKenzie, Lachaine et al. 2002). The output of HELAX TMS is a dose distribution relative to the dose at the normalization point. Following evaluation of the dose calculations one can relate the dose to the 5 x 5 cm^2 field to the dose delivered by the IMBs. Using this technique, the point doses to isocentre, as well as, to the improved detector positions were calculated.

Chapter 3 References

Almond, P. R., P. J. Biggs, B. M. Coursey, W. F. Hanson, M. S. Huq, R. Nath and D. W. Rogers (1999). "AAPM's TG-51 protocol for clinical reference dosimetry of high-energy photon and electron beams." Med Phys **26**(9): 1847-70.

Fowler, J. F. and F. H. Attix (1966). Solid state electrical conductivity doseimeters. Radiation Dosimetry. F. H. Attix and W. C. Roesch. New York, Academic. **1**.

Greer, P. B. and C. C. Popescu (2003). "Dosimetric properties of an amorphous silicon electronic portal imaging device for verification of dynamic intensity modulated radiation therapy." Med Phys **30**(7): 1618-27.

MacKenzie, M. A., M. Lachaine, B. Murray, B. G. Fallone, D. Robinson and G. C. Field (2002). "Dosimetric verification of inverse planned step and shoot multileaf collimator fields from a commercial treatment planning system." J Appl Clin Med Phys **3**(2): 97-109.

Martens, C., C. De Wagter and W. De Neve (2000). "The value of the PinPoint ion chamber for characterization of small field segments used in intensity-modulated radiotherapy." Phys Med Biol **45**(9): 2519-30.

Mobit, P. N. and G. A. Sandison (1999). "A Monte Carlo comparison of the response of the PTW-diamond and the TL-diamond detectors in megavoltage photon beams." Med Phys **26**(11): 2503-7.

Partridge, M., M. Ebert and B. M. Hesse (2002). "IMRT verification by three-dimensional dose reconstruction from portal beam measurements." Med Phys **29**(8): 1847-58.

Pychlau, C. (2003). E. Barnett. Freiburg, Germany.

Steciw, S., B. Warkentin, S. Rathee and B. G. Fallone (2003). "A Monte Carlo based method for accurate IMRT verification using the aS500 EPID." Med Phys **30**: 1331.

Warkentin, B., S. Steciw, S. Rathee and B. G. Fallone "Dosimetric IMRT verification with a flat-panel EPID." Med Phys **in press**.

Chapter 4 Results and Discussion

This chapter will summarize the results of the measurements described in the preceding chapter. The results of the basic characterization measurements of the diamond detector including pre-irradiation dose, detector stability, spatial resolution, dose rate dependence and detector sensitivity are presented in the first half of this chapter in sections 4.1 to 4.5. Following the basic characterization measurements, the effect of the well documented dose-rate dependence of this diamond detector was observed by comparing the doses measured with the diamond detector and an ion chamber during the delivery of an arc treatment where the dose rate varies. These results are summarized in section 4.6. A further theoretical investigation into the effect of the dose-rate dependence was conducted and is summarized in section 4.7. Diamond detectors offer several advantages over commonly employed point dosimeters such as ion chambers and diodes. The remaining chapter sections serve as a comparison among dose measurements made with the diamond detector, two ion chambers, namely the PTW-Freiburg PinPoint and Exradin A12 ion chamber and a Varian aS500 EPID. The performance of each of these dosimeters is compared in field sizes as small as 1 x 1 cm^2, in simple IMBs with no high dose gradients at the point of measurement and in a clinical IMB. The comparison of the responses of these dosimeters in these situations illustrates the strength of the diamond detector in the field of radiation dosimetry.

4.1 Pre-Irradiation

The pre-irradiation responses of the diamond detector as a function of dose to cobalt, 6 and 15 MV beam qualities are shown in Figure 4.1. During the delivery of each pre-irradiation dose, the dose rates were different. This explains the difference in the diamond current for irradiations of different beam qualities.

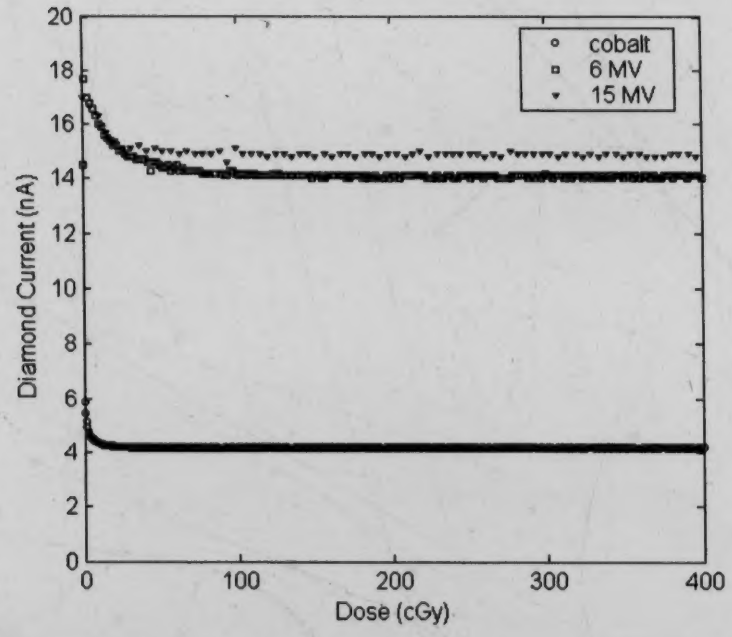

Figure 4.1 Diamond detector pre-irradiation response to beams of cobalt, 6 MV and 15 MV photons

The effect of removing the bias voltage on the detector's signal was observed. Following the measurement of the cobalt pre-irradiation dose, the power supply that provides the bias voltage to the detector was turned off for five minutes and then turned back on. Again an initial increase in the detector sensitivity was observed followed by a leveling off as the detector's response stabilized. A dose of 18.6 cGy was required to achieve a stable detector response. This effect suggests that a sufficient pre-irradiation dose is required each time that the bias voltage is turned off. Table 4.1 summarizes the doses required to a stable detector response for the three beam qualities investigated in this study.

Table 4.1 Dose required to stabilize PTW-Freiburg type 60003 diamond detector (S/N 9-032) response following period of unbiased conditions

Beam Quality	Stabilization Dose (cGy)
Cobalt 60	29.1
6 MV	67.8
15 MV	35.7

The difference in the dose required to stabilize the detector response for the different beam qualities are attributed to the amount of time between successive uses of the diamond dosimeter. When the diamond remains unused and subsequently in an unbiased state for long periods of time the amount of trap emptying within the sensitive volume is greater than when the detector was used more frequently. The differing periods of time between detector use affect the dose required to stabilize the response of the diamond detector.

It was decided that a pre-irradiation dose of 500 cGy was sufficient to ensure detector stability for megavoltage energies. This pre-irradiation dose was delivered for all subsequent measurements.

4.2 Stability

The stability of the diamond detector was observed by varying the time between identical exposures to irradiation from the cobalt-60 beam. A slight effect on the leading edge of the detector response curve as a function of time becomes noticeable with increases in time between successive measurements. For these measurements, it takes slightly longer for the signal to reach a stable level. The detector responses to radiation following gaps of 1 minute and 60 minutes between successive measurements are shown in Figure 4.2. The average signal during irradiation has been plotted as a function of the time between successive irradiations in Figure 4.3. This figure indicates that the time between irradiations up to a period of an hour has very little effect on the response of the diamond detector. The diamond detector's response decreases by approximately 0.01 nC (0.2% of the signal) after a period of 6 minutes has elapsed between successive measurements. However it should be noted that when the standard deviation of the signal during irradiation is considered all diamond currents are the same within the statistical error of the measurements.

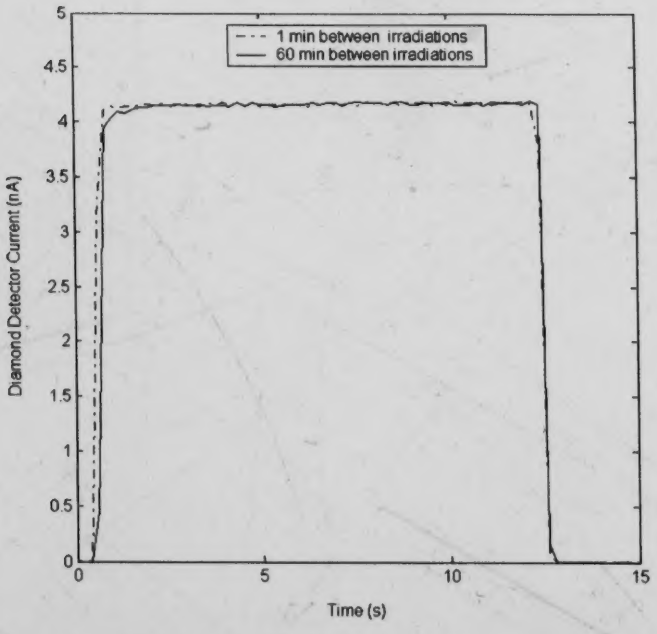

Figure 4.2 Diamond detector response to pulse of cobalt-60 radiation following 1 minute and 60 minutes of no irradiation

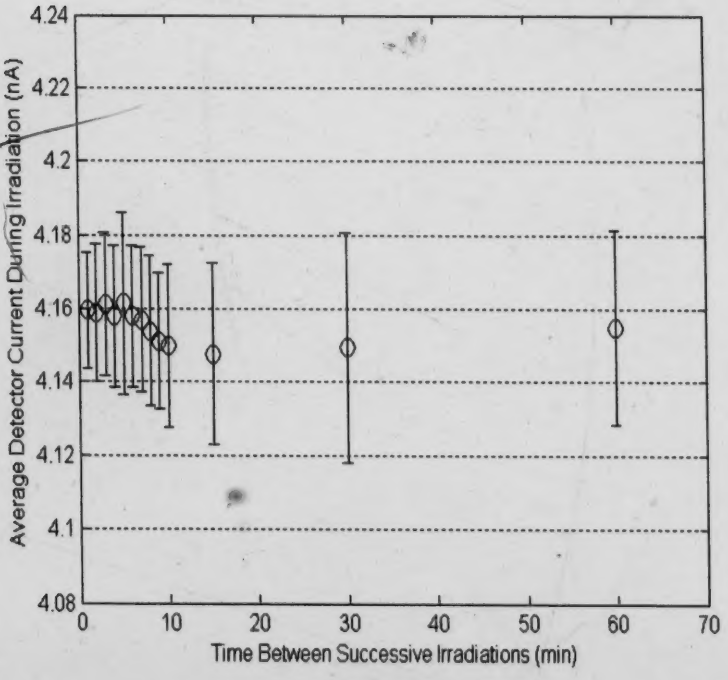

Figure 4.3 Variations in detector response to Cobalt-60 irradiation with increasing time between subsequent irradiations

4.3 Beam Profile Measurements

Figure 4.4 and Figure 4.5 illustrate cross-plane profiles measured with the diamond detector orientated both parallel and perpendicular to the beam CAX and the IC10 chamber oriented with its axis perpendicular to the beam CAX.

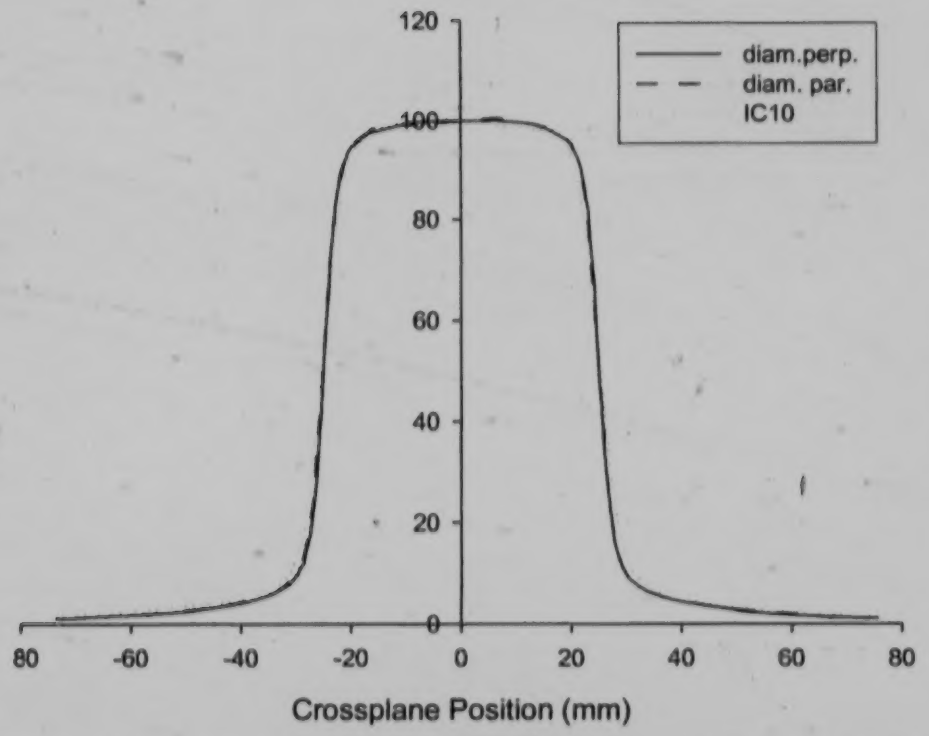

Figure 4.4 Crossplane beam profiles at 10 cm depth with SSD = 90 cm of 5 x 5 cm^2 Varian 600C generated 6 MV photon beam as measured with diamond detector with perpendicular and parallel orientations as well as IC10 ion chamber

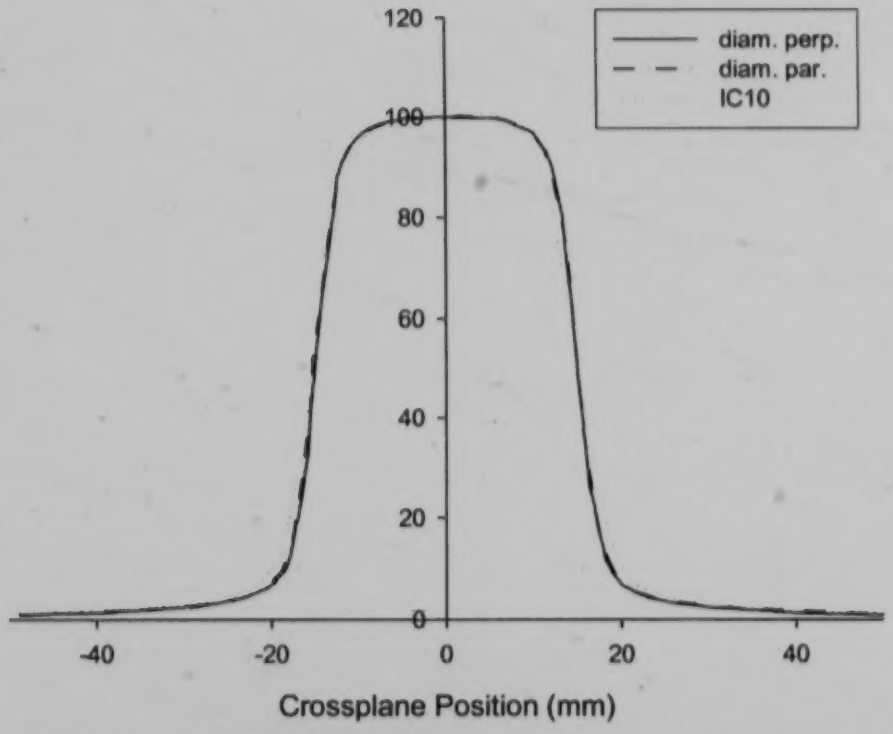

Figure 4.5 Crossplane beam profiles at 10 cm depth with SSD = 90 cm of 3 x 3 cm^2 Varian 600C generated 6 MV photon beam as measured with diamond detector with perpendicular and parallel orientations as well as IC10 ion chamber

The improvement in the sharpness of the beam profile introduced by using the diamond detector can be seen by comparison between the IC10 and diamond detector measurements shown in Figure 4.4 and Figure 4.5. An increased broadening of the penumbral region can be seen when the IC10 ion chamber is used. This result arises directly from volume averaging of the signal within the 0.14 cm^3 sensitive volume of the ion chamber. The improved spatial resolution of the diamond detector over the IC10 chamber can be seem by comparison of the 20-80% and 10-90% penumbral widths summarized in Table 4.2 and Table 4.3, respectively.

Table 4.2 20-80 % dose level penumbral widths measured with diamond detector and IC10 ion chamber for 6 MV photon beam generated with a Varian 600C linac

Field Size	Depth (cm)	Measurement	Penumbral Width (mm)		
			Diamond Perpendicular (mm)	Diamond Parallel (mm)	IC10 (mm)
3 x 3 cm^2	1.5	Cross-plane	3.1 ± 0.2	3.6 ± 0.2	5.2 ± 0.1
		In-plane	3.9 ± 0.1	3.9 ± 0.2	5.6 ± 0.1
	10	Cross-plane	3.9 ± 0.2	4.1 ± 0.2	5.7 ± 0.2
		In-plane	3.9 ± 0.1	5.0 ± 0.1	6.7 ± 0.1
5 x 5 cm^2	1.5	Cross-plane	3.5 ± 0.3	3.7 ± 0.1	5.3 ± 0.1
		In-plane	3.4 ± 0.1	4.3 ± 0.4	6.0 ± 0.2
	10	Cross-plane	4.1 ± 0.1	4.5 ± 0.2	6.0 ± 0.2
		In-plane	4.9 ± 0.2	5.0 ± 0.2	7.1 ± 0.2
10 x 10 cm^2	1.5	Cross-plane	3.5 ± 0.2	3.8 ± 0.2	5.4 ± 0.2
		In-plane	3.6 ± 0.1	3.9 ± 0.1	6.5 ± 0.2
	10	Cross-plane	4.8 ± 0.2	5.3 ± 0.2	7.1 ± 0.2
		In-plane	5.9 ± 0.1	6.0 ± 0.2	7.9 ± 0.1

For all penumbral widths appearing in Table 4.2 and Table 4.3 the measurements obtained with the diamond detector oriented perpendicular to the beam CAX are smaller than the diamond oriented parallel to the beam CAX and the ion chamber measurements. It is expected that the diamond detector exhibits its highest spatial resolution when used in this orientation because the thickness of the diamond in this dimension is 0.25 mm. Thus the beam "sees" an area of approximately 0.65 mm^2. However when the probe is used with its stem axis parallel to the CAX the beam "sees" a sensitive volume having an area of 6.8 mm^2, thus there is an increase in the volume averaging effect and hence a broadening of the penumbral widths when compared with the perpendicular orientation. It should be noted that when the error estimates are included in the values appearing in Table 4.2 and Table 4.3 the differences in the penumbral widths measured with the diamond in different orientations are small. The differences of penumbral widths measured with the diamond perpendicular to beam CAX and IC10 ion chamber range

between 1.5 and 2.9 mm with an average difference of 2.1 mm. This emphasizes the superior spatial resolution that the diamond detector is capable of as compared with air-filled ion chambers.

Table 4.3 10-90 % dose level penumbral widths measured with diamond detector and IC10 ion chamber for 6 MV photon beam generated with a Varian 600C linac

Field Size	Depth (cm)	Measurement	Penumbral Width (mm)		
			Diamond Perpendicular (mm)	Diamond Parallel (mm)	IC10 (mm)
3 x 3 cm^2	1.5	Cross-plane	5.2 ± 0.1	5.9 ± 0.1	7.8 ± 0.1
		In-plane	5.7 ± 0.2	6.7 ± 0.5	9.4 ± 0.2
	10	Cross-plane	6.5 ± 0.1	6.9 ± 0.2	9.0 ± 0.4
		In-plane	7.2 ± 0.2	8.0 ± 0.2	10.4 ± 0.2
5 x 5 cm^2	1.5	Cross-plane	5.6 ± 0.2	6.1 ± 0.1	8.0 ± 0.2
		In-plane	6.3 ± 0.2	7.2 ± 0.4	9.5 ± 0.1
	10	Cross-plane	8.1 ± 0.1	8.2 ± 0.1	10.5 ± 0.2
		In-plane	8.8 ± 0.2	9.6 ± 0.4	11.6 ± 0.1
10 x 10 cm^2	1.5	Cross-plane	6.3 ± 0.1	6.8 ± 0.1	8.9 ± 0.1
		In-plane	7.0 ± 0.3	7.6 ± 0.4	10.2 ± 0.4
	10	Cross-plane	13.0 ± 0.1	14.2 ± 0.2	15.3 ± 0.1
		In-plane	14.9 ± 0.5	15.4 ± 0.3	17.5 ± 0.5

4.4 Dose Rate Dependence Measurements

The determination of the diamond detector's under-response parameter with dose rate, Δ, by means of SSD variation, PDD measurement, PRF variation and TMR measurement are summarized in Tables 4.4, 4.5, 4.6 and 4.7 respectively. In all cases, the diamond responses and the dose rates were normalized to the lowest diamond response and lowest dose rate respectively. The Δ value corresponds to the slope of a log-log plot of the normalized diamond detector response to the normalized dose rate. For these four measurement series ion chamber measurements were used to calculate the abscissa values of the log-log plot. In all cases the ion chamber measurements were corrected for both polarity and recombination effects and then normalized to the lowest dose rate.

Log-log plots of the normalized diamond responses as a function of the normalized dose rates were generated. According to expressions 2.6.13 the slope of such a plot corresponds to the Δ value. In this manner the Δ value was established for the diamond detector in each of the beam energies and methods investigated. The dose rate ranges over which each of the dose rate dependence experiments were conducted are also included in the following four tables. The average value of the Δ values appearing in Table 4.4 through Table 4.7 is 0.995 ± 0.002. The estimates of the error in the Δ values appearing in Tables 4.4 through 4.7 are solely statistical. Figure 4.6 shows the log-log plot of the normalized diamond response as a function of the normalized dose rate for 15 MV photons when dose rate variations are induced by changes in the SSD. The inset in this figure shows the relationship between the correction factors, P_{pol} and P_{ion} as a function of dose rate. The inset in Figure 4.6 illustrates the importance of correcting ion chamber measurements for recombination effects within the chamber. It is clear from the inset figure that P_{ion} varies with dose rate. If corrections for this effect are not made then the dose rate dependence of the diamond detector can go undetected.

Table 4.4 Δ Values determined from SSD variation

Energy (MV)	Δ Value	Dose Rate Range (cGy/min)
^{60}Co	0.998 ± 0.001	11-227
6	0.999 ± 0.001	58-1047
15	0.998 ± 0.001	61-1165

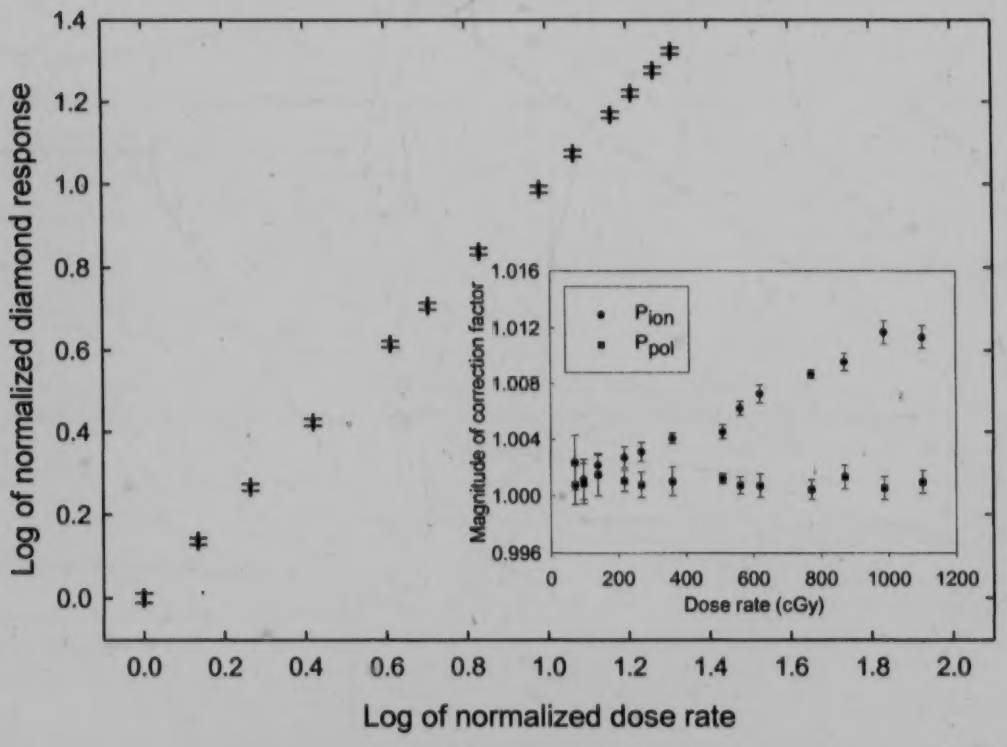

Figure 4.6 Linear Relationship between logarithms of normalized diamond response and normalized dose rate for 15 MV photons generated by a Varian 2300 EX linac. Variations in SSD were used to obtain dose rate variations. The inset shows the variation in the ion chamber correction factors with dose rate

Table 4.5 Δ Values determined from PDD measurements

Energy (MV)	Δ Value	Dose Rate Range (cGy/min)
^{60}Co	0.984 ± 0.002	42-174
6	0.992 ± 0.001	175-600
15	0.995 ± 0.001	241-600

Table 4.6 Δ Values determined from TMR variation

Energy (MV)	Δ Value	Dose Rate Range (cGy/min)
^{60}Co	0.988 ± 0.002	44 – 178
6	0.997 ± 0.002	136 - 396
15	0.997 ± 0.002	199 – 400

Table 4.7 Δ Values determined from PRF variation

Energy (MV)	Δ Value	Dose Rate Range (cGy/min)
6	0.999 ± 0.001	77-465
15	0.999 ± 0.001	88-527

Each method of Δ value determination employed in this investigation offers advantages and disadvantages. Variation of the SSD allows for the largest variation of dose rate. However positioning of the probe in phantom during the acquisition of these measurements may be prone to errors. For such large variation in the SSD, the gantry is positioned at 90° and the couch at 270° and the phantom surface is beyond the range of the optical distance indicator for the majority of the measurements. Therefore SSD position measurements must be made with a measuring tape thereby introducing an additional source of error to the measurements. The set-up of this experiment is also the most time consuming. In spite of these considerations, the errors considered in this study are purely statistical and assume random experimental variations only.

The estimates of the error in the Δ values appearing in Table 4.4 to Table 4.7 are a result of performing a weighted linear regression (see Appendix B) on the log of the normalized diamond currents and the log of the normalized dose rate. Errors in the diamond responses were the standard deviation of the electrometer readings over multiple measurements for the SSD, PDD and TMR measurements and the standard deviation of the diamond current during the delivery for the PRF measurements. Errors in the ion chamber measured dose rate considered differences in electrometer readings. The error in the diamond current and dose rate were then propagated through the normalization of the data and taking the logarithm of the data (see Appendix C). These error estimates were then used in the weighted linear regression as described in Appendix B.

The average value of the Δ values appearing in Tables 4.4, 4.5, 4.6 and 4.7 is 0.995 ± 0.002. It is interesting to note that the Δ values obtained for the ^{60}Co beam using the PDD and TMR measurements are significantly lower than the Δ

values obtained for the corresponding measurements made for 6 and 15 MV photons. Although the sensitive volume of these detectors is essentially water equivalent, this result suggests that there may be a slight energy dependence of the Δ value. If these two Δ values are neglected in the average, a Δ value of 0.997 ± 0.002 is obtained and all but one of the Δ values included in the average are contained within two standard errors of the average Δ value. An energy dependence can arise from the contact materials employed in the detector (Laub, Kaulich et al. 1997). Some groups have found a slight dose rate dependence on the Δ value; they have noted a decrease in the Δ value with increasing dose rate (Planskoy 1980; Hoban, Heydarian et al. 1994) however this effect was not observed in this study. Alternatively the cause of the difference between the Δ values determined using a ^{60}Co beam and the linear accelerated generated beams using the PDD and TMR measurements could arise due to the difference in the nature of the beams – pulsed versus continuous. It has been suggested in the literature that the dose rate dependence of diamond detectors is sensitive to average dose and not instantaneous dose implying that there should exist no difference in the Δ values measured in a continuous or pulsed beam (Hoban, Heydarian et al. 1994). The results of this investigation suggest that this may not be the case.

4.5 R Value Determination

According to expression 2.6.9, *R* is the constant of proportionality relating the diamond current to the dose rate. The *R* values that were determined for cobalt-60, 6 and 15 MV beam qualities are summarized in Table 4.8 assuming a Δ value of 0.995 ± 0.002.

Table 4.8 R values of PTW-Freiburg type 60003 Diamond detector (S/N 9-032) for different beam qualities used in this investigation

Beam Quality	R (10^{-11} A/cGy/min)
Cobalt-60	2.57 ± 0.02
6 MV	2.60 ± 0.02
15 MV	2.56 ± 0.02

Multiple determinations of the R value for different beam qualities were made. The R values appearing in Table 4.8 are the average values of these multiple measurements. The error estimate of each R value was assigned such that all R value determinations would be included within error of the average value of R for a given beam quality. The error associated with each R value is relatively large (on the order of 1 %) and consequently the R value was determined at all subsequent diamond detector uses and these average values were not used in diamond detector current to dose rate conversion.

4.6 Arc Treatment

The diamond current measured during the delivery of the 6 MV arc treatment is shown in Figure 4.7. The dose rate correction was applied to both the 6 and 15 MV diamond detector current and the corrected dose rates as a function of time were subsequently integrated to obtain the doses of the treatment, using the previously determined Δ value of 0.995 ± 0.002 and expression 2.6.9. The dose rate corrected integrated diamond detector doses are summarized in Table 4.9. Also included in this table are the integrated doses measured with the PR-06C ion chamber.

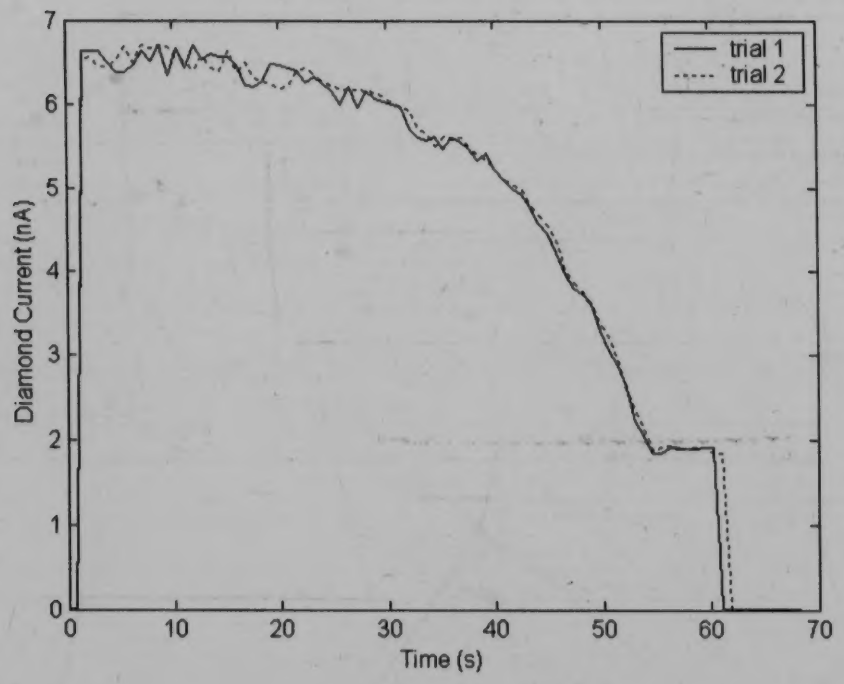

Figure 4.7 Diamond detector current as a function of time during 6 MV arc treatment

Table 4.9 Doses measured with PR-06C ion chamber and diamond detector during 6 and 15 MV arc treatment

Dose (cGy)			
6 MV		15 MV	
Ion Chamber	Diamond Dose rate corrected	Ion Chamber	Diamond Dose rate corrected
204.0 ± 1.0	202.5 ± 1.5	235.0 ± 1.2	233.7 ± 2.4

The results summarized in Table 4.9 indicate good agreement is obtained between doses measured with the PR-06C ion chamber and the diamond detector for both 6 and 15 MV arc treatments. A percent error of 0.5 was assumed for the ion chamber measurements, while the errors associated with diamond detector were propagated in quadrature as shown in Appendix A.

4.7 Theoretical Effect of Dose Rate Dependence

The theoretical effect of the dose rate dependence was investigated using the diamond detector current measured during the delivery of the 6 and 15 MV arc treatments. Δ values ranging from 0.5 to 1 were assumed and the corresponding R values were calculated and used in the subsequent calculation conversion from current to dose rate. These hypothetical dose rates were integrated to obtain the doses during the arc treatments. The error associated with each of these hypothetical doses is the standard deviation of the multiple arc treatment measurements converted to dose rates for different Δ values. The results of this investigation are summarized in Table 4.10 and Table 4.11. Included in these tables are the percent differences between the dose rate dependence corrected doses and the dose for a linearly responding device (Δ = 1) and the percent difference between the dose rate dependence corrected doses and the dose measured with the ion chamber.

Table 4.10 Theoretical doses calculated for 6 MV arc treatment illustrating effect of diamond detector's Δ value on conversion from diamond current to dose rate

Δ value	Dose (cGy)	% difference between dose rate dependent diamond and linear diamond	% difference between diamond and ion chamber
0.5	143.6 ± 2.3	29.2	29.6
0.7	173.4 ± 2.0	14.5	15.0
0.9	194.5 ± 1.8	4.1	4.7
0.95	198.8 ± 1.7	2.0	2.5
0.995	202.5 ± 1.7	0.2	0.7
1	202.9 ± 1.7	-	0.5

Table 4.11 Theoretical doses calculated for 15 MV arc treatment illustrating effect of diamond detector's Δ value on conversion from diamond current to dose rate

Δ value	Dose (cGy)	% difference between dose rate dependent diamond and linear diamond	% difference between diamond and ion chamber
0.5	164.0 ± 2.8	30.0	30.2
0.7	199.8 ± 2.4	14.7	15.0
0.9	224.5 ± 2.2	4.1	4.5
0.95	229.5 ± 2.1	2.0	2.3
0.995	233.7 ± 2.1	0.2	0.5
1	234.2 ± 2.1	-	0.4

The results summarized in Tables 4.10 and 4.11 illustrate that the dose rate dependence of the PTW-Freiburg type 60003 diamond detector (S/N 9-032) has a small effect. The percent difference that is introduced by assuming that this device responds linearly with dose rate is only 0.2 for both 6 and 15 MV arc treatments. Also the percent difference between the ion chamber measured dose and the dose if a Δ value of 0.995 is used is 0.7 and 0.5 for 6 and 15 MV photon beams. While this percent difference between the ion chamber and dose if a Δ value of 1 is used is 0.5 and 0.4 for 6 and 15 MV photons. It should be noted that the ion chamber measured doses and the doses for Δ values of 0.995 and 1 agree within the experimental error. The results summarized in this table indicate that excellent agreement is obtained between diamond doses and ion chamber doses when Δ values of 0.995 and 1 are used. This result suggests that correction for the dose rate dependence is not required for the diamond detector employed in this study over the dose rate range encountered in the delivery of this arc treatment. For diamond detectors with a dose rate dependence of larger magnitude, correction for this effect may be necessary. However for the dose rate variations present during the delivery of this arc treatment, correction for this effect is not necessary.

4.8 Small field dosimetry

The doses measured as a function of the length of a side of the square field are illustrated in Figure 4.8 and Figure 4.9 for 6 and 15 MV photons, respectively. For field sizes above 4 x 4 cm^2 there is good agreement among all dosimeters for both 6 and 15 MV photons. It is for smallest fields that the ion chambers show an under-response in the measured dose as compared with the dose measured with the diamond. The doses measured with the A12 chamber and the diamond detector agree very well with a percent difference of less than 0.5 % and 0.7 % for square field sizes 4 x 4 cm^2 and larger for 6 and 15 MV photons respectively. With increasingly small field sizes, the A12 measurements show increasing deviations from the diamond detector measured doses reaching 58 % and 46 % differences at a field size of 1 x 1 cm^2 for 6 and 15 MV photons respectively. For these small field sizes, the dimensions of this large volume chamber become comparable with the field size and dose gradients within the sensitive volume are responsible for the underestimate of dose measured with this chamber.

The PinPoint chamber performs better than the large volume A12 ion chamber particularly for field sizes smaller than 3 x 3 cm^2. For field sizes 2 x 2 cm^2 and larger, the doses measured with the PinPoint chamber agree within 0.4 % and 1 % of the diamond detector for 6 and 15 MV photons respectively. It is only for the smallest field used in this study that there is an appreciable deviation between the PinPoint chamber and the diamond detector measured doses. The doses measured with the PinPoint chamber are 8 % and 5 % lower than that measured with the diamond detector for the 1 x 1 cm^2 field for 6 and 15 MV photons respectively. This result is consistent with that reported by Martens *et al.* where it is recommended that for output measurements of field sizes smaller than 1.5 x 1.5 cm^2 a diamond detector is a more appropriate dosimeter than a PinPoint chamber (Martens, De Wagter et al. 2000).

Both air filled ion chambers experience a loss of signal resulting in an underestimate of dose when the field sizes reach a size comparable to the size of the sensitive volume. According to the manufacturer's specification, the collecting electrode within the A12 chamber is 21.1 mm long with the air filled

volume extending beyond this length. The dose measured with this chamber started to deviate from the diamond detector measurement at a field size of 3 x 3 cm^2. The length of the PinPoint chamber's collection volume is 5 mm. The PinPoint dose measurements deviated from the diamond detector measurements only at a field size of 1 x 1 cm^2 which is twice the length of the sensitive volume of this device.

In our center, individual segments that make up an IMB are limited in size by the physical dimensions of the multi-leaf collimator, which can be as small as 0.5 cm projected width at isocentre. Therefore, segments can be smaller that the limiting field size for which a small volume ion chamber such as the PinPoint fails to give an accurate dose reading. For square field sizes with side length less than twice the maximum lateral range of electrons set in motion by primary photons, lateral electronic equilibrium may not exist at the beam CAX (Heydarian, Hoban et al. 1996). Thus, at the beam CAX lateral electronic equilibrium may not exist for field sizes 3 x 3 cm^2 and 6 x 6 cm^2 and smaller for 6 and 15 MV photons respectively. This requirement for the existence of lateral electronic equilibrium is significantly more restrictive than that outlined by Bjarngard *et al.* as mentioned previously (Bjarngard, Tsai et al. 1990). For both 6 and 15 MV dosimetry measurements there is good agreement between all dosimeters down to field sizes of 4 x 4 cm^2. This suggests that the reason for the discrepancy between the ion chamber and diamond measurements is not due to a lack of lateral electronic equilibrium but to a different effect such as volume averaging effects within the sensitive volume.

The doses measured with the diamond detector and the EPID agree well for all field sizes having a maximum percent difference of 1.4 %. The EPID is a pixilated imaging device with pixel size of 0.736 x 0.736 mm^2 thus volume averaging effects that plague large volume point dosimeters are not an issue for a EPID dosimetry. This agreement between the diamond detector and the EPID is an encouraging result indicating that the diamond detector is an effective dosimeter for small field measurements. In a characterization study of radiosurgical beams conducted by Rustgi *et al.* total scatter factors measured with

a PTW diamond detector and a silicon diode were higher than measurements made with a Markus ion chamber. It was suggested that the measurements made with the solid state dosimeters approach the true values of the total scatter factors of these radiosurgical beams due to the small size of the sensitive volume. High dose gradients across the sensitive volume of the larger volume ion chambers are offered as an explanation for the underestimate of the total scatter factor (Rustgi 1995).

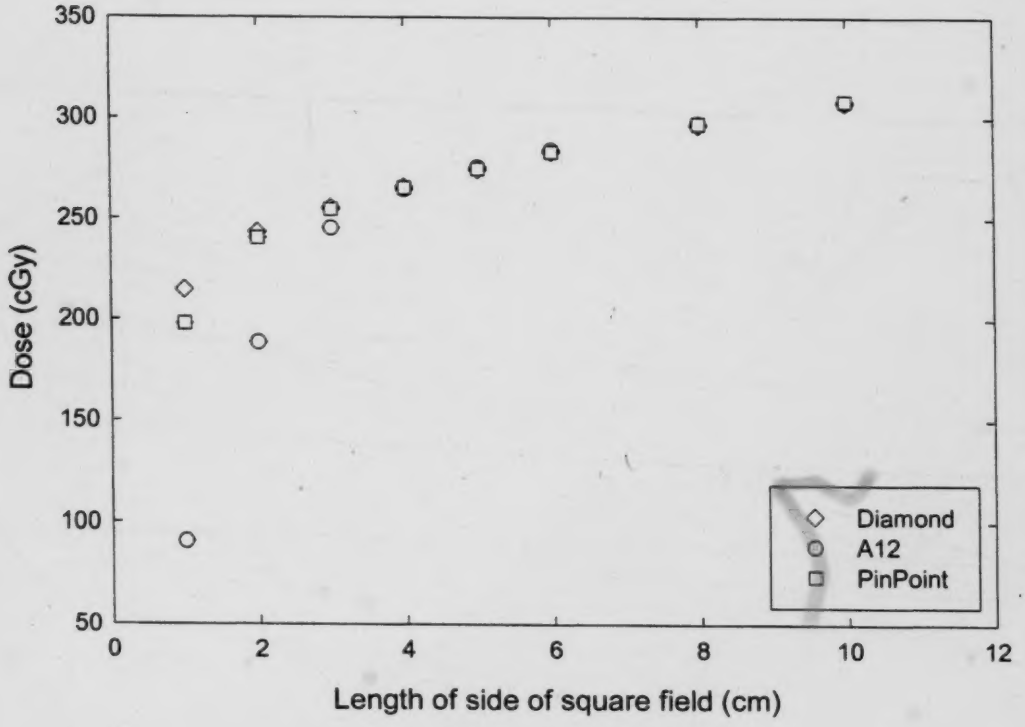

Figure 4.8 Doses measured at field sizes ranging from 1 x 1 cm^2 to 10 x 10 cm^2 using diamond detector, A12 and PinPoint for 6 MV irradiations

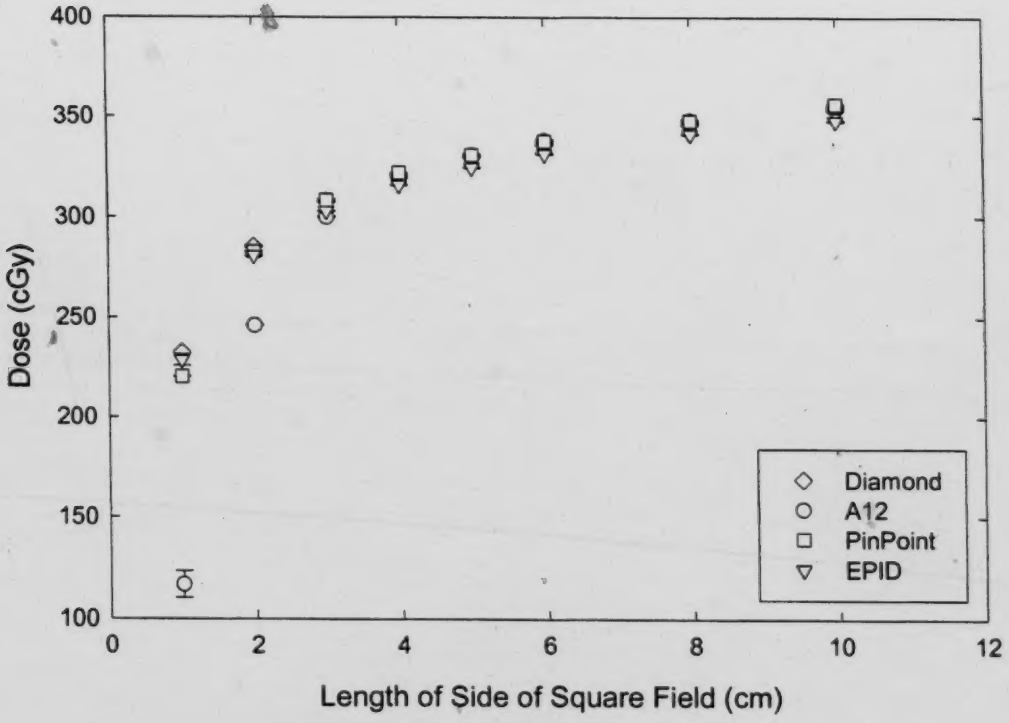

Figure 4.9 Doses measured at field sizes ranging from 1 x 1 cm^2 to 10 x 10 cm^2 using diamond detector, A12, PinPoint and EPID for 15 MV irradiations

4.9 Dosimetry of simple intensity modulated beams

The five segments that comprise the first simple IMRT test case are shown in Figure 4.10 with the co-ordinates (0,0) denoting the position of isocenter. The dose rates at isocenter at a depth of 10 cm in phantom as a function of time measured with diamond detector and the A12 ion chamber are shown in Figure 4.11 during the delivery of the first simple IMB. The PinPoint response coincided with the diamond detector and was therefore not included in Figure 4.11 for ease of viewing. By viewing Figure 4.11 it can be seen that with the exception of the third segment, all segments were centered at isocenter. By examining the geometry of the segments, the performance of the point dosimeters can be understood. Segments one and two were 2 x 2 cm^2 and 2 x 4 cm^2 fields respectively. Due to the large physical dimensions of the A12 ion chamber,

volume averaging effects within the sensitive volume give rise to the under-response of this chamber during the delivery of these segments. The third segment measured 2 x 3 cm^2 and was centered at (3 cm, -6 cm) where the numbers in parenthesis are the in-plane and cross-plane position relative to isocenter. Thus the dose to the point of measurement during the delivery of this segment can be attributed to scatter and leakage. There was a slight over-response of the PinPoint relative to the diamond detector and A12 chamber during the third segment. This slight over-response is attributed to the presence of the steel electrode which causes an over-response to low energy photons as documented by Martens *et al.* Good agreement was obtained for the diamond detector and the A12 during the delivery of this segment. The forth segment is sufficiently large (4 x 5 cm^2 centered at isocenter) that volume averaging within the sensitive volume of the large volume chamber does not occur. For this reason good agreement was obtained among the dosimeters for this segment. The final segment was a 1 x 1 cm^2 field centered at isocenter. The smallness of this segment gave rise to an increase in the magnitude of the volume averaging effects for the large volume chamber as can be seen in Figure 4.11. Although not shown in Figure 4.11 there was a slight decrease in the response of the PinPoint chamber relative to the diamond response for this segment. This result is consistent with the results of the preceding section where a slight under-response of the PinPoint was found for 1 x 1 cm^2 fields.

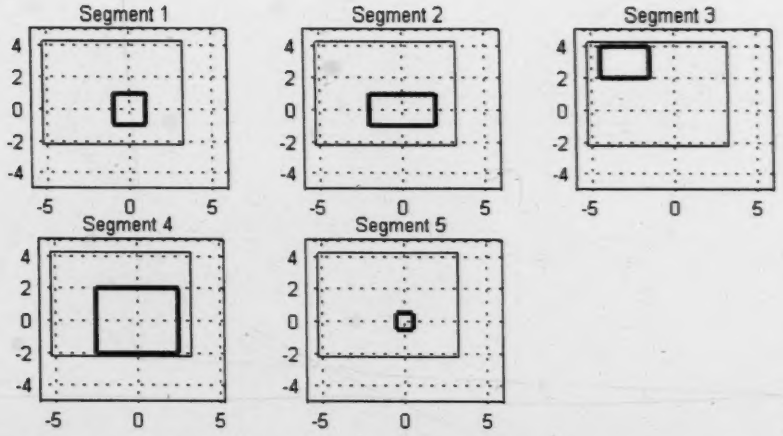

Figure 4.10 Shape of individual segments comprising 5 segment simple step and shoot intensity modulated beam – thick lines illustrate segment geometry, thin lines illustrate main collimator settings

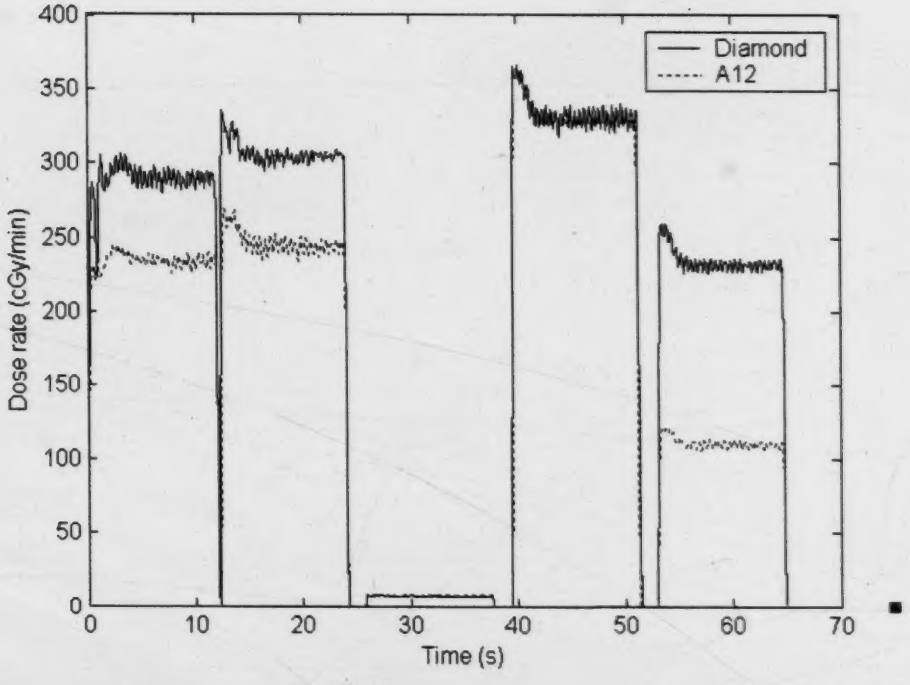

Figure 4.11 Dose rate during delivery of 5 segment step and shoot IMRT field at isocentre at 10 cm depth in phantom as measured with diamond detector and Exradin A12 ion chamber

The integrated doses measured with each of the point dosimeters for the three simple IMRT plans are summarized in Table 4.12. These results show that for these simple IMBs, the doses measured with the PinPoint, diamond detector and EPID agree within error for the beams 1 and 2. For both of these beams, the A12 chamber under-responds significantly. For the third beam, the PinPoint over-responds slightly as compared with the responses of the A12, diamond detector and EPID. Four of the five segments making up the third simple IMB, were situated off the CAX. As a result of this segment geometry during the majority of the beam delivery, the dose to the point of measurement was due to scatter giving rise to the over-response of the PinPoint as described by Martens *et al* (Martens, De Wagter et al. 2000).

Table 4.12 Doses at isocenter for simple IMRT plans measured using A12, PinPoint, diamond detector and aS500 EPID

	Dose to Isocenter (cGy)			
	A12	PinPoint	Diamond	EPID
Beam 1	183 ± 1	230 ± 1	231 ± 1	231.5 ± 0.9
Beam 2	290 ± 1	311 ± 1	312 ± 1	311.6 ± 0.5
Beam 3	71.3 ± 0.5	75.8 ± 0.4	72.4 ± 0.7	71.9 ± 0.2

In all three of the simple plans that were delivered there is excellent agreement between the doses measured with the diamond detector and the EPID. For the first two simple IMBs delivered the PinPoint ion chamber also agrees well with the diamond detector and the EPID. However for the third simple IMB the PinPoint chamber over-responds when compared with the diamond detector and the EPID. The third IMRT plan consisted of four segments that were distanced from the CAX by at least 1 cm in the plane of isocenter and one segment that coincided with the CAX. This indicates that for the majority of the treatment the dose to isocentre, the point of measurement in this case, is a result of scatter. The over-response of the Pin Point ion chamber to low energy photons due to the

presence of the steel electrode has been previously documented (Martens, De Wagter et al. 2000). This over-response to low energy photons may explain the higher dose measured with the Pinpoint chamber as compared with the diamond detector and EPID doses.

The dose rate spikes occurring at the beginning of segments two, four and five of Figure 4.11 are an effect of the dose servo mechanism of the linear accelerator. When the dose servo is enabled, it functions to maintain a uniform dose rate. The dose servo responds to the zero dose rate during the leaf motion of step and shoot IMRT by overshooting the selected dose rate when the beam is turned back on. When the dose servo is disabled this overshoot effect is not observed.

4.10 Dosimetry of clinical prostate intensity modulated beam

The higher dose gradients at isocentre introduced by the clinical IMRT prostate plan complicate point dosimetry in these regions. Dosimetric measurements in high dose gradients are extremely sensitive to positioning in these areas. Although efforts were made to choose an IMRT plan with a low dose gradient at isocentre when selecting a clinical IMRT plan, volume effects of the various point dosimeters employed in this study became apparent. Figure 4.12 illustrates the dose rate as a function of time during the delivery of one of the IMBs comprising the IMRT prostate treatment as measured with the diamond detector, as well as the A12 and PinPoint ion chambers.

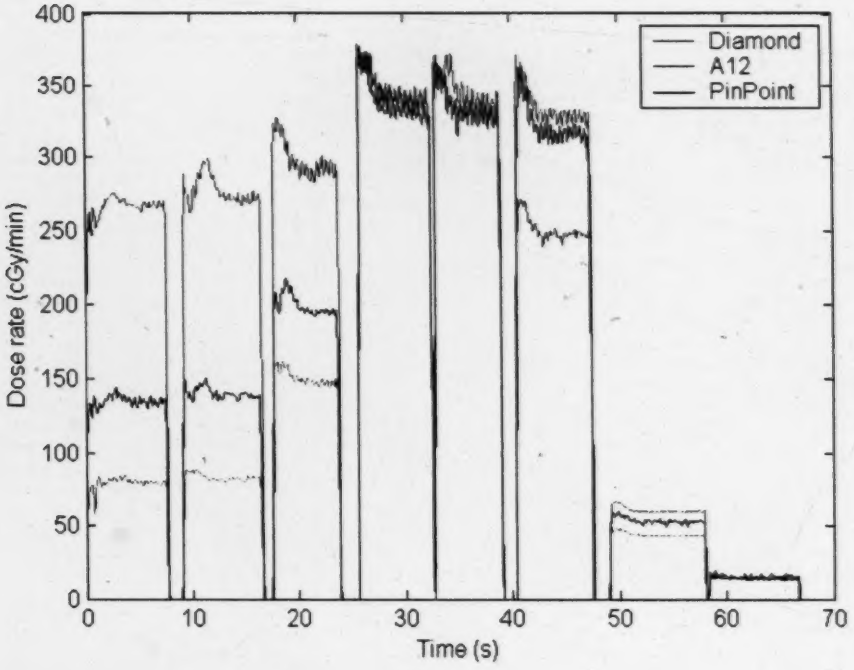

Figure 4.12 Comparison of response of three point dosimeters' response to 8 segment intensity modulated field at isocentre

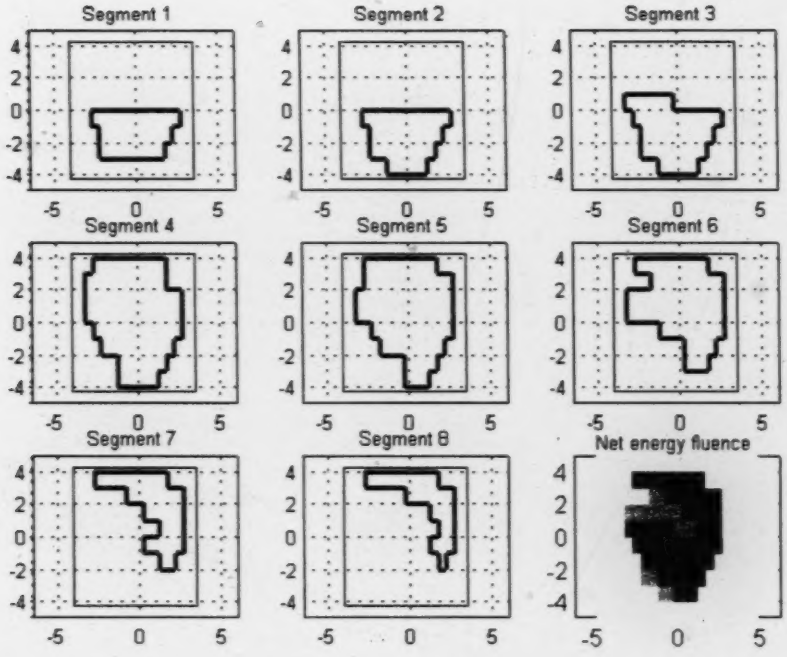

Figure 4.13 Shape of eight segments that comprise single IMB and "fluence map" resulting from delivery of eight step and shoot segments - thick lines illustrate segment geometry, thin lines illustrate main collimator settings

By viewing Figure 4.12 it is apparent that there is good agreement between the response of the three point dosimeters for the forth, fifth and eighth segments. Poor agreement is obtained for the other segments. The shape of the individual segments is related to the agreement obtained by the three different dosimeters employed in this portion of the study. Figure 4.13 is an illustration of the geometry of the eight segments that make up the intensity modulated field for which the dose rate responses are shown in Figure 4.12 above. The (0,0) coordinate of each of the segments corresponds to isocentre. By viewing Figure 4.13 it is evident that the beam edge corresponds exactly or is very near to isocentre for segments 1, 2, 3 and 7. Placement of the centre of the sensitive volume of the point dosimeters at isocentre is therefore placing these detectors in the penumbral region of these segments. There are a number of complications introduced by making dosimetric measurement in these high gradient regions and

measurements in these regions are extremely sensitive to positioning errors. If we consider the geometry of the sensitive volume of the dosimeters employed in this study, the differences in the responses illustrated in Figure 4.12 can be understood. The length of the sensitive volume of the A12 chamber is over 2 cm long. By centering the sensitive volume at isocentre one can see that a large portion of the sensitive volume extends both into the region outside the field and into the beam. Volume averaging effects are extremely pronounced for this large volume chamber. It is interesting to note that the dose rate measured by the large volume A12 chamber both underestimates and overestimates the response of the other smaller volume chambers. The diamond detector having such a small sensitive volume is extremely sensitive to positioning. If the centre of the sensitive volume is displaced by a fraction of a millimeter from isocentre the dose measured will differ significantly from the dose at isocentre. The beam profile measurements made in this study with the diamond detector oriented perpendicularly to the CAX indicate that the 10-90% penumbra widths are 13.0 ± 0.1 and 14.9 ± 0.5 mm for in-plane and crossplane respectively at 10 cm depth for a 6 MV beam. A slight error in positioning can lead to a significant difference in the measured dose. This result stresses the importance of probe positioning particularly in the vicinity of beam edges. Thus it is not surprising that there is poor agreement between the dose rate measured with diamond and the ion chambers.

The following table summarizes the results of the point dose measurements made at isocentre in this IMB as well as those dose measurements made using the aS500 EPID. The EPID pixels corresponding to the beam CAX were established by placement of a lead BB at the crosshairs. The estimates of error in the measurements using the EPID reflect the finite size of the BB used. Pixel values that were distanced by less than the radius of the BB from the CAX were considered in the estimate of error in the doses appearing in Table 4.13.

Following the establishment of the pixels that correspond to isocentre on the EPID images, the HELAX dose distributions for each segment were registered with the EPID images. The image registration algorithm used here has an

associated error of ± 1 pixel. Therefore the error associated with the HELAX dose calculations at a given point reflect the error associated with the error process. Dose values were then extracted from the registered HELAX dose distribution.

It is also of importance to see how well the TPS employed in this centre performs when compared with these dosimeters. The doses calculated for isocentre are also included in this table.

Table 4.13 Doses measured at isocentre during delivery of 8 segment clinical prostate intensity modulated beam

Segment	Dose (cGy)				
	A12	PinPoint	Diamond Detector	EPID	HELAX-TMS
1	25.5 ± 0.4	29.0 ± 0.2	10.9 ± 0.1	19 ± 4	23.6
2	25.9 ± 0.4	29.5 ± 0.2	11.2 ± 0.1	19 ± 4	23.8
3	26.1 ± 0.4	28.2 ± 0.2	15.2 ± 0.2	21 ± 4	21.7
4	40.3 ± 0.6	40.0 ± 0.3	40.2 ± 0.5	39.9 ± 0.1	39.5
5	36.0 ± 0.4	35.9 ± 0.2	36.1 ± 0.5	35.9 ± 0.1	35.6
6	34.9 ± 0.5	38.9 ± 0.3	40.2 ± 0.5	39.7 ± 0.1	40.5
7	9.3 ± 0.1	10.8 ± 0.1	7.5 ± 0.1	10 ± 2	2.7
8	2.18 ± 0.03	2.24 ± 0.01	2.26 ± 0.01	2.5 ± 0.1	0.0
Total	200 ± 1	214.5 ± 0.5	164 ± 1	186 ± 7	187

There are a number of conversions that must occur in order to arrive at the dose for each segment using each of the point dosimeters appearing in Table 4.13. The raw signal for the A12 and the PinPoint chambers obtained from the Wellhöfer is in the form of a percent dose rate that must be converted to a dose rate by means of a conversion factor. The dose rate as a function of time is then integrated with respect to time to arrive at the integrated dose during each segment. The raw signal during the irradiation is also noisy due to the pulsed nature of the linac output. The use of this conversion factor, the integration and noise in the raw signal introduce error to the dose per segment. These effects have been considered in the error estimates appearing in Table 4.13. The error in the dose resulting from the integration is estimated by equation A.3. In order to arrive at

doses measured with the diamond detector, the raw signal measured with the Wellhöfer dosimetry system must be converted to a diamond current. This current must then be converted to a dose rate by means of expression 2.6.9 and the previously determined Δ and R values, each of which has an associated error. The error in these quantities was propagated through the conversion from current to dose rate as shown in Appendix A.

4.11 Dosimetry of clinical prostate intensity modulated beam at improved detector positions

The presence of high dose gradients in IMBs complicates dosimetry within these fields. This effect is illustrated by the results that were obtained in the previous section where isocentre (point of measurement) coincided with high dose gradients in four out of the eight segments making up the IMB. These poor results prompted the investigation into the effects of more appropriate probe positions. Probe positions were considered acceptable for an individual segment if the probe position was separated by a user-defined distance from the segment edge and the position was within the field. In order to find appropriate positions for an IMB, the acceptable probe positions for each segment were weighted according to the segment weightings in the IMB. In this way the map shown in Figure 4.14 was generated. The positions with the highest value correspond to probe positions that avoid high dose gradients best for an IMB.

Following initial measurements made with the various probes at isocentre, it became apparent that differences between the doses measured using detectors of different sensitive volumes may have arisen from sensitive volumes that abutted the field edges. For large volume chambers where a large portion of sensitive volume does not intersect with the beam segment, the measured dose at isocentre is significantly less than the dose measured for a detector with its sensitive volume contained entirely in the segment. Doses measured in segments that did not have a segment edge near the detectors' sensitive volumes agreed better than those in which the segment edges coincided with the sensitive volume of one

detector and not another. This difference provided the motivation to seek out more appropriate detector positions that would help to eliminate this effect.

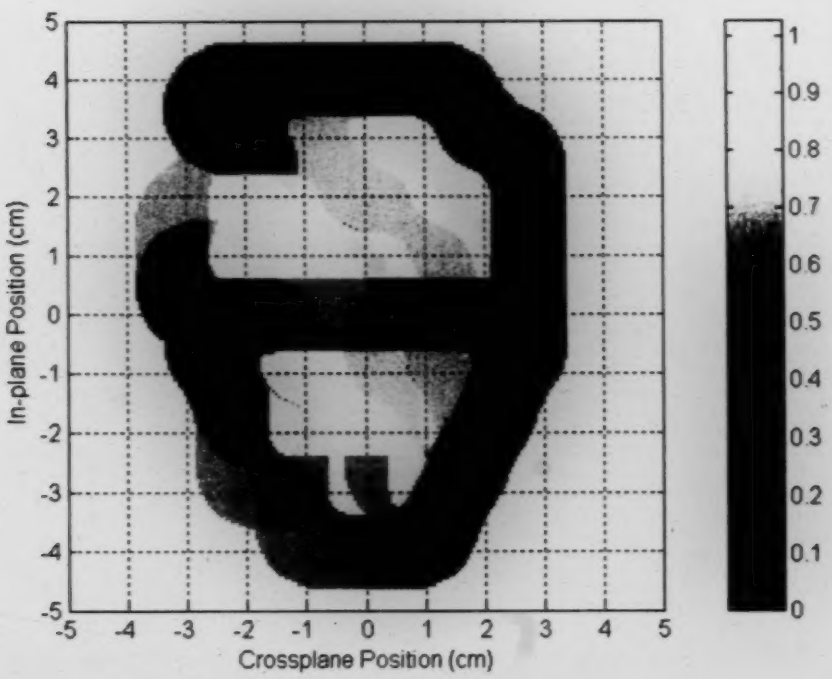

Figure 4.14 Map used to determine appropriate probe positions for a clinical prostate IMB

The positions within the treatment field with the highest value assigned to them are the most appropriate positions to make point measurements according to the criteria described in the preceding section. According to the exclusion of segment edges to find better probe positions used in this work shown in Figure 4.14, it is apparent that there are two probe positions that avoid the high dose gradients: (-1.3 cm, 1.7 cm) and (0.7 cm, 3.0 cm) where the first and second numbers in parenthesis are the positions in the cross-plane and in-plane direction respectively. The dose rate as a function of time during the delivery of the same IMB as in the preceding section are shown at these better probe positions are shown in Figure 4.15 and Figure 4.16. By viewing these figures it is apparent that by avoiding point dose measurements in the regions of high dose gradients, better agreement between the PinPoint and the diamond detector dose rate measurements are

obtained. The dose rates as a function of time for these dosimeters track well at both of the improved detector positions. The large volume A12 chamber does not agree with the measurements made with the other point dosimeters. This result is not surprising when one considers the dimensions of this dosimeter.

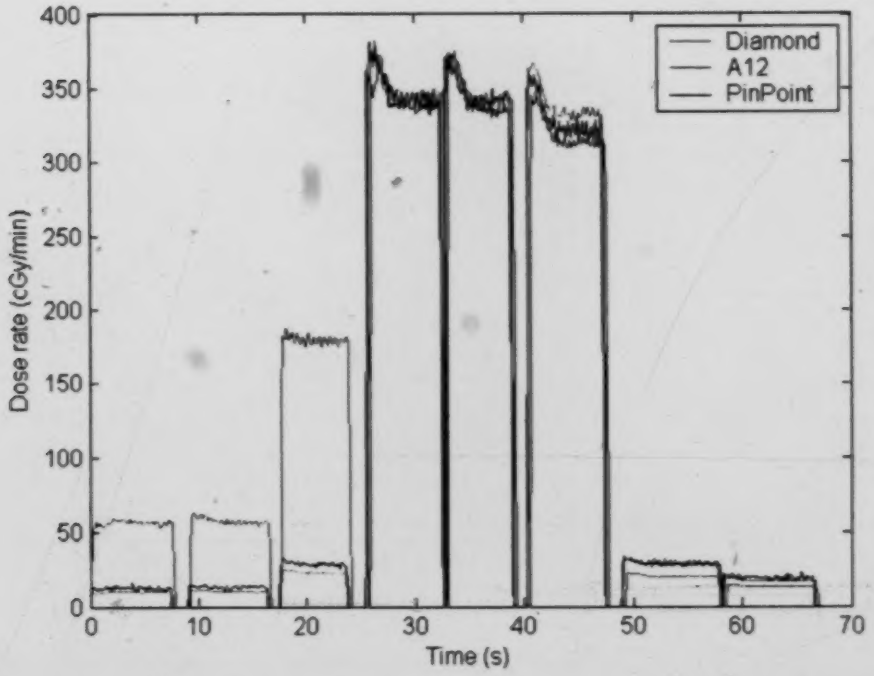

Figure 4.15 Comparison of response of three point dosimeters' response to 8 segment IMRT field at improved detector position 1 (-1.3 cm, 1.7 cm) as determined by edge exclude software

Table 4.14 Doses measured at improved detector position 1 (-1.3 cm 1.7 cm) during delivery of 8 segment IMRT field

Segment	Dose (cGy)				
	A12	PinPoint	Diamond Detector	EPID	HELAX-TMS
1	2.58 ± 0.04	1.61 ± 0.02	1.40 ± 0.02	1.7 ± 0.1	1.1
2	2.63 ± 0.04	1.65 ± 0.02	1.47 ± 0.02	1.7 ± 0.1	1.1
3	10.1 ± 0.2	3.23 ± 0.05	2.61 ± 0.04	3.0 ± 0.3	2.6
4	40.6 ± 0.7	41.0 ± 0.6	40.9 ± 0.6	40.2 ± 0.1	39.5
5	36.4 ± 0.7	36.9 ± 0.6	36.5 ± 0.6	36.2 ± 0.1	35.6
6	39.4 ± 0.6	40.6 ± 0.5	40.2 ± 0.5	40.0 ± 0.2	39.9
7	5.0 ± 0.1	4.69 ± 0.05	4.61 ± 0.05	4.5 ± 0.5	1.3
8	3.17 ± 0.04	2.75 ± 0.03	2.72 ± 0.03	2.8 ± 0.2	0.0
Total	140 ± 1	132 ± 1	130 ± 1	130.1 ± 0.7	121.2

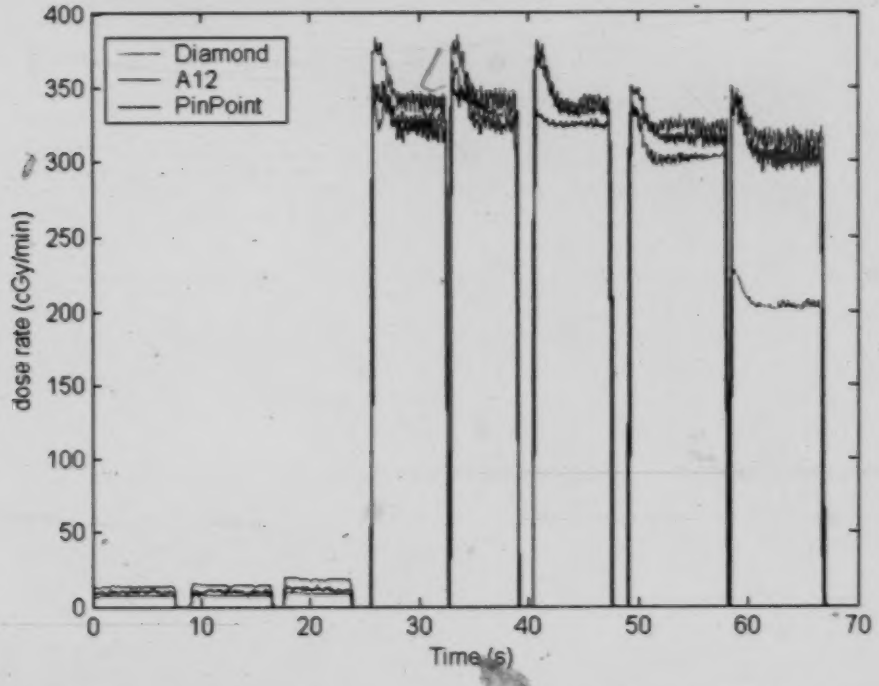

Figure 4.16 Comparison of response of three point dosimeters' response to 8 segment IMRT field at improved detector position 2 (0.7 cm, 3.0 cm) as determined by edge exclude software

Table 4.15 Doses measured at improved detector position 2 (0.7 cm, 3.0 cm) during delivery of 8 segment IMRT field

Segment	Dose (cGy)				
	A12	PinPoint	Diamond Detector	EPID	HELAX-TMS
1	1.23 ± 0.02	1.15 ± 0.01	1.00 ± 0.01	1.36 ± 0.05	0.2
2	1.26 ± 0.02	1.22 ± 0.01	1.04 ± 0.01	1.35 ± 0.04	1.1
3	1.26 ± 0.02	1.18 ± 0.01	1.00 ± 0.01	1.26 ± 0.04	0.9
4	37.3 ± 0.6	39.7 ± 0.3	39.2 ± 0.5	38.4 ± 0.3	39.2
5	33.8 ± 0.5	36.3 ± 0.2	35.6 ± 0.5	35.0 ± 0.2	35.5
6	38.2 ± 0.6	41.2 ± 0.3	40.4 ± 0.5	39.7 ± 0.3	36.6
7	45.6 ± 0.7	49.9 ± 0.3	49.8 ± 0.7	48.7 ± 0.2	49.6
8	36.9 ± 0.6	44.9 ± 0.3	45.6 ± 0.4	44.9 ± 0.1	46.1
Total	196 ± 1	216 ± 1	214 ± 1	210.8 ± 0.5	209.1

The results summarized in Table 4.14 and Table 4.15 indicate that improved agreement between doses measured with various dosimeters can be obtained by appropriate selection of probe positioning. Avoidance of high dose gradient regions improves agreement between measured doses particularly for the PinPoint chamber, the diamond detector and the EPID. Excellent results are obtained by measuring the dose at the first improved detector position as determined by the technique previously described. The total doses measured by the PinPoint chamber, diamond detector and EPID are very nearly in agreement within one standard error. Although the agreement between the doses measured at the second improved detector position is not as good as at the first improved detector position, the PinPoint and EPID values differ by less than 1.5 % from the diamond detector measured value. Comparison of the results summarized in Table 4.13, Table 4.14 and Table 4.15 indicates that drastic improvement in the agreement between doses measured with various dosimeters can be obtained by choosing measurement points appropriately. Avoidance of high dose gradient regions is necessary to decrease volume averaging effects that greatly affect large volume chamber and to eliminate the high sensitivity of dosimeters to small errors in positioning.

Chapter 4 References

Bjarngard, B. E., J. S. Tsai, et al. (1990). "Doses on the central axes of narrow 6-MV x-ray beams." Med Phys **17**(5): 794-9.

Heydarian, M., P. W. Hoban, et al. (1996). "A comparison of dosimetry techniques in stereotactic radiosurgery." Phys Med Biol **41**(1): 93-110.

Hoban, P. W., M. Heydarian, et al. (1994). "Dose rate dependence of a PTW diamond detector in the dosimetry of a 6 MV photon beam." Phys Med Biol **39**: 1219-1229.

Laub, W. U., T. W. Kaulich, et al. (1997). "Energy and dose rate dependence of a diamond detector in the dosimetry of 4-25 MV photon beams." Med Phys **24**(4): 535-6.

Martens, C., C. De Wagter, et al. (2000). "The value of the PinPoint ion chamber for characterization of small field segments used in intensity-modulated radiotherapy." Phys Med Biol **45**(9): 2519-30.

Planskoy, B. (1980). "Evaluation of diamond radiation dosemeters." Phys Med Biol **25**(3): 519-32.

Rustgi, S. N. (1995). "Evaluation of the dosimetric characteristics of a diamond detector for photon beam measurements." Med Phys **22**(5): 567-70.

Chapter 5 Conclusions

The PTW-Freiberg type 60003 diamond detector (S/N 9-032) has been characterized in this work. Various effects of its operation have been observed including the required pre-irradiation dose to ensure detector stability for the following beam qualities: ^{60}Co, 6 and 15 MV photon beams. From this portion of this study it was confirmed that a pre-irradiation dose of 500 cGy is sufficient radiation dose to stabilize the response of the diamond detector for the beam qualities investigated. By increasing time periods between successive ^{60}Co irradiations the stability of the diamond was observed. For delays between measurements ranging from 1 minute to 1 hour, a drop in sensitivity of 0.2 % was observed. The spatial resolution of the diamond detector was quantified by making beam profile measurements at depths of d_{max} and 10 cm in a 6 MV linear accelerator beam. 20-80 % penumbral widths determined using the diamond detector beam profiles are on average 2.1 mm narrower than those measured with the IC10 ion chamber. In all cases the penumbral widths measured with the diamond were smaller than those measured with an ion chamber with a sensitive volume measuring 0.14cm^3. This superior spatial resolution is one of the features of diamond detectors that has made these dosimeters attractive for clinical dosimetric measurements.

The dose rate dependence of this diamond detector was quantified using four different methods of dose rate variation: SSD variation, TMR measurement, PDD measurement and PRF variation. The average value of the Δ value determined from these measurement series for beam qualities of ^{60}Co, 6 and 15 MV was determined to be 0.995 ± 0.002. It was found that in order to observe the dose rate dependence of this diamond detector, dose rate measurements made with an ion chamber needed to be corrected for recombination effects. If these corrections are not made, then the dose rate dependence of the diamond detector may not be observed. It was found that a Δ value of 0.995 introduces a negligible effect when the diamond current is converted to dose rate over this variation in dose rate. A slight sensitivity of the diamond detector dose rate dependence to beam type, pulsed or continuous, was observed. The Δ value determined using a

^{60}Co irradiation was lower than the Δ value determined using linear accelerator generated beam. Diamond detectors due to the similarity of the atomic number of carbon with water have a response that is essentially energy independent. Thus, it is believed that this reduction in the Δ value from pulsed to continuous may arise not from the difference in the energy but rather from the nature of the beam.

In order to verify our ability to correct for the dose rate dependence, 6 and 15 MV arc treatment was delivered and the diamond current was observed as a function of time during the delivery. Agreement within error was obtained between the dose rate dependence corrected diamond and ion chamber dose measurements for both the 6 and 15 MV treatments.

A theoretical investigation of the effect of the dose rate dependence on the conversion of diamond current to dose rate was conducted using diamond current data measured in phantom during the delivery of an arc treatment. It was found that the percent difference between the integrated dose when the dose rate dependence ($\Delta = 0.995$) is taken into account and the integrated dose when the diamond detector is assumed to operate linearly with changes in dose rate is 0.5 % for both 6 and 15 MV photons. That is to say that when the error associated with the integrated doses is considered, the application of the dose rate correction has essentially no effect on the integrated dose for the treatment. This result suggests that dose rate corrections do not need to be applied to diamond detector current data if the Δ value is sufficiently close to unity.

Dose measurements were made for 6 and 15 MV photons for field sizes ranging from 1 x 1 cm^2 to 10 x 10 cm^2. Measurements were made with the diamond detector, PinPoint ion chamber, Exradin A12 ion chamber as well as a Varian aS500 EPID. This study revealed that good agreement in dose measurements is obtained between the diamond detector and the EPID even at field sizes as small as 1 x 1 cm^2. Deviations in the doses measured with the ion chambers at small field sizes were observed. At small field sizes the effects of volume averaging within the sensitive volume and the loss of lateral electronic equilibrium combine to give a loss of sensitivity and a corresponding under-representation of the dose. This result confirms that ion chamber dosimetry is not

adequate for field sizes of this magnitude, and that other dosimeters are required for this situation.

The performance of the diamond detector in three simple IMBs was then compared with the performance of different dosimeters. These beams were created such that there were no high dose gradients at isocenter (the point of measurement). Similar results to those of the small field measurements were obtained. Good agreement was obtained in all cases between the diamond and the EPID measured doses. The response of the other dosimeters was less than ideal with the large volume chamber being greatly affected by volume averaging effects and the PinPoint chamber over-responding to low energy scattered photons.

The sensitivity of the diamond detector to positioning errors was emphasized when point dose measurements were made in a clinical prostate IMB at isocentre. For a number of the segments comprising the IMB isocenter corresponded to the segment edge. Thus, positioning the probe at the isocentre corresponded to placing the probe in a high dose gradient. Although, one of the most attractive features of the diamond detector is its small sensitive volume resulting in high spatial resolution, this same feature also makes diamond detector dosimetry extremely sensitive to positioning.

The appropriateness of this dosimeter as a possible clinical dosimetry has been demonstrated in this thesis. The improved performance of this detector over other clinically used dosimeters in small field dosimetry and IMBs has been demonstrated. After the success achieved by making diamond detector point dose measurements in IMBs at improved detector positions, future work could include a comparison between PinPoint chamber and diamond response in tomotherapy modulated treatment.

Appendix

Appendix A - Calculation of error in dose rate for diamond detector

Expression A.1 describes the relationship between the dose rate, $\dot{D}$, the diamond current, i, the under-response parameter of the diamond detector, Δ, and the constant of proportionality, R.

$$\dot{D} = \left(\frac{i}{R}\right)^{\frac{1}{\Delta}} \tag{A.1}$$

The three variables on the right hand side of the above equation have errors associated with them. The following expression was used to propagate the error in these quantities to arrive at an estimate in error the dose rate.

$$\delta\left(\dot{D}\right) = \sqrt{\left(\frac{\partial \dot{D}}{\partial i}\cdot \delta i\right)^2 + \left(\frac{\partial \dot{D}}{\partial R}\cdot \delta R\right)^2 + \left(\frac{\partial \dot{D}}{\partial \Delta}\cdot \delta \Delta\right)^2} \tag{A.2}$$

$$\delta\left(\dot{D}\right) = \sqrt{\left(\frac{1}{\Delta \cdot R}\cdot\left(\frac{i}{R}\right)^{\left(\frac{1}{\Delta}-1\right)}\cdot \delta i\right)^2 + \left(\frac{i}{\Delta \cdot R^2}\cdot\left(\frac{i}{R}\right)^{\left(\frac{1}{\Delta}-1\right)}\cdot \delta R\right)^2 + \left(\left(\frac{i}{R}\right)^{\frac{1}{\Delta}}\cdot \ln\left(\frac{i}{R}\right)\cdot \delta \Delta\right)^2} \tag{A.2A}$$

The dose rates are then integrated to obtain the total dose during the delivery. Thus the error in the individual dose rates is summed over the time of the irradiation to give an estimate of the error in the dose according to expression A.3.

$$\delta D = \sum_t \delta\left(\dot{D}\right)\cdot \Delta t \tag{A.3}$$

Appendix B – Weighted Regression

When error in data points varies from point to point it may be desirable to weight certain points more heavily in the determination of the equation of the function best fitting the data. The equations contained in this appendix are extracted from *Data reduction and error analysis for the physical sciences* (Bevington 1969). Linear relationships described by expression B.1

$$y = m \cdot x + b \tag{B.1}$$

may have error associated with both x and y values, σ_x and σ_y respectively. In many cases the error in the independent variable is significantly larger than the error in the dependent variables. As a result error in x values are considered to be negligible. In other cases σ_x and σ_y values are of the same order of magnitude and both should be considered in the weighted regression. In these cases the weighting assigned to a data point is given by equation B.2.

$$\sigma^2 = \sigma_x^2 + \sigma_y^2 \tag{B.2}$$

The parameters, m and b, are established by the following equations.

$$b = \frac{1}{\Delta} \cdot \left[\left(\sum \frac{x^2}{\sigma^2} \right) \cdot \left(\sum \frac{y}{\sigma^2} \right) - \left(\sum \frac{x}{\sigma^2} \cdot \sum \frac{x \cdot y}{\sigma^2} \right) \right] \tag{B.3}$$

$$m = \frac{1}{\Delta} \left[\left(\sum \frac{1}{\sigma^2} \right) \cdot \left(\sum \frac{y \cdot x}{\sigma^2} \right) - \left(\sum \frac{x}{\sigma^2} \right) \cdot \left(\sum \frac{y}{\sigma^2} \right) \right] \tag{B.4}$$

$$\Delta = \sum \frac{1}{\sigma^2} \cdot \sum \frac{x^2}{\sigma^2} - \left(\sum \frac{x}{\sigma^2} \right)^2 \tag{B.5}$$

Estimates of the error in the slope and intercept of the weighted regression fit are calculated according to equations B.6 and B.7.

$$\delta b = \left(\frac{1}{\Delta} \cdot \sum \frac{x^2}{\sigma^2} \right)^{\frac{1}{2}} \tag{B.6}$$

$$\delta m = \left(\frac{1}{\Delta} \cdot \sum \frac{1}{\sigma^2} \right)^{\frac{1}{2}} \tag{B.7}$$

Appendix C – Error Propagation

For all estimates of error in this study the rules of error propagation as outlined in *An Introduction to Error Analysis* by J. R. Taylor were employed (Taylor 1997). For the normalization of diamond response shown in the following equation C.1

$$i_{norm} = \frac{i}{i_{ref}} \tag{C.1}$$

the following equation was used to estimate the error in the normalized current value.

$$\delta i_{norm} = \sqrt{\left(\frac{\partial i_{norm}}{\partial i} \cdot \delta i \right)^2 + \left(\frac{\partial i_{norm}}{\partial i_{ref}} \cdot \delta i_{ref} \right)^2} \tag{C.2}$$

$$\delta i_{norm} = \sqrt{\left(\frac{\delta i}{i_{ref}} \right)^2 + \left(\frac{i}{i_{ref}^2} \cdot \delta i_{ref} \right)^2} \tag{C.3}$$

Bibliography

Almond, P. R., P. J. Biggs, B. M. Coursey, W. F. Hanson, M. S. Huq, R. Nath and D. W. Rogers (1999). "AAPM's TG-51 protocol for clinical reference dosimetry of high-energy photon and electron beams." Med Phys **26**(9): 1847-70. (14, 56, 57, 58, 59)

Arcovito, G., A. Piermattei, G. D'Abramo and F. A. Bassi (1985). "Dose measurements and calculations of small radiation fields for 9-MV x rays." Med Phys **12**(6): 779-84. (13)

Attix, F. H. (1986). Introduction to Radiological Physics and Radiation Dosimetry. New York, John Wiley & Sons. ((13, 15, 17, 18, 32)

Barrett, H. H. and W. Swindell (1981). Radiological Imaging - The Theory of Image Formation, Detection and Processing. New York, Academic Press, Inc. (20)

Beddar, A. S., D. J. Mason and P. F. O'Brien (1994). "Absorbed dose perturbation caused by diodes for small field photon dosimetry." Med Phys **21**(7): 1075-9. (14, 17, 18)

Bevington, P. R. (1969). Data reduction and error analysis for the physical sciences. New York, McGraw-Hill. (109)

Bjarngard, B. E., J. S. Tsai and R. K. Rice (1990). "Doses on the central axes of narrow 6-MV x-ray beams." Med Phys **17**(5): 794-9. (12, 88)

Bjork, P., T. Knoos and P. Nilsson (2000). "Comparative dosimetry of diode and diamond detectors in electron beams for intraoperative radiation therapy." Med Phys **27**(11): 2580-8. (27)

Boyer, A. L., L. Xing and P. Xia (1999). Chapter 12 Beam Shaping and Intensity Modulation. The Modern Technology of Radiation Oncology. J. Van Dyk. Madison, Wisconsin, Medical Physics Publishing: 437-479. (8)

Brady, L. W., S. Kramer, S. H. Levitt, R. G. Parker and W. E. Powers (2001). "Radiation Oncology: Contributions of the United States in the Last Years of the 20th Century." Radiology **219**: 1-5. (5)

Burgemeister, E. A. (1981). "Dosimetry with a diamond operating as a resistor." Phys Med Biol **26**(2): 269-75. (28, 32, 37)

Chuang, C. F., L. J. Verhey and P. Xia (2002). "Investigation of the use of MOSFET for clinical IMRT dosimetric verification." Med Phys **29**(6): 1109-15. (18,19)

De Angelis, C., S. Onori, M. Pacilio, G. A. Cirrone, G. Cuttone, L. Raffaele, M. Bucciolini and S. Mazzocchi (2002). "An investigation of the operating characteristics of two PTW diamond detectors in photon and electron beams." Med Phys **29**(2): 248-54. (25, 27, 29, 35, 36, 37, 38)

Fidanzio, A., L. Azario, R. Miceli, A. Russo and A. Piermattei (2000). "PTW-diamond detector: dose rate and particle type dependence." Med Phys **27**(11): 2589-93. (27, 29, 37)

Fowler, J. F. and F. H. Attix (1966). Solid state electrical conductivity doseimeters. Radiation Dosimetry. F. H. Attix and W. C. Roesch. New York, Academic. **1**. (24, 63)

Glasgow, G. P. (1999). Chapter 10 Cobalt-60 Teletherapy. The Modern Technology of Radiation Oncology. J. Van Dyk. Madison, Wisconsin, Medical Physics Publishing: 313-348. (6)

Glasgow, G. P. (1999). Chapter 18 Brachytherapy. The Modern Technology of Radiation Oncology. J. Van Dyk. Madison, Wisconsin, Medical Physics Publishing: 695-752. (6)

Greer, P. B. and C. C. Popescu (2003). "Dosimetric properties of an amorphous silicon electronic portal imaging device for verification of dynamic intensity modulated radiation therapy." Med Phys **30**(7): 1618-27. (48)

Hall, E. J. (2000). Radiobiology for the radiologist. Philidelphia, Lippincott Williams & Wilkins. (5)

Heydarian, M., P. W. Hoban, W. A. Beckham, I. M. Borchardt and A. H. Beddoe (1993). "Evaluation of a PTW diamond detector for electron beam measurements." Phys Med Biol **38**: 1035-1042. (15, 30, 32, 33, 38)

Heydarian, M., P. W. Hoban and A. H. Beddoe (1996). "A comparison of dosimetry techniques in stereotactic radiosurgery." Phys Med Biol **41**(1): 93-110. (12, 88)

Hoban, P. W., M. Heydarian, W. A. Beckham and A. H. Beddoe (1994). "Dose rate dependence of a PTW diamond detector in the dosimetry of a 6 MV photon beam." Phys Med Biol **39**: 1219-1229. (16, 24, 26, 27, 28, 32, 34, 35, 36, 82)

Houdek, P. V., J. M. VanBuren and J. V. Fayos (1983). "Dosimetry of small radiation fields for 10-MV x rays." Med Phys **10**(3): 333-6. (13)

Hugtenburg, R. P., K. Johnston, G. J. Chalmers and A. H. Beddoe (2001). "Application of dimaond detectors fo the dosimetry of 45 and 100 kVp therapy beams: comparison with a parallel-plate ionization chamber and Monte Carlo." Phys Med Biol **46**: 2489-2501. (36)

ICRU (1984). "Radiation dosimetry: electron beams with energies between 1 and 50 MeV." ICRU Report 35. (33)

Johns, H. E. and J. R. Cunningham (1983). The Physics of Radiology. Springfield, Charles C. Thomas. (15, 17, 21, 30)

Ju, S. G., Y. C. Ahn, S. J. Huh and I. J. Yeo (2002). "Film dosimetry for intensity modulated radiation therapy: dosimetric evaluation." Med Phys **29**(3): 351-5. (21)

Kanda, H., M. Akaishi and S. Yamaoka (1999). "Synthesis of diamond with the highest nitrogen concentration." Diamond and Related Materials **8**: 1441-1443. (23)

Keddy, R. J., T. L. Nam and R. C. Burns (1987). "Synthetic diamonds as ionisation chamber radiation detectors in biological environments." Phys Med Biol **32**(6): 751-9. (28)

Khan, F. M. (1994). The Physics of Radiation Therapy. Baltimore, Williams and Wilkins. (5, 8, 15, 20, 21, 32)

Laub, W. U., T. W. Kaulich and F. Nusslin (1997). "Energy and dose rate dependence of a diamond detector in the dosimetry of 4-25 MV photon beams." Med Phys **24**(4): 535-6. (26, 82)

Laub, W. U., T. W. Kaulich and F. Nusslin (1999). "A diamond detector in the dosimetry of high-energy electron and photon beams." Phys Med Biol **44**(9): 2183-92. (35)

Mack, A., S. G. Scheib, J. Major, S. Gianolini, G. Pazmandi, H. Feist, H. Czempiel and H. J. Kreiner (2002). "Precision dosimetry for narrow photon beams used in radiosurgery-determination of Gamma Knife output factors." Med Phys **29**(9): 2080-9. (12, 13)

MacKenzie, M. A., M. Lachaine, B. Murray, B. G. Fallone, D. Robinson and G. C. Field (2002). "Dosimetric verification of inverse planned step and shoot multileaf collimator fields from a commercial treatment planning system." J Appl Clin Med Phys **3**(2): 97-109. (67, 68)

Mainwood, A. (2000). "Recent developments of diamond detectors for particles and UV radiation." Semicond Sci Technol **15**: R55-R63. (23, 27, 30, 37)

Martens, C., I. Claeys, C. De Wagter and W. De Neve (2002). "The value of radiographic film for the characterization of intensity-modulated beams." Phys Med Biol **47**(13): 2221-34. (9, 10)

Martens, C., C. De Wagter and W. De Neve (2000). "The value of the PinPoint ion chamber for characterization of small field segments used in intensity-

modulated radiotherapy." Phys Med Biol **45**(9): 2519-30. (12, 13, 47, 87, 93, 94)

Menon, G. V. and R. S. Sloboda (2003). "Compensator quality control with an amorphous silicon EPID." Med Phys **30**(7): 1816-24. (22)

Mobit, P. N., A. E. Nahum and P. Mayles (1997). "A Monte Carlo study of the quality dependence of diamond thermoluminescent dosimeters in radiotherapy beams." Phys Med Biol **42**: 1913-1927. (33)

Mobit, P. N. and G. A. Sandison (1999). "A Monte Carlo comparison of the response of the PTW-diamond and the TL-diamond detectors in megavoltage photon beams." Med Phys **26**(11): 2503-7. (46)

NCIC (2003). National Cancer Institute of Canada. http://www.ncic.cancer.ca, accessed September 2003. (4)

Olivera, G. H., D. M. Shepard, K. Ruchala, J. S. Aldridge, J. Kapatoes, E. E. Fitchard, P. J. Reckwerdt, G. Fang, J. Balog, J. Zachman and T. R. Mackie (1999). Chapter 15 Tomotherapy. The Modern Technology of Radiation Oncology. J. Van Dyk. Madison, Wisconsin, Medical Physics Publishing: 521-587. (7, 11)

Partridge, M., M. Ebert and B. M. Hesse (2002). "IMRT verification by three-dimensional dose reconstruction from portal beam measurements." Med Phys **29**(8): 1847-58. (48)

Planskoy, B. (1980). "Evaluation of diamond radiation dosemeters." Phys Med Biol **25**(3): 519-32. (16, 26, 27, 32, 34, 35, 36, 37, 82)

Podgorsak, E. B. and M. B. Podgorsak (1999). Chapter 16 Stereotactic Irradiation. The Modern Technology of Radiation Oncology. J. Van Dyk. Madison, Wisconsin, Medical Physics Publishing: 589-639. (16)

Pychlau, C. (2003). Personal communication with E. Barnett. Freiburg, Germany. (46)

Radiology Centennial, I. (1993). Magical Roentgen Rays in Early Therapy. (5)

Rustgi, S. N. (1995). "Evaluation of the dosimetric characteristics of a diamond detector for photon beam measurements." Med Phys **22**(5): 567-70. (18, 88, 89)

Rustgi, S. N., A. K. Rustgi, S. B. Jiang and K. M. Ayyangar (1998). "Dose perturbation caused by high-density inhomogeneities in small beams in stereotactic radiosurgery." Phys Med Biol **43**: 3509-3518. (13)

StatsCanada (1999). Mortality - Summary List of Causes, 1997. http://www.statcan.ca/english/IPS/Data/84F0209XPB.htm#abstract, accessed September 2003. (4)

Steciw, S., B. Warkentin, S. Rathee and B. G. Fallone (2003). "A Monte Carlo based method for accurate IMRT verification using the aS500 EPID." Med Phys **30**: 1331. (22, 49, 65, 66)

Tapper, R. J. (2000). "Diamond detectors in particle physics." Rep Prog Phys **63**: 1273-1316. (25, 27)

Taylor, J. R. (1997). An Introduction to Error Analysis. Sausalito, University Science Books. (10)

Tromson, D., V. N. Amosov, A. Brambilla, C. Mer, F. Foulon, R. Barrett and P. Bergonzo (2001). "Influence of defect inhomogeneities in high quality natural diamond detectors." Diamond and Related Materials **10**: 469-473. (23)

Van Dyk, J. (1999). Chapter 1 Radiation Oncology Overview. The Modern Technology of Radiation Oncology. J. Van Dyk. Madison, Wisconsin, Medical Physics Publishing: 1-17. (5)

Vatnitsky, S. and H. Jarvinen (1993). "Application of a natural diamond detector for the measurement of relative dose distributions in radiotherapy." Phys Med Biol **38**(1): 173-84. (30, 32, 33, 35, 37)

Warkentin, B., S. Steciw, S. Rathee and B. G. Fallone (2003). "Dosimetric IMRT verification with a flat-panel EPID." Med Phys **30**(12): 3143-3155. (22, 49, 65, 66)

Webb, S. (1997). The Physics of Conformal Radiotherapy. Bristol, Institute of Physics Publishing Ltd. (7)

Webb, S. (2001). Intensity-Modulated Radiation Therapy. Bristol, Institute of Physics Publishing Ltd. (7, 8, 9, 10)

Wilkins, D., X. A. Li, J. Cygler and L. Gerig (1997). "The effect of dose rate dependence of p-type silicon detectors on linac relative dosimetry." Med Phys **24**(6): 879-81. (18)

Williams, L. E., A. Liu and G. Wong (1999). Chapter 25 Monoclonal Antibody and Other Internal Emitter Therapies. The Modern Technology of Radiation Oncology. J. Van Dyk. Madison, Wisconsin, Medical Physics Publishing: 1021-1042. (6)

Zhu, X. R., J. J. Allen, J. Shi and W. E. Simon (2000). "Total scatter factors and tissue maximum ratios for small radiosurgery fields: comparison of diode

detectors, a parallel-plate ion chamber, and radiographic film." Med Phys **27**(3): 472-7. (13)

Zhu, X. R., P. A. Jursinic, D. F. Grimm, F. Lopez, J. J. Rownd and M. T. Gillin (2002). "Evaluation of Kodak EDR2 film for dose verification of intensity modulated radiation therapy delivered by a static multileaf collimator." Med Phys **29**(8): 1687-92. (21)